UNIVERSITEIT VAN PRETORIA
UNIVERSITY OF PRETORIA
YUNIBESITHI YA PRETORIA

Denkleiers • Leading Minds • Dikgopolo tša Dihlalefi

SUBLIMATION/DESUBLIMATION SEPARATION OF ZrF_4 AND HfF_4

Jakkie Postma

2018

SUBLIMATION/DESUBLIMATION SEPARATION OF ZrF_4 AND HfF_4

By

Jakkie Postma

Submitted in partial fulfilment of the requirements for the degree of MASTER IN ENGINEERING (CHEMICAL ENGINEERING)

in the

Faculty of Engineering, Built Environment and Information Technology

Department of Chemical Engineering

University of Pretoria

South Africa

2018

EXECUTIVE SUMMARY

SUBLIMATION/DESUBLIMATION SEPARATION OF ZrF_4 AND HfF_4

Supervisor: Prof PL Crouse

Co-supervisor: Mr HF Niemand

This dissertation details research aimed at the separation of Zr and Hf in the tetrafluoride form. Separation of ZrF_4 and HfF_4 was achieved using sublimation followed by desublimation. The separation involves the sublimation of the tetrafluorides in an inert atmosphere under controlled parameters. The sublimed mass (700 °C to 800 °C) diffuses into nitrogen which then flows across a water-cooled desublimer (annulus) with the aim of desubliming the one metal fluoride in preference to the other. This implies that separation was achieved in both the sublimer and the desublimer, due to differences in both the sublimation and desublimation rates. The aim was for the sublimer residue to be Hf-rich and the desublimer content to be Zr-rich. The Zr/Hf content was determined by means of ICP-OES analysis. It must be noted that the work reported in this thesis is based on only a first sublimation step. The reason for this is that the equipment used was on laboratory scale and that the mass collected from the desublimer was not sufficient to allow a second or third step to be carried out.

Little information was available in the literature on the sublimation separation of Zr and Hf, especially in the fluoride form, most of it being sublimation under vacuum conditions. On an industrial scale, only vacuum sublimation of ZrF_4 has been introduced into the industry, and no information was found for sublimation of ZrF_4 in an inert atmosphere on an industrial scale. There was also limited information on the sublimation rate of ZrF_4 or HfF_4 in an inert atmosphere.

In the process described in this dissertation, optimal temperature selection is crucial since low temperatures result in a low sublimation rate, and high temperatures not only increase the level of impurities in the sublimed product, but also increase the cost of construction material and energy consumption. The aim was to determine the experimental conditions, i.e. sublimation time, temperature and position on the desublimer, which will provide optimal separation conditions. These conditions must, however, be compared with the operating cost, as this will be higher at a higher temperature and for longer sublimation runs.

A model was developed to predict the respective sublimation rates of the two tetrafluorides and to use these rates to determine the separation within the sublimer as well as the partial pressures of the two tetrafluorides in the gas phase. The partial pressures were then used to further model the desublimation of the tetrafluorides on a water-cooled annular surface. The model sufficiently predicted the sublimation rates at lower temperatures, but over-predict at higher temperatures.

A major problem of the experiments was that the sublimation rate formed a plateau before complete sublimation had been achieved. This can be the formation of a crust-like surface or sintered cake which prevented further sublimation from occurring, which may be due to the presence of impurities originating from the zircon. The sublimation temperature remained the same, but sintering of the cake negatively influenced the sublimation kinetics.

The conclusion is that sublimation in an inert atmosphere may be feasible depending on the extent of separation achieved along the length of the desublimer as well as within the sublimer residue. A lower sublimation temperature resulted in better separation but with lower sublimation rates. Vacuum sublimation, however, results in higher fluxes and requires lower temperatures. It is therefore recommended that this work be repeated under vacuum conditions to determine the extent of separation that can be achieved along the length of the desublimer. To stress the importance of the recommendation, it must be noted that sublimation provides dry methods with no liquid waste. It may require fewer steps, which is less labour intensive and requires lower capital cost than other commercial technologies. The major drawback is the high energy requirements to obtain the high separation temperatures, which results in costly construction materials.

Keywords: Sublimation, desublimation, zirconium tetrafluoride, hafnium tetrafluoride

Declaration

I, Catharina Jacoba (Jakkie) Postma, hereby declare that:

- This dissertation has not been submitted, in full or in part, for any degree or examination at any other university;
- This dissertation, along with the research reported therein, is my own wok and is expressed in my own words. All the sources that I have used, or partially used, of authors in any form have been indicated and acknowledged at the point of their use as full references.

Mrs. Jakkie Postma

2018/11/27

Date

Acknowledgements

I wish to express my sincerest gratitude and appreciation to the following organisations, colleagues and family members who made this dissertation possible:

- To my Heavenly Father for giving me the strength and wisdom to complete this research.
- To my whole family, especially my husband, who supported and encouraged me all along the way; to my precious son who motivated me to complete this work; to my parents who encouraged and supported me to study after I had completed my matric; and special thanks to my father-in-law for his motivating words during my studies.
- To the Nuclear Materials Development Network (NMDN) of the Advanced Metals Initiative (AMI), funded by the South African Department of Science and Technology (DST), for their financial assistance.
- To Necsa, for financial support throughout this project.
- To my professor, Philip Crouse, for his advice and guidance throughout the writing of this dissertation.
- To my co-supervisor, Hennie Niemand, for his valued moral support and continued engineering inputs which are much appreciated.
- To Salmon Lubbe for his support with my experimental work, several meaningful discussions and the ICP-OES analysis.
- To Pat Smith and Johan Havenga for their valued support and assistance in building the experimental setup used to carry out this research.
- To John Barry and Ettienne Snyders for their continuous encouragement to complete this work; and special thanks to John Barry for the editorial work on sections of this thesis.
- To Gerard Puts and Andrew Pienaar for all the thermogravimetric analyses.
- To Ryno van der Merwe for the SEM and other particle analyses.
- To Tshepo Ntsoane for the invaluable XRD analyses.
- To Steven Lotter, Milton Makhofane and others for their assistance with several matters during the course of producing this dissertation.

Publications

Publications that resulted from this work

Pretorius, CJ, Pienaar, AD, Crouse, PL and Niemand, HF (2014) Sublimation kinetics of zirconium tetrafluoride. *Advanced Materials Research* 1019: 398-405.

Postma, CJ, Niemand, HF and Crouse, PL (2015) A theoretical approach to the sublimation separation of zirconium and hafnium in the tetrafluoride form. *Journal of the South African Institute of Mining and Minerals,* 115: 961-966.

Postma, CJ, Lubbe, SJ and Crouse, PL (2017) Selective sublimation/desublimation separation of ZrF_4 and HfF_4. *Journal of the South African Institute of Mining and Minerals*, 117: 939-946.

Contents

EXECUTIVE SUMMARY i

Declaration iii

Acknowledgements iv

Publications v

List of figures ix

List of tables xii

Nomenclature xiii

Chapter 1: Introduction 1-1

Chapter 2: Literature 2-1

2.1 Zirconium and hafnium 2-1

2.2 Processes for the separation of Zr and Hf 2-2

2.2.1 Fractional crystallisation 2-3

2.2.2 Fractional crystallisation of the double fluorides 2-3

2.2.3 Solvent extraction 2-5

2.2.4 Ion exchange 2-10

2.2.5 Reduction processes 2-11

2.2.6 Extractive distillation in molten salts 2-12

2.2.7 High-pressure vapour-liquid distillation 2-13

2.3 Sublimation as a purification and separation process 2-14

2.3.1 Sublimation for the separation of Zr from Hf 2-15

2.3.2 Sublimation purification of ZrF_4 from non-volatile impurities (excluding Hf) 2-16

2.4 Apparatus used for sublimation purification of ZrF_4 2-19

2.4.1 Vacuum sublimation purification (excluding Hf) 2-19

2.4.2 Vacuum sublimation purification (separation of Zr and Hf) 2-21

2.4.3 Sublimation purification in an inert atmosphere (excluding Hf) 2-23

2.5 Typical sublimation rates of ZrF_4 and HfF_4 2-25

2.5.1 Vacuum sublimation 2-25

2.5.2 Sublimation in an inert atmosphere 2-31

2.5.3 Scaled-up sublimation processes 2-31

2.6 Nuclear specification for Zr 2-32

Chapter 3: Experimental 3-1

3.1 Process description and concept discussion 3-1
3.2 Experimental procedure 3-4

Chapter 4: Preparation and characterisation of $Zr(Hf)F_4$ 4-1

4.1 Preparation of $Zr(Hf)F_4$ 4-1
4.1.1 Impurities in ZrF_4 4-2
4.1.2 System description 4-2
4.2 Characterisation of $Zr(Hf)F_4$ used in sublimation experiments 4-5
4.2.1 X-Ray diffraction 4-5
4.2.2 Thermogravimetric analysis 4-6
4.2.3 Scanning electron microscope 4-7
4.2.4 Particle analysis 4-8

Chapter 5: Model development 5-1

5.1 Properties of ZrF_4, HfF_4 and N_2 5-1
5.1.1 Vapour pressures 5-1
5.1.2 Physical properties of nitrogen 5-3
5.1.3 Physical properties of ZrF_4, HfF_4 and other metal fluoride impurities 5-3
5.1.4 Thermodynamic properties of ZrF_4 and HfF_4 5-6
5.1.5 Diffusion coefficients 5-8
5.1.6 Flow properties 5-13
5.1.7 Heat transfer 5-14
5.1.8 Mass transfer 5-15
5.1.9 Lewis number 5-17
5.2 Development of a model for the pre-heating of the nitrogen 5-17
5.2.1 Model of pre-heating 5-17
5.3 Development of a sublimation rate model 5-19
5.3.1 Predicting sublimation rates 5-19
5.3.2 Sublimation mode 5-20
5.3.3 Continuity equation 5-23
5.3.4 Sublimation rate model 5-23
5.3.5 Flow diagram for calculations of the sublimation process 5-24
5.4 Development of a desublimation rate model 5-26
5.4.1 Concentration and thermal diffusion contributions to the mass flux 5-26
5.4.2 Desublimation mode 5-27
5.4.3 Desublimation rate model 5-29
5.4.4 Flow calculations for the desublimation rate model 5-29

Chapter 6: Results and discussion 6-1
6.1 Model parameters 6-1
6.1.1 Variables 6-1
6.1.2 Constants 6-1
6.2 Nitrogen preheating 6-1
6.3 Sublimation rate 6-2
6.4 Separation within the sublimer 6-6
6.5 Separation within the desublimer 6-8
6.5.1 Experimental results 6-8
6.5.2 Model predictions 6-11
6.5.3 Bulk gas temperature 6-11
6.6 Modelled partial pressures 6-12
6.6.1 Partial pressures of ZrF_4 and HfF_4across the sublimer and desublimer section 6-12
6.6.2 Partial pressures exiting the sublimer section 6-13
6.7 Number of sublimation steps determined by the model 6-15
6.7.1 Model run at 790 °C sublimation temperature and 30 minutes' sublimation time 6-15
6.7.2 Model run at 760 °C sublimation temperature and 30 minutes' sublimation time 6-16
6.7.3 Model run at 760 °C sublimation temperature and 60 minutes' sublimation time 6-17
Chapter 7: Conclusions and recommendations 7-1
7.1 Conclusions 7-1
7.2 Recommendations 7-2
Chapter 8: References 8-1

List of figures

Figure 2-1: Established technologies for the separation of Zr and Hf 2-3
Figure 2-2: Sublimation apparatus used by Abate and Wilhelm for the purification of ZrF_4 2-20
Figure 2-3: Sublimation and desublimation system with baffles for the purification of ZrF_4 2-20
Figure 2-4: Sublimation apparatus used by Kotsar *et al.* for the purification of ZrF_4 2-21
Figure 2-5: Vacuum sublimation apparatus used by Monnahela *et al.* for the separation of ZrF_4 and HfF_4 2-22
Figure 2-6: Vacuum sublimation apparatus (Solov'ev & Malyutina, 2002a) 2-22
Figure 2-7: Sublimation apparatus for the purification of ZrF_4 used by Dai *et al.* 2-23
Figure 2-8: Chemical vapour deposition apparatus used by Fujiura *et al.* for the synthesis of high-purity ZrF_4 2-23
Figure 2-9: Sublimation setup used for the purification of ZrF_4 2-24
Figure 2-10: A highly efficient sublimation purification system using baffles with orifices 2-25
Figure 2-11: Influence of temperature on the sublimation rate under vacuum conditions 2-27
Figure 2-12: Area-dependent rate as a function of temperature 2-28
Figure 2-13: Langmuir expression for the sublimation of ZrF_4 under vacuum conditions 2-28
Figure 2-14: Approximate dimensions of the crucible used by MacFarlane (Figure 2-9) 2-31
Figure 3-1: Block flow diagram (BFD) for the sublimation separation of ZrF_4 and HfF_4 3-1
Figure 3-2: Schematic of the sublimer used 3-2
Figure 3-3: Schematic of sublimer and desublimer inside tube furnace 3-2
Figure 3-4: Experimental setup for the sublimation/desublimation separation of ZrF_4 and HfF_4 3-3
Figure 3-5: Illustration of the sublimation/desublimation setup 3-3
Figure 3-6: Image showing sublimer and desublimer in tube oven set at 850 °C. 3-4
Figure 3-7: Piping and instrumentation diagram 3-5
Figure 4-1: Batch reactor system for the production of $Zr(Hf)F_4$ from DPDZ and ABF 4-4
Figure 4-2: XRD pattern of $Zr(Hf)F_4$ overlaid with stick pattern of ZrF_4 4-5
Figure 4-3: TGA result of three samples of $Zr(Hf)F_4$ prepared for sublimation experiments 4-7
Figure 4-4: (a) SEM image indicating very small $Zr(Hf)F_4$ particles along with the larger zircon and PDZ particles, (b) 30 μm magnification indicating agglomerates of small Zr(Hf) particles 4-8
Figure 5-1: Vapour pressures for ZrF_4 and HfF_4 as reported in the literature 5-1
Figure 5-2: Transparent crystals formed by recrystallisation at 650 °C over a 3-day time period (Robinson & Fuller, 1987) 5-6
Figure 5-3: Heat capacity as a function of temperature 5-7
Figure 5-4: Enthalpy as a function of temperature 5-8
Figure 5-5: Entropy as a function of temperature 5-8

Figure 5-6: Pre-heating of nitrogen featuring ¼'' copper tubing spiralled around the pipe for sublimation in a tube oven 5-18
Figure 5-7: Illustration of the sublimation mode and definition of a control volume within the sublimation pan 5-21
Figure 5-8: Cross-section of the sublimer in the tube oven 5-21
Figure 5-9: Flow calculations for the sublimation of ZrF_4 and HfF_4 as a function of the sublimation time and the length of the bed 5-25
Figure 5-10: Definition of coordinates in annulus section of the desublimer 5-27
Figure 5-11: Cross-section of annular probe indicating the driving forces resulting in mass transport to the surface 5-28
Figure 5-12: Flow calculations for desublimation of ZrF_4 and HfF_4 as a function of length of time .. 5-30
Figure 6-1: Sublimation rate of $Zr(Hf)F_4$ as a function of the sublimation temperature 6-2
Figure 6-2: Sublimer residue indicating cake formation 6-3
Figure 6-3: Sublimer residue indicative of hump formation 6-3
Figure 6-4: Linear section of the sublimation rate as a function of the temperature 6-4
Figure 6-5: Modelled sublimation rates compared with experimental results 6-4
Figure 6-6: Slope of the fraction sublimed vs. time as a function of the sublimation temperature.... 6-5
Figure 6-7: Modelled result for the total sublimation time as a function of the sublimation temperature 6-6
Figure 6-8: ZrF_4 and HfF_4 sublimer residue as a function of sublimation time at 790 °C..... 6-6
Figure 6-9: Zr/Hf mole ratio of the sublimer residue as a function of time and temperature 6-7
Figure 6-10: Slope of Zr/Hf mole ratio vs. time as a function of the sublimation temperature 6-7
Figure 6-11: Sample positions on the desublimer 6-8
Figure 6-12: Zr/Hf mole ratio across the length of the desublimer 6-9
Figure 6-13: Temperature-dependent mole ratios as a function of desublimer position 6-9
Figure 6-14: Linear relationship for the slope of the Zr/Hf mole ratio versus temperature graphs as a function of the position on the desublimer 6-10
Figure 6-15: The amount of mass that desublimes is a function of the sublimation temperature ... 6-10
Figure 6-16: Experimental and model results obtained for separation along the length of the desublimer 6-11
Figure 6-17: Schematic of sublimer and desublimer inside tube furnace indicating the position of X_1 thermocouple 6-11
Figure 6-18: Modelled result for cooling of the bulk gas after exiting the sublimer section with the sublimation temperature set at 790 °C 6-12
Figure 6-19: Partial pressures of ZrF_4 within the sublimer and desublimer 6-13
Figure 6-20: Partial pressures of HfF_4 within the sublimer and desublimer 6-13

Figure 6-21: Partial pressures of ZrF_4 and HfF_4 exiting the sublimer section at 790 °C 6-14
Figure 6-22: Partial pressures of ZrF_4 and HfF_4 exiting the sublimer section at 760 °C 6-14
Figure 6-23: Number of calculated sublimation steps required to obtain < 100 ppm Hf at a sublimation temperature of 790 °C and removal of the sublimer after 30 minutes..... 6-16
Figure 6-24: Number of calculated sublimation steps required to obtain < 100 ppm Hf at a sublimation temperature of 760 °C and removal of the sublimer after 30 minutes..... 6-17
Figure 6-25: Number of sublimation steps required to obtain < 100 ppm Hf with a sublimation temperature of 760 °C and removal of the sublimer after 60 minutes..... 6-17
Figure 7-1: Cascade of sublimer/desublimer systems for the separation of Zr and Hf 7-3

List of tables

Table 2-1: Summary of the sublimation rates obtained for ZrF_4 from the literature data 2-26
Table 2-2: Area-dependent sublimation rates 2-27
Table 2-3: Specification for nuclear grade Zr sponge 2-32
Table 2-4: Permissible impurities in ZrF_4 2-33
Table 4-1: Quantitative XRD results for three batches $Zr(Hf)F_4$ prepared from DPDZ and ABF 4-5
Table 4-2: Calculated low-temperature volatiles in the three respective batches 4-6
Table 4-3: Average particle size distributions 4-8
Table 5-1: Combined vapour pressure correlations for ZrF_4 and HfF_4. 5-2
Table 5-2: Vapour pressures of metal fluoride impurities (Robinson, 1986: 189) 5-2
Table 5-3: Physical properties of nitrogen at several temperatures and at 100 kPa 5-3
Table 5-4: Melting, boiling and/or sublimation temperatures of some metal fluorides 5-4
Table 5-5: Free energy of formation 5-7
Table 5-6: Chemical thermodynamic data for ZrF_4 in the solid and gaseous state 5-7
Table 5-7: Estimating the Lennard-Jones diameter using Spartan software 5-10
Table 5-8: Estimating collision diameters for ZrF_4 and HfF_4 with N_2 5-10
Table 5-9: Collision integral parameters 5-11
Table 5-10: Diffusion coefficients for ZrF_4 and HfF_4 in nitrogen at 1 atmosphere 5-11
Table 5-11: Comparison of calculated diffusivities with literature values 5-12
Table 5-12: Relationships between fluxes and driving forces 5-26

Nomenclature

Abbreviations and Definitions

Abbreviation	Definition
ABF	Ammonium bifluoride
Alamine 300	Tri-n-octyl amine
Alamine 336	Tri-(C8-C10) amine
Aliquat 336	Tri-(C_8-C_{10}) methyl ammonium chloride
Amberjet 4200 Cl	Poly(styrene-co-divinylbenzene) with quaternary amine functionality, chloride form
Amberlite IRA-400	Strong basic anion resin
AMI	Advanced Metals Initiative
ASTM	American Society for Testing and Materials
Baddeleyite	ZrO_2 (mineral)
Caustic soda	Sodium hydroxide
CEZUS	Compagnie Européenne de Zirconium Ugine Sandvik
CYANEX 272	Bis(2,4,4-trimethylpentyl)phosphinic acid
CYANEX 921	Trioctylphosphine oxide (TOPO)
CYANEX 923	A mixture of four trialkyl-phosphine oxides
CYANEX 925	A mixture of branched chain alkylated phosphine oxides
D2EHPA	Di-2-ethylhexylphosphoric acid
DBBP	Dibutyl butylphosphonate
DIBK	Diisobutyl ketone
DMHP	Di-(1-methylheptyl) methylphosphonate
Dowex-1	Strong basic anion resin
Dowex-50	Strong acid cation resin
DPDZ	Desilicated Plasma Dissociated Zircon ($Zr(Hf)\cdot O_2$)
DST	Department of Science and Technology
GD-OES	Glow Discharge optical emission spectroscopy
HSC	Chemical reaction and equilibrium software with extensive thermochemical database and flowsheet simulation
HSCN	Thiocyanic acid
kerosene	A mixture of liquid hydrocarbons
LIX 63	5,8-diethyl-7-hydroxy-6-dodecanone oxime
LM	Liquid membrane

Abbreviation	Definition
Mercaptans	Organosulphur compounds that contain a carbon-bonded sulfhydryl group
MIBK	Methyl isobutyl ketone
Necsa	The South African Nuclear Energy Corporation SOC. Ltd.
NMDN	Nuclear Materials Development Network
PDZ	Plasma-dissociated zircon ($Zr(Hf)O_2 \cdot SiO_2$)
ppm	Parts per million
SCN	Thiocyanate
SEM	Scanning Electron Microscope
SLM	Supported liquid membrane
Solvesso 150	Heavy aromatic solvent naphtha
TBP	Tributyl phosphate
TNOA	Tri-n-octylamine
TODGA	N,N,N',N'-tetraoctyldiglycolamide
XRD	X-Ray Diffraction
Zircon	$ZrSiO_4$ or $Zr(Hf)SiO_4$ to place emphasis on Hf impurity

Description of symbols

Symbols	Description
$\boldsymbol{A_{flow}}$	Flow area
$\boldsymbol{A_{sub}}$	Sublimation area
$\boldsymbol{A_{pipe}}$	Surface area of the pipe used for pre-heating the nitrogen
$\boldsymbol{b}$	Half the base of the sublimer bulk mass width
$\boldsymbol{c}$	Constant
$\boldsymbol{Cp}$	Heat capacity
$\boldsymbol{D_e}$	Equivalent diameter
$\boldsymbol{D_{eH}}$	Equivalent diameter of heat transfer
$\boldsymbol{D_{i,N2}}$	Diffusion coefficient of either ZrF_4 or HfF_4 in nitrogen
$\boldsymbol{D_i^T}$	Thermal diffusion coefficient
$\boldsymbol{D_1}$	Outer diameter of the inner pipe of the annulus
$\boldsymbol{D_2}$	Inner diameter of the outer pipe annulus
$\Delta \boldsymbol{G_f^\circ}$	Standard Gibbs energy of formation
$\boldsymbol{Gr}$	Grashof number
$\boldsymbol{Gz}$	Graetz number

Symbols	Description
ΔH_{sub}	Enthalpy of sublimation
$\mathbf{h}_{conv}$	Convective heat transfer coefficient
ΔH_{form}	Free energy of formation
ΔH_f°	Standard enthalpy of formation
ΔH	Incremental height of the fraction of the bed that sublimed
J_i^{ω}	Contribution of concentration to mass flux in the desublimer
J_i^{T}	Contribution of thermal diffusion to mass flux in the desublimer
k	Thermal conductivity
K	Boltzmann constant
k_i	Mass transfer coefficient
k_i^{ω}	Mass transfer coefficient in the desublimer
$L_{c,desub}$	Characteristic length for the annulus section of the desublimer
$L_{c,sub}$	Characteristic length in the sublimer
Le	Lewis number
$\dot{m}$	Mass flow
$M_{i,t+1_s}$	Residual mass of ZrF_4 or HfF_4 at time *t* in the sublimer
MM	Molecular weight
M_B	Mass of a Brownian particle
N_i	Number of moles
$\dot{n}_j$	Molar flux at a specific position in the sublimer
Nu	Nusselt number
P	Pressure
P_i^*	Vapour pressure
p_i'	Partial pressure
Pr	Prandtl number
Re	Reynolds number
r_i	Rate of sublimation
Sc	Schmidt number
Sh	Sherwood number
S_w	Walk speed
S_T	Soret coefficient
S°	Standard entropy of formation
$\mathbf{S}$	Source term used in the continuity equation

Symbols	Description
T_w	Temperature at the wall
T_b	Temperature in the bulk
t	Time
u	Velocity
x_i	Mole fraction
Δz	The length of the segment between positions j and $j+1$ in the sublimer and/or desublimer

Description of Greek letters

Greek letter	Description
α-ZrF_4	Tetragonal ZrF_4
β-ZrF_4	Monoclinic ZrF_4
β	Gas expansion coefficient
γ_i	Activity coefficient
ϵ	Molecular interaction
μ	Dynamic viscosity
ρ	Density
ρ_B	Density of the bulk material
$\sigma_{i,N2}$	Collision diameter of nitrogen with either ZrF_4 or HfF_4
σ_i	Lennard-Jones diameter of the respective spherical molecule
ω_i	Mass fraction
Ω_D	Collision integral

Description of subscripts

Subscript	Description
b	Bulk phase
f	Film
g	Gas phase
i	Represents either ZrF_4 or HfF_4
j	Incremental length in the sublimer and desublimer in the direction of the gas flow
k	Incremental length indicator for the pre-heating section of the nitrogen
s	Sublimer
t	Time
w	Wall

Chapter 1: Introduction

Zirconium (Zr) ores typically contain between 1 % and 3 % hafnium (Hf) (Xu *et al.,* 2012). The use of Zr metal in the nuclear industry requires an Hf content of <100 ppm, owing to its high neutron cross-section (Brown & Healy, 1978). Therefore the separation step is key in the preparation of nuclear-grade Zr metal, which is considered to be very difficult due to the various similarities of their chemical properties (Smolik *et al.*, 2009). Generally the preparation of Hf-free Zr relies on the traditional wet routes, for example solvent extraction systems. In contrast to the traditional aqueous chloride systems, the dry processes have the advantage of producing much less hazardous chemical waste.

The New Metals Development Network (NMDN) of the Advanced Materials Initiative (AMI) was created by the Department of Science and Technology (DST) in 2006, with the mandate to develop new processes for beneficiation relating to the elements Zr, Hf, Ta and Nb. The current work attempts to develop a process involving the beneficiation of the mineral zircon ($ZrSiO_4$) to produce nuclear-grade Zr metal. The zircon contains Hf as an impurity. To indicate this, the formula $Zr(Hf)SiO_4$ is used throughout this text. Zr and Hf occur in the zircon crystal structure in identical crystallographic positions.

The proposed Zr metal recovery process involves the plasma dissociation of the $Zr(Hf)SiO_4$,which results in a much higher chemical reactivity. Here the zircon particles condense upon cooling as microcrystals of $Zr(Hf)O_2$ embedded in the amorphous silica matrix, which is referred to as plasma-dissociated zircon (PDZ, i.e. $Zr(Hf)O_2{\cdot}SiO_2$). The PDZ is then desilicated (DPDZ or $Zr(Hf)O_2$) and fluorinated with ammonium bifluoride (ABF) to produce $Zr(Hf)F_4$. Separation of Hf from the Zr can be achieved either by the tetrafluoride or tetrachloride form, although the latter will require an additional chlorination step. The next step is the plasma reduction of the tetrahalide to the metal and finally purification of the metal powder in a high-temperature vacuum furnace (Nel *et al.*, 2013; Retief *et al.*, 2011). The nomenclature $Zr(Hf)F_4$ defines a ZrF_4 crystal structure in which 1 % to 3 % of the Hf is substituted for Zr. ZrF_4 and HfF_4 behave differently according to temperature in the vapour phase, i.e. due to the difference in vapour pressures. This implies that HfF_4 is thermodynamically more stable than ZrF_4 at a specific temperature. It is therefore assumed that ZrF_4 will sublime separately from the HfF_4 due to the differences in the thermodynamic stability of the two compounds.

Sublimation, together with distillation techniques, is considered the most convenient and effective method for removing metal fluoride impurities from ZrF_4. Sublimation and distillation processes provide dry methods with no liquid waste. They may require fewer steps, which is less labour intensive and requires lower capital costs compared to other commercial technologies. The major drawbacks are the high energy requirements to obtain the high separation temperatures, resulting in expensive construction materials. Purification by sublimation and subsequent crystallisation is normally more effective than distillation because no liquid is present from which impurities have to be extracted from the vapours in the cooling chamber. There is also no significant extent of dissolution of gaseous impurities by the crystallised product as compared to the liquid. The partial vapour pressures of the impurities are also insignificant and therefore do not permit the formation of a new independent liquid or solid phase (Robertson, 1932).

In this process, separation of the ZrF_4 and HfF_4 is achieved using sublimation followed by desublimation. The separation involves the sublimation of the tetrafluorides in an inert atmosphere under controlled parameters. The sublimed mass (700 °C to 800 °C) diffuses into nitrogen which is then allowed to flow across a water-cooled desublimer (annulus) with the aim of desubliming the one metal fluoride in preference to the other. This implies that separation is achieved in both the sublimer and desublimer, due to differences in both the sublimation and desublimation rates. Separation is further achieved along the length of the desublimer. The sublimation rates depend on the vapour pressures at the respective temperatures as well as the concentration and/or partial pressure differences. The aim is for the sublimer residue to be Hf-rich and the desublimer content Zr-rich. The Zr/Hf content is determined by means of ICP-OES analysis.

A sublimation and desublimation model was developed to predict the sublimation and desublimation rates of both ZrF_4 and HfF_4 in the tetrafluoride form in an inert gas. These rates were then used to determine the Zr/Hf mole ratios to those obtained experimentally. The aim is to provide experimental conditions, i.e. sublimation time, temperature and position on the desublimer, which provide optimal separation conditions. These conditions must, however, be compared to the operating cost, as this will be higher at a higher temperature and for longer sublimation runs.

Chapter 2: Literature

2.1 Zirconium and hafnium

Zirconium was discovered in 1789 by Martin Heinrich Klaproth, in Berlin, Germany. The name zirconium originates from the Arabic word "*zargun*" meaning "*gold colour*", which describes the colour of the gemstone now known as zircon. It is the eleventh most abundant element in the earth's crust, which amounts to approximately 0.028 % (Benedict *et al.*, 1981). Zr and Hf occur together in nature and can be found in minerals such as zircon and Baddeleyite, with zircon being the most commercially available source (Banda *et al.*, 2013). These ores typically contain between 1 % to 3 % Hf (Xu *et al.*, 2012).

There is currently a worldwide production (the largest producers being Australia, South Africa and the US) of approximately 1 million metric tons of zircon per year, of which 5 % is used for the production of Zr metal and alloys (Konings *et al.*, 2012), while the rest ends up in the refractory industry or ceramics.

Hafnium was discovered in 1923 by Hevesy and Coster (Hevesy, 1925; Hansen *et al.,* 1950; Kragh & Robertson, 1979). Separation of these two elements then became a concern. Soon after the discovery, the mineral was fused with acidic potassium fluoride and the melt was extracted with hot water containing HF and the potassium Zr fluoride was re-crystallized from a water solution. Separation of the two elements was achieved after several re-crystallisations steps.

Another attempt at separation was made shortly thereafter by van Arkel and De Boer in 1924, who were able to demonstrate considerable separation between the two elements by means of fractional distillation. Gruen and Katz continued this research and reported an Hf reduction from 2.5 % to 0.2 % (Gruen & Katz, 1949).

Currently the key producers of low-hafnium zirconium for the nuclear industry are France (AREVA), the US (Westinghouse), Russia (Rusatom, TVEL), Global Nuclear Fuel (the US and Japan) and South Korea (KEPCO Nuclear Fuel) (Ux Consulting, 2013).

The use of Zr in the nuclear industry requires an Hf content of less than 100 ppm(Smolik *et al.*, 2009). Recent articles reported Zr metal specifications with Hf values of less than 50 ppm (Banda *et al.*, 2013; Waseda & Isshiki, 2001). Separation of these two elements is extremely difficult due to their

chemical similarities in both their metallic and compound states. These similarities are greater than any other homologous elements in the periodic table (Yang *et al.*, 2002). Zr and Hf have similar atomic radii, similar configurations of valence electrons (Favre-Réguillon *et al.*, 2007) along with various other chemical and physical similarities. Furthermore, Zr and Hf have a very high reactivity towards oxygen, nitrogen, carbon and hydrogen, which emphasizes the extreme difficulty of producing Hf-free Zr of high purity (Waseda & Isshiki, 2001). Even so, by the 1960s, Hf-free Zr had already been produced by several US companies (Benedict *et al.*, 1981).

The Zr grade used in alloy production, which is used for the construction of nuclear fuel elements and other reactor core components, has a direct effect on the efficiency of the reactor core and therefore the cost of producing nuclear power (Yang *et al.*, 2002).The use of Zr is possible due to the low thermal neutron capture cross-section of Zr (0.18 barns), whereas that of Hf is 640 times higher (Yang *et al.*, 2002). The key to preparing nuclear grade Zr therefore lies in the separation technology of Zr and Hf (Xu *et al.*, 2012).

2.2 Processes for the separation of Zr and Hf

Metals can be separated by taking advantage of occurrences where there are substantial differences in water solubilities, organic solvents, fused salts or liquid metals. These occurrences are, however, very rare for Zr and Hf (Benedict *et al.*, 1981).

One of the major processes used for the separation of Zr and Hf is solvent extraction. Solvent extraction is, however, a complex and expensive process to use for the separation of Zr and Hf (Begovich & Sisson, 1983). Additionally, the solvent extraction process using methyl isobutyl ketone (MIBK) as the extractant has several disadvantages and several attempts at direct separation of the two metals in their chloride form have been made. These include fractional sublimation, distillation of the chlorides under pressure and extractive distillation using several solvents. Up to 1984, none of these methods had been developed into industrial processes due to the many technological problems that could not be reliably resolved (Moulin *et al.*, 1984).

The three technologies currently used in industry for the separation of Zr and Hf are multiple crystallisation of potassium Zr/Hf fluoride ($K_2Zr(Hf)F_6$), solvent extraction using MIBK or tributyl phosphate (TBP) and extractive distillation with a potassium chloride–aluminium chloride mixture ($KCl\text{-}AlCl_3$) – solvent extraction and distillation being the two major processes (Barberis, 2008; Favre-Réguillon *et al.*, 2007; Konings *et al.*, 2012). Poriel *et al.* summarized some of the established technologies (Figure 2-1) for the separation of Zr and Hf (Poriel *et al.*, 2006).

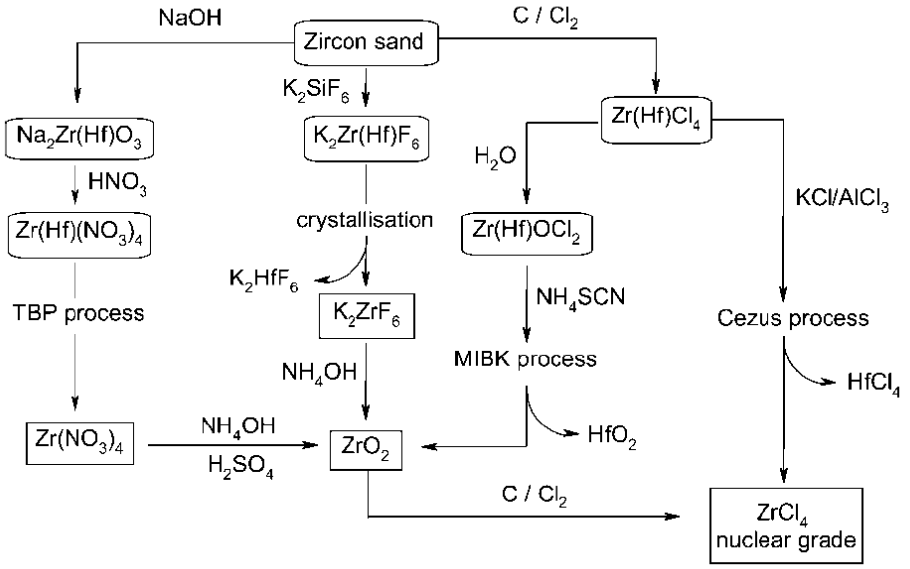

Figure 2-1: Established technologies for the separation of Zr and Hf

These processes for the separation of Zr and Hf, along with others listed in the literature, are discussed in more detail in the following sections.

2.2.1 Fractional crystallisation

Some of the most successful methods of fractional crystallisation are those using phosphates, potassium, ammonium double fluorides and ferrocyanides (Hansen *et al.*, 1950).

Others include the crystallisation of ammonium or potassium zirconium oxalate, crystallisation of zirconium oxychloride with basic chlorides or with organic acids and zirconium sulphate with hydrogen peroxide, to name but a few (Hevesy, 1925).

2.2.2 Fractional crystallisation of the double fluorides

The original method used for separation of Hf from Zr was the fractional crystallisation of the double potassium fluorides, in which multiple recrystallisations are necessary since these salts form solid solutions and have a solubility ratio close to unity (Benedict *et al.*, 1981). Both hexafluorides and heptafluorides can be obtained by the addition of potassium or ammonium fluoride to ZrF_4. The solubilities of the heptafluorides of Hf and Zr are practically the same, whereas the solubilities of the hexafluorides are such that separation of the two elements is possible (Hevesy, 1925). The ammonium hexafluorides of Zr and Hf have higher solubilities, whereas the corresponding potassium hexafluorides have larger differences between the solubilities of the Zr and Hf compounds. The

solubility of the Hf compound is greater than that of the Zr compound, resulting in the crystallisation of the Zr compounds in preference to the Hf compounds (Branken, 2009; Hevesy, 1925).

In 1955 it was found that 10 recrystallisation steps are required to reduce the Hf content from 2 % to 0.1 %. Optimisation of the operation temperatures and solubilities of a similar process was done in 1956. It was found that up to 18 recrystallisation steps were necessary to reduce the Hf content to 0.003 %, with a Zr yield of 80 % (Benedict *et al.* 1981).

In 2010, Branken *et al.* studied the influence of potassium fluoride (KF) and hydrogen fluoride (HF) on the selectivity of Zr and Hf separation by fractional crystallisation of $K_2Zr(Hf)F_6$. Their work indicated that crystallisation from KF solutions leads to the formation of $K_3Zr(Hf)F_7$ with an increasing KF concentration, which leads to a decrease in the selectivity. This is in good agreement with the work done by Hevesy (Hevesy, 1925) who showed that the heptafluorides of ammonium and potassium are practically insoluble. Branken *et al.* showed that the addition of HF to the crystallisation solution suppressed the formation of the $K_3Zr(Hf)F_7$. Although selectivities obtained were still very low, they were much higher than the crystallisation selectivities from solutions of high KF concentrations without HF and also from water only solutions (Branken & Lachmann, 2010). The addition of HF to the KF solution was also suggested by Coster and Hevesy (Coster & Hevesy, 1927).

Fractional crystallisation of the phosphates

Appreciable differences exist between the solubilities of the phosphates of Zr and Hf, with the Hf phosphate being less soluble in strong mineral acids (Hevesy & Kimura, 1925). The phosphate precipitate can be dissolved in HF and allowed to crystallize, resulting in a compound containing Zr, phosphorus and fluorine (Hevesy, 1925). According to Hevesy, preference is to be given to the crystallisation of the phosphates among all other crystallisation methods. One possible disadvantage to this process is that the phosphate compounds formed are not readily converted to other compounds (Hansen *et al.,* 1950).

Recent work on fractional crystallisation

A patent was recently issued which claims to remove traces of Zr from Hf compounds by making particular use of Zr containing Hf tetrakis (dimethylamide). The mixtures are melted and held at a set temperature thereby obtaining two phases, one crystalline and one liquid, with the liquid phase containing the lowest Zr concentration (Reuter *et al.,* 2009).

2.2.3 Solvent extraction

Traditional liquid-liquid extraction

Extraction is the process of drawing a compound out of a mixture by means of a solvent. Liquid-liquid extraction, also known as solvent extraction and partitioning, is more specific. It is a separation method in which compounds are separated based on their relative solubilities in two different solvents.

A limited number of extractants and extraction systems have been used in the separation of Zr and Hf for selectively extracting either Zr or Hf (Deorkar & Khopkar, 1991; Xu *et al.,* 2012).

The major solvent extraction process used for the purification and removal of Hf is the MIBK-thiocyanate (SCN) process (Konings *et al.,* 2012). Other processes include TBP, CYANEX and amine-based extractants.

MIBK-SCN

In a study noted around 1957 (Benedict *et al.,* 1981), the Oak Ridge National Laboratory concluded that solvent extraction of SCN was the best commercial method, in which an HCl solution of the oxychloride as the aqueous phase was recommended, with a mixture of MIBK and thiocyanic acid (HSCN) as an organic solvent. In this system an Hf-Zr separation factor of 5 is obtained. Operating plants with a capacity of 400 $kg \cdot h^{-1}$ have been reported (Benedict *et al.,* 1981).

In the solvent extraction system of the US Bureau of Mines Plant (Benedict *et al.*, 1981), commercial grade $Zr(Hf)Cl_4$ was dissolved in water together with ammonium thiocyanate (NH_4SCN) and ammonium hydroxide (NH_4OH). Zr and Hf form SCN complexes ($(Zr/Hf)O(SCN)_2$) which can be extracted with the use of HSCN and MIBK in a counter-current solvent extraction system, preferentially extracting the Hf into the organic phase. Sulphuric acid (H_2SO_4) was added to the organic phase for stripping of the Hf. A hydrochloric acid (HCl) scrub solution was used to transfer the remaining Zr from the MIBK stream back into the aqueous phase, after which zirconium hydroxide ($Zr(OH)_4$) was precipitated from the aqueous product stream containing 0.004 % Hf.

Disadvantages of the widely used MIBK-thiocyanic solvent extraction process include(Brown & Wain, 1978; Da Silva & Distin, 1998):

- the high aqueous solubility of the MIBK
- the low flash point of the MIBK

- the formation of gaseous contaminants such as hydrogen sulphide (H_2S), hydrogen cyanide (HCN) and mercaptans from the decomposition of the SCN complexes in HCl medium
- the aqueous raffinate containing SCN, which could have disposal implications.

TBP

In contrast to the MIBK process, when using TBP as the extractant, Hf is concentrated in the aqueous phase and Zr in the organic phase.

The feed stream to the TBP process can be obtained by the reaction of zircon sand with molten caustic soda (also known as sodium hydroxide or NaOH). This process is also referred to as caustic fusion. The product of this process is washed with cold water and centrifuged to give hydrated Zr oxide. Cox *et al.* found that initial dissolution of the washed product in HCl or sulphuric acid (H_2SO_4) followed by secondary dissolution in nitric acid (HNO_3) resulted in a product of the required specification. A solution of TBP with n-heptane and HNO_3 is used for the extraction of Zr from the feed stream (Cox *et al.* 1958; Stephens, 1984).

The French Atomic Energy Commission (Benedict *et al.*, 1981) fractionally extracted Zr from Hf with an organic phase consisting of TBP and kerosene and an aqueous phase consisting of $Zr(NO_3)_4$ and $Hf(NO_3)_4$ in a mixture of HNO_3 and $NaNO_3$. A separation factor of 10 with a plant capacity of 24 kg Zr per day containing less than 0.02 % Hf was obtained.

The work by Cox *et al.* indicated that the use of only HNO_3 as a salting agent (i.e. no $NaNO_3$) is more preferable for use in a commercial process. Zr and Hf nitrates were separated by extracting them with TBP diluted with n-heptane, which shortens the time required for separation of the phases. Separation factors of up to 36 were reported and the Hf content in the Zr was reduced to less than 100 ppm (Cox *et al.*, 1958). The information gathered in the pilot plant provided the design data for separation on a commercial scale (Benedict *et al.,* 1981). Disadvantages (Branken, 2009; Brown and Wain, 1978) were:

- the requirement for high TBP concentrations at high acidities
- Hf purification from Zr is difficult from a practical standpoint
- high consumption rates of chemicals
- constraints regarding low metal concentrations in both phases.

CYANEX as an extractant

Several types of CYANEX extractants have been reported in the literature. These include CYANEX 272, 921, 923 and 925, of which the latter two have shown better performance. However, the disadvantages to the two extractants are that CYANEX 925 has a high cost compared to conventional TBP and CYANEX 923 on its own causes third phase formation at Zr concentrations exceeding 8 g/L (Nayl *et al.,* 2009; Taghizadeh *et al.,* 2011).

CYANEX 923

In 2011, the separation of Zr and Hf was studied using a mixture of TBP and CYANEX 923 (Taghizadeh *et al.,* 2011). The process of Zr and Hf separation was successful, without the risk of third phase formation. Higher metal extractions were obtained with lower acid concentrations when compared to the conventional TBP/HNO_3 processes. This process has the advantage of lower chemical consumption rates as well as lower disposal costs. Separation factors as high as 186 were obtained.

CYANEX 272

Taghizadeh *et al.* determined optimum process conditions for the extraction and separation of Zr and Hf. The extractants studied were TBP, D2EHPA and CYANEX 272. They found the optimum for selective extraction of Zr to be 80 % when using HNO_3 and CYANEX 272 as extractant. The same was true for the separation of Zr and Hf with a separation factor of 34 (Taghizadeh *et al.,* 2008). They continued to study the stoichiometric relation of this extraction process in 2009 (Taghizadeh *et al.,* 2009).

In 2013, Banda *et al.* selectively extracted Zr over Hf from H_2SO_4 solutions using D2EHPA or CYANEX 272 or a mixture thereof with LIX 63. D2EHPA gave better separation than CYANEX 272 with separation factors of approximately 30, whereas mixtures of D2EHPA or CYANEX 272 with LIX 63 did not indicate sufficient selectivity towards extracting Hf over Zr (Banda *et al.,* 2013).

CYANEX 921

Nayl *et al.* studied the extraction of Zr and Hf from nitrate mediums by using CYANEX 921, CYANEX 923 or CYANEX 925 in kerosene. At optimum conditions, separation factors of 17, 21.4 and 40.7 were obtained for the respective extractants, with reasonably fast extraction rates (Nayl *et al.,* 2009).

Amine extraction

Takahashi (Takahashi *et al.,* 1984) separated Zr from Hf in a counter-current mixer-settler by means of an anionic exchange mechanism and replacing the MIBK with a high-molecular alkyl amine. The

organic phase was a mixture of tri-n-octyl amine, tridecanol, tri-n-paraffin (kerosene) and sulphuric acid. The aqueous phase was prepared by digesting sodium zirconate in sulphuric acid to produce Zr and Hf oxysulphates. Here the Hf content is concentrated in the organic phase while the Zr is concentrated in the aqueous phase, with separation factors of up to 20. Pure $Zr(OH)_4$ is precipitated by neutralizing the aqueous solution with NaOH. One advantage of this process is that most trace element impurities are also separated from Zr, except for uranium (U), which can be removed by adding a pre-extraction step to the process.

Poriel *et al.* studied the extraction in a solution of HCl and Aliquat 336 as the extractant (Poriel *et al.,* 2006) to preferentially extract Zr by means of an anionic exchange mechanism. Their work indicated that separation is possible with separation factors of up to 14, provided that the feed solution is a mixture of $Zr(Hf)Cl_4$ in concentrated HCl. This is necessary to maintain the extraction equilibrium since it inhibits the formation of polynuclear hydroxy-bridged compounds.

Van der Westhuizen also employed separation with amine extractants Alamine 336 and Aliquat 336, with recovery of the Zr species in the organic phase. Extraction was tested on both fluoride and chloride-based compounds ($(K_2Zr(Hf)F_6)$ and $Zr(Hf)Cl_4$ respectively) and only the chloride compounds provided successful separation (Van der Westhuizen, 2009).

Van der Westhuizen highlighted the following advantages of using amines as extractants (Van der Westhuizen, 2009):

- they reduce cost
- they are more environmentally and user friendly
- no requirement for stripping chemicals for the recovery of the Zr solutes
- high solute loading capacity relative to chemical consumption
- high selectivity towards Zr.

The major disadvantage of the process discussed above is the requirement of high acidities in the aqueous feed solution, which poses some economic and engineering problems.

In 2012, Banda *et al.* (2012) separated Zr from Hf in a HCl solution using amine-based extractants. They found that Alamine 300 and Alamine 336 produced better separation than other amine-based extractants and Alamine 336 gave the highest separation factor. These were based on a batch simulation of counter-current extraction, yielding extractions of Zr and Hf of 98.5 % and 12.5 % respectively (Banda *et al.,* 2012).

Other solvent extraction processes for the separation of Zr and Hf

Brown *et al.* investigated the solvent extraction of Zr from Hf in HNO_3 solutions using a new extractant, dibutyl butylphosphonate (DBBP), in Solvesso 150. This process required lower acidities compared to the TBP process and the new extractant did not require the use of a salting agent. In this process the Hf content could be reduced to below nuclear specifications and purification from uranium was also achieved in a 10-stage Croda mixer-settler. Separation coefficients for Zr/Hf ranged from 6 to 42 depending on the acidity and Zr concentrations. Separation factors for Zr/U of 40 to 150 were obtained and depended on the acidity of the HNO_3 solution (Brown & Healy, 1978).

XU *et al.* optimized a solvent extraction system for the separation of Zr and Hf in an HSCN medium using a mixture of diisobutyl ketone (DIBK) and TBP as the extractant. A separation factor of Hf from Zr of 9.3 was obtained. It was found that the DIBK selectively extracted the minor metal (Hf) from HSCN solutions to meet the high grade specifications, but with lower separation coefficients than that obtained with MIBK. DIBK is preferred to MIBK in industrial applications due to its high flash point, high boiling point and low solubility, whereas MIBK has a high water solubility and it burns and volatilizes easily (Xu *et al.,* 2012).

The research of Da Silva and Distin also describes how the problems with MIBK could be overcome by using organophosphorous extractants (Da Silva & Distin, 1998).

Other extractants used for the extraction of Zr and Hf from HCl solutions include dicyclohexyl-18-crown-6 in dichloromethane (Deorkar & Khopkar, 1991) and TODGA for extraction from HNO_3 solutions (Saleh, 2012).

The above are only a few of the numerous methods reported in the literature for the separation of Zr and Hf using solvent extraction.

Membrane-based solvent extraction and pertraction

Separation with solvent extraction can be achieved in multi-stages of two separate steps (extraction and stripping) with the use of an extractant. Solvent extraction is regarded as a promising method for the separation of metallic elements (Banda *et al.,* 2013), but it has the disadvantages of emulsification, flooding and loading limits, phase disengagement and large solvent inventory (Yang *et al.,* 2002).

The use of a liquid membrane (LM) offers high selectivity in a single operation since it combines both extraction and stripping. A liquid membrane is formed if two miscible fluids are separated by a third immiscible liquid that enables mass transport between the fluids. The idea of using a liquid membrane for separations in three-phase systems is quite new and its use has been very limited for the difficult Zr and Hf separation (Štefan Schlosser, 2009; Yang *et al.,* 2002).

Supported liquid membranes (SLM) using microporous membranes feature simultaneous extraction and stripping, therefore equilibrium limitations and ratios of aqueous/organic ratios are not applicable. This thin microporous membrane is impregnated with an organic solvent which assists in separating the feed and stripping solutions and eliminates the disadvantages associated with solvent extraction (Yang *et al.,* 2002).

In 2002, Yang *et al.* studied SLMs with hollow fibres (polypropylene with 600 µm inner diameter and 0.2 µm pore diameter) as substrates and TNOA or Aliquat 336 as extracting agents. This process has very high efficiencies with a high surface-to-volume ratio and low organic extractant inventory, but for various economic and technical reasons, it was found that this process is only useful for laboratory and pilot scale production units (Yang *et al.,* 2002).

Pertraction, however, has the advantage of increased stability compared to SLMs, but it has the disadvantage of requiring two membranes, one for the organic phase and another for the stripping of the metal back into the aqueous phase (Van der Westhuizen *et al.,* 2012). This problem can be overcome with emulsified pertraction. Van der Westhuizen *et al.* registered a patent in 2012 which claimed a method to separate Zr and Hf by using membrane-based solvent extraction and in particular pertraction and emulsified pertraction (Van der Westhuizen *et al.,* 2012).

2.2.4 Ion exchange

Several ion exchange processes for the separation of Zr and Hf can be found in the literature. This technology has been extensively applied in analytical separations, which have been shown to be much more effective than conventional solvent extraction techniques (Yang *et al.,* 1999). Different anion and cation ion exchangers are employed, with the most often used being the strong-base anion exchange resins to adsorb Zr in preference to Hf and cation exchange resins, where Hf is preferentially adsorbed (Smolik *et al.,* 2009).

One of the most often studied cation exchange resins is Dowex 50 with the use of several different acid mediums (Street & Seaborg, 1948; Benedict *et al.,* 1954; Qureshi & Husain, 1971; Hurst, 1983; Begovich & Sisson, 1983).

Kraus and Moore studied the separation of Zr and Hf with a Dowex-1 anion exchanger with a mixture of HCl and HF as effluent (Kraus & Moore, 1949). Similar work was done by Huffman and Lilly but with the use of an Amberlite IRA-400 in place of the Dowex-1 (Huffman & Lilly, 1951).

Byers *et al.* registered two patents on the separation using continuous ion exchange chromatography in sulphate solutions with an anionic exchange resin (Byers *et al.,* 1997) and in chloride solutions with either anionic or cationic resins (Byers *et al.*, 1998). No mention is made of the type of resin. These processes promise very good efficiencies as well as separation factors.

Yang *et al.* (1999) studied the separation using TNOA and/or Aliquat 336 on a styrene/divinylbenzene copolymer resin and HCl. Aliquat 336 showed the best selectivity towards Zr and Hf separation, with separation factors up to 164.

More recent investigations of the separation of Zr and Hf with the use of ion exchange with commercially available resins have been reported. These include the Amberjet 4200 Cl anion exchange resin (Favre-Réguillon *et al.*, 2007) and the Diphonix® resin used in chelating cation exchangers (Smolik *et al.*, 2009).

2.2.5 Reduction processes

Newnham separated Zr and Hf by preferential reduction of their tetrachlorides. This was achieved by heating the crude tetrachloride with Zr powder to thereby reduce the tetrachloride to the non-volatile trichloride, without reducing the Hf tetrachloride. After sublimation separation, the Hf content in the residual Zr trichloride was reduced to less than 0.05 % (Newnham, 1956).

In the “Megy Process” a very high separation factor is obtained if a mixture of Na_2ZrF_6 and Na_2HfF_6 is reduced by aluminium dissolved in liquid zinc. This partial reduction reaction occurs in a graphite-lined container at 900 °C. Two immiscible salt phases are formed, a light phase rich in Hf and a heavy phase rich in Zr, which can then be separated from each other. Reducing the Hf content to below 0.01 % required contacting of the Zr-rich phase with a liquid mixture consisting of ZnF_2 and NaF to again produce a mixture of Na_2ZrF_6 and Na_2HfF_6 , making the production of reactor-grade Zr possible in as few as two salt-metal contacting stages (Megy, 1978; Benedict *et al.*, 1981).

2.2.6 Extractive distillation in molten salts

Soon after the discovery of the element Hf, de Boer wrote a paper in which he discussed the preparation of pure Zr compounds by means of double compounds with phosphorus chlorides, in which $(ZrCl_4)_2 \cdot PCl_5$ and $(ZrCl_4)_2 \cdot POCl_3$ are formed which melt and provide a means for purification of impurities after a single distillation of the salts (excluding $HfCl_4$ and double compounds). Purification from Hf was achieved with further fractional distillations (Boer, 1927).

In the majority of cases the extractive distillation process used is a counter-current vapour phase distillation column whereby $Zr(Hf)Cl_4$ vapours are contacted with a $KCl\text{-}AlCl_3$ solvent at 350 °C and at atmospheric pressure (the CEZUS process). The solvent (Zr enriched) is passed through a stripping column where nitrogen gas is passed through the solvent for the recovery of $ZrCl_4$. Pure $HfCl_4$ can be produced from the vapour phase (Hf enriched) with a few alterations to the process (Branken, 2009; Konings *et al.*, 2012; Moulin *et al.*, 1984; Niselson *et al.*, 2009).

This process was patented in 1977 (Besson *et al.*, 1977), in which the authors claimed a continuous process for recovering $ZrCl_4$ with less than 200 ppm Hf with a molten solvent selected from the group consisting of an alkali metal chloroaluminate, an alkali metal chloroferrate and mixtures thereof. Besson *et al.* specified the pressure as atmospheric pressure and the alkali metal as potassium. This patent was based on information gained from pilot plant operation. A full-scale production plant was built which corresponded to a Zr sponge production of 1 600 tons per year (Moulin *et al.*, 1984). This process does, however, require an additional sublimation step for the removal of the remaining impurities as with the solvent extraction system (Moulin *et al.,* 1984).

In 2010, Delons *et al.* registered a patent with many similarities to the process patented by Besson *et al.,* with added claims to the process of recovering pure Hf. Hf-enriched fractions containing as little as 20 molar ppm Zr are reported (Delons *et al.,* 2010).

Ishizuka registered a patent for a process to refine $ZrCl_4$ containing $HfCl_4$. The refining was done by repeatedly subliming and condensing $Zr(Hf)Cl_4$ between a pair of coaxially disposed cylinders, one being at a higher temperature than the other. This process is also referred to as fractional distillation or gradient sublimation. The condensed phase collected at the low temperature zone was dissolved in an alkali metal chloride, an alkaline earth metal chloride or a double salt thereof. Overall separation factors of 10 and 20 were reported and the final $ZrCl_4$ proved to contain as little as 0.005 % Hf (Ishizuka, 1974).

McLaughlin and Stolz registered a patent in 1988 to separate Zr and Hf tetrachloride with a molten zinc chloride lead chloride solvent, claiming fewer corrosion problems and that the stripping temperature (360 °C to 450 °C) is lower than that of prior Hf-Zr chloride extractive distillation processes (McLaughlin & Stoltz, 1988). In 1989 they registered a patent in which they provide improvements for extractive distillation separation of Zr or Hf, whereby mixtures of fused alkali metal or alkali metal and alkaline earth chlorides are used as the solvent (McLaughlin & Stoltz, 1989).

Energy requirements for a distillation process are comparable to those of a solvent extraction process, since the energy requirement for the higher temperature needed in the distillation process more or less equals the additional energy required for rechlorination, which is required in the MIBK process (Branken, 2009).

Although sublimation purification of ZrF_4 is regarded as the most convenient and rapid method, distillation of ZrF_4 from a mixture of 70 % ZrF_4 and 30 % barium fluoride (BaF_2) at 827 °C gives considerably better purification results, especially as regards Fe content. Separation in molten salts or extractive distillation in molten salts is one of the most effective processes currently used for Zr purification (Delons *et al.,* 2010).

Distillation of fused salts to remove impurities (excluding Hf)

MacFarlane *et al.* studied the purification of ZrF_4 by distillation of ZrF_4-BaF_2 melts and reported the method to be superior to the sublimation method. Operation temperatures of up to 875 °C are required to achieve a distillation rate of 15 $g \cdot h^{-1}$. The Fe, Ni and Cu impurities were reduced to a factor of 8 to 10 compared to a factor of 2 obtained through sublimation (MacFarlane *et al.,* 2002).

2.2.7 High-pressure vapour-liquid distillation

High-pressure vapour-liquid distillation has also been employed for the separation of Zr and Hf in the tetrachloride form, but these operations require pressures of up to 60 atm which require the use of expensive equipment. Continuous operation is also difficult with regard to the solid feed stream. Furthermore, this process requires stringent temperature control due to the narrow range of the operating temperature which is between the triple point (437 °C) and the critical point (505 °C) (Skaggs *et al.,* 1984).

2.3 Sublimation as a purification and separation process

Sublimation is an endothermic process whereby a solid is directly converted into a gas or vapour (Green, 2000) and desublimation is the process whereby a vapour state is directly converted to the solid state without passing through a liquid state. It is widely employed in purification processes and is used to separate volatile from non-volatile components (Green, 2000; Kodde & Mewes, 1995). For sublimation to occur, the vapour pressure of the subliming components must be greater than its partial pressure in the surrounding gas that is in contact with the solid (Hanson & Corder, 2004). In order to encourage sublimation, the total system needs to be controlled (usually by vacuum), or the partial pressure needs to be reduced (usually by introducing a high-vapour pressure gas) (Raouzeos & Schwenk, 1996).

In order to obtain satisfactory separation and/or purification results, sufficient differences should exist between the vapour pressures of the substances to be separated and if they do not, satisfactory separation may in some instances be unobtainable (Jacque & Dumez, 1960).

Raouzeos and Schwenk specified three types of sublimation process: vacuum sublimation, sublimation with a sweep gas and fractional sublimation (Raouzeos & Schwenk, 1996). Gradient sublimation techniques are also used and are among the most useful and common means of purification. In this technique, separation is achieved in a long tube with a constant temperature gradient so that the target material deposits on the wall of the heated tube, separating it from the more volatile and less non-volatile impurities (Jeon *et al.,* 2008).

Almost no information was available on the sublimation purification of ZrF_4 from impurities up to the early 1970s (Solov'ev & Malyutina, 2002a). By the 1990s, sublimation was regarded as the most wide-spread, convenient and rapid method for the purification of ZrF_4 (Murskii *et al.,* 1989; Robinson, 1986).

The lower separation factors obtained through sublimation compared to the more efficient distillation process can be explained by the following (Murskii *et al.,* 1989):

- the non-equilibrium nature of the ZrF_4 sublimation process
- the interaction of the impurities with the purified substance
- the transfer of impurities as fluidized particles.

2.3.1 Sublimation for the separation of Zr from Hf

The separation of Zr from Hf is mostly studied in the tetrahalide form, mostly fluorides, chlorides and in some instances bromides.

Vacuum sublimation for the separation of Zr and Hf

The separation of Zr and Hf by means of vacuum sublimation consists of multiple sublimation steps in order to achieve the required degree of separation. Monnahela *et al.* studied vacuum sublimation in a system operated at temperatures of around 550 °C and pressures of 10^{-5} mbar. According to the authors, the presence of oxyfluorides resulted in much lower recoveries of product although they found better Hf reduction in samples with higher amounts of oxyfluorides and suggested that this might be due to a "gettering" activity. The formation of oxyfluorides during the manufacture of the ZrF_4 is detrimental to the recovery of the sublimates, but it is a requirement for purification since it can drastically reduce the number of steps required to achieve reactor-grade ZrF_4. Theoretical calculations were based on the percentage recoveries per run and the starting mass required to obtain 2 g of reactor- grade ZrF_4. It was established that, with an average reduction in Hf of 40 % per sublimation step and 80 % recovery, a multi-sublimation process consisting of 10 steps is required. This 10-step process therefore requires a starting mass of 20 g ZrF_4 to produce 2 g of reactor-grade ZrF_4 (Monnahela *et al.,* 2013).

Earlier work by Solov'ev and Malyutina established that the addition of difluorides, especially those of the iron subgroup, act as good sorbents for use in the purification of ZrF_4 from HfF_4 by means of multiple sublimations. It is hypothesized that the HfF_4 forms compounds of lower volatility, thereby increasing the separation between the ZrF_4 and HfF_4. The authors obtained ZrF_4 with an Hf content of 0.05 % with the addition of NiF_2 as a sorbent (or "getter") with eight sublimation cycles and a degree of sublimation of 60 % to 80 %. Temperatures in the range of 700 °C to 850 °C and pressures of 3 Pa to 5 Pa are required for this purpose (Solov'ev & Malyutina, 2002b).

It can therefore be assumed that vacuum sublimation requires additional compounds to provide a "gettering" activity in order to reduce the number of steps required to achieve reactor-grade ZrF_4.

Sublimation in an inert atmosphere for the separation of Zr and Hf

Sublimation techniques described in a review done in 1984 on the production of Hf-"free" Zr include thin film sublimation as another technique used to separate $ZrCl_4$ and $HfCl_4$ in a counter-current sublimation column. Mechanical transfer of solids down the column was, however, required since

the solids tends to adhere to the column surfaces. The technique of thin film sublimation was used by Gillot and Goldberger in 1968, where sublimated $Zr(Hf)Cl_4$ was passed through a moving bed of glass beads in the presence of an inert gas. Separation was achieved by differential condensation and re-sublimation on the surface of the beads. This method gave some separation of Zr from Hf on a laboratory scale and it was reported that operation on an industrial scale may be less attractive but that the process definitely offers advantages over other conventional processes (Gillot & Goldberger, 1969; Royston & Alfredson, 1970; Skaggs *et al.,* 1984).

2.3.2 Sublimation purification of ZrF_4 from non-volatile impurities (excluding Hf)

Several sublimation techniques are described in the literature that is being used for the purification of ZrF_4 and/or HfF_4 from other metal fluoride impurities. Some of these techniques are discussed in the following paragraphs.

The details on the equipment for vacuum sublimation and sublimation in an inert atmosphere are given in Sections 2.4.1 and 2.4.3 and information on the rate of sublimation is given in Section 2.5.

Vacuum sublimation

Vacuum sublimation is widely used for the purification of components from other volatile impurities. For the purification of Zr or Hf from metal impurities in the tetrafluoride form, vacuum sublimation is as efficient as sublimation in an inert gas due to the lower operation temperature which increases the separation coefficients. The vacuum heat treatment ensures the removal of volatile impurities from the surface of the tetrafluorides and at a given temperature the rate of sublimation is faster than that of operating in an inert gas (Kotsar *et al.,* 2001).

Vacuum sublimation has the following advantages over sublimation in an inert atmosphere (Kotsar *et al.,* 2001; Raouzeos & Schwenk, 1996):

- Higher efficiency in removing volatile impurities owing to preliminary vacuum heat treatment
- No need for costly materials to sustain high temperatures
- A low partial pressure of the component to be purified is required when sublimating in an inert atmosphere. This suggests high energy consumption due to the repetitive cooling and reheating of the system.

Abate and Wilhelm operated a 2 kg ZrF_4 charge vacuum sublimation purification system for ZrF_4 from Fe, Ni, Cu and C and found that the optimum temperature for sublimation was 800 °C to 850 °C and

that the optimal pressure was 40 Pa with respect to sublimation rate, purity and total time required for sublimation. They also investigated the influence of the fluoride content in the starting material on the sublimation yield (Abate & Wilhelm, 1951).

Yeatts and Rainey employed single and multi-stage vacuum sublimation purification of ZrF_4 with the use of baffles to reduce the Fe, Ni, O_2 and Cr content on a 50 g commercial ZrF_4 sample at temperatures of 750 °C to 800 °C and a system pressure that was never greater than 53 Pa. They studied the influence of the sublimation rate, condensation rate, number of successive sublimations, number and arrangement of baffles as well as the pre-treatment of the starting material in order to fluorinate the oxides to fluorides. They concluded that the O_2 and Fe levels can be reduced to 500 ppm and 100 ppm respectively without great difficulty. Successive sublimations (three steps) and an increase in the number of baffles from 6 to 10 did not reduce the O_2 any further and they concluded that their procedure had reached its maximum purification level (Yeatts & Rainey, 1965).

Kotsar *et al.* (2001) studied the purification of ZrF_4 and HfF_4 from metal impurities in a sublimation barrel operating at pressures of 10^{-2} to 10^{-4} Pa and temperatures as high as 850 °C. They calculated separation coefficients and found them to decrease in the order $CrF_2 > MnF_2 > NiF_2 > CoF_2 > MnF_3 > FeF_2 > AlF_3 > CrF_3 > CuF_2 > FeF_3$. They also optimized the conditions for vacuum sublimation purification of ZrF_4 and HfF_4 and found that the concentration of impurities increased with the product of the evaporation rate per unit area and the degree of evaporation.

Vacuum sublimation at pressures of 3 Pa to 5 Pa and in the temperature range 700 °C to 850 °C has been used as a purification technique that easily purifies ZrF_4. It has been introduced into industry with excellent economic results. The oxygen contents were reduced to 0.02 % and it was reported that it is impossible to produce ZrF_4 with oxygen levels below 0.1 % (Solov'ev & Malyutina, 2002a).

Sublimation in an inert atmosphere

Purification in an inert atmosphere has also been studied. Dai *et al.* proposed a new route to purify ZrF_4 to a high purity whereby $ZrO(NO_3)_2$ replaces the conventional $ZrOCl_2$ used to purify ZrF_4. In their sublimation experiments, they prepared $ZrO(NO_3)_2$ using HF to produce $ZrF_4 \cdot xH_2O$, which was sublimed at 900 °C and 200 Pa in an argon atmosphere. The second zone was operated at a temperature of 500 °C to 700 °C with the aim of collecting the sublimed ZrF_4. Impurity levels of Fe in the final ZrF_4 were 20 ppb to 50 ppb and below 5 ppb for Co, Ni and Cu. No mention is made of the oxygen content in the final purified sample (Dai *et al.,* 1992).

MacFarlane *et al.* sublimated 20 g of ZrF_4 in a dry helium atmosphere at temperatures of 850 °C to 875 °C for 1 hour. A maximum yield of 50 % was obtained after only 3 hours and the Fe, Ni and Cu impurities were reduced by a factor of only 2 (MacFarlane *et al.,* 2002).

Robinson investigated the purification of heavy metal fluoride glass and studied both the sublimation and the distillation of ZrF_4-BaF_2 melts. Results indicated that one sublimation step under dry HF atmosphere reduced the Fe content by a factor of 10 with a 70 % yield (Robinson, 1986). It was mentioned that the limiting value of Fe cannot be reduced to below 1 ppm to 2 ppm, even after several successive iterations.

Sublimation of ZrF_4 in a chlorine flow was also investigated for purification from metal impurities. Sublimation was carried out on a 50 g sample at 800 °C and the cold zone for product collection was kept between 690 °C and 710 °C. Results indicated that sublimation in chlorine gave a product with lower Cu, Al and Fe impurities compared with sublimation in a helium atmosphere (Murskii *et al.,* 1989).

Purification starting from the impure metal and involving sublimation

Other purification techniques for the purification of ZrF_4 from metal impurities have been studied that do not use ZrF_4 as a starting material, but rather obtain high-purity ZrF_4 from an impure metal or other starting material. Folweiler invented a chemical vapour purification process for preparing high-purity metal fluorides. The process involves the reaction of a metal (in excess) with a reactive transport agent to generate a gaseous metal-containing compound. Isolation and fluorination of the gaseous metal-containing compound follow, thereby forming a solid metal fluoride (Folweiler, 1987).

Fujiura *et al.* used a technique of chemical vapour deposition in $ZrBr_4$-HF, in which Zr metal is reacted with Br_2 to produce $ZrBr_4$ and is then fluorinated with HF in an argon atmosphere to produce ZrF_4 of the required purity. This technique is more efficient than the normal sublimation purification and/or solvent extraction processes for the removal of transition metal impurities, since the vapour pressure of $ZrBr_4$ is ten orders of magnitude higher than the vapour pressures of the transition metal bromides at a temperature of 350 °C. Impurity levels indicated Fe contents in ZrF_4 of less than 10 ppb (Fujiura *et al.,* 1989).

Withers *et al.* registered a patent for a process to produce ZrF_4, HfF_4 and AlF_3 of high purity. The process involved incomplete reaction of the metal or metal compound (preferably its oxide, i.e. ZrO_2) with elemental fluorine, followed by high-temperature sublimation of the metal fluoride. It is

suggested that the unreacted metal or metal compound act as a getter with the aim of converting volatile impurities to non-volatile metals or metal compounds. The "gettering" activity thereby acts to selectively sublime the required metal fluoride for recovery from the reaction product. A heating rate of 1 °C·min^{-1} up to 850 °C at 12.5 kPa was reported as the preferred condition for the operation, with an overall ZrF_4 yield of 91 % from the starting ZrO_2. In order to maximize the "getter" activity, i.e. to improve purity, lower conversion of oxide to fluorides is preferred (Withers *et al.,* 1991).

Other purification techniques that involve sublimation

Purification techniques combined with a sublimation process are also reported in the literature. Such techniques are necessary, since sublimation and/or distillation techniques for the removal of Fe have proven to be very difficult due to the high vapour pressure of Fe^{3+}, to name but one drawback. A combined vaporisation-electrolytic separation procedure used in the preparation of pure ZrF_4 and HfF_4 was patented by Pastor and Robinson, who disclosed an efficient single-step process to reduce Fe impurities below 1 ppm (Pastor & Robinson, 1986).

2.4 Apparatus used for sublimation purification of ZrF_4

Some of the sublimation equipment illustrated in the literature for the purification of ZrF_4 is discussed in the following sections. Other apparatus used for sublimation, but not in particular for purification of ZrF_4, is also given in the literature (Gosling & Bowen, 1973; Jang *et al.,* 2005; Jeon *et al.,* 2008; Kawato *et al.,* 2014).

2.4.1 Vacuum sublimation purification (excluding Hf)

The sublimation unit used by Abate and Wilhelm for the sublimation purification of ZrF_4 is shown in Figure 2-2 (Abate & Wilhelm, 1951). The impure ZrF_4 was added in the bottom of the retort and heated to the required temperature. Baffle plates were incorporated to help reduce the mechanical carrying of impurities. The purified ZrF_4 was collected on a condenser. Here (G) is the nickel-lined retort, 5 inches in diameter and 31 inches high, (H) nickel sheet, (I) rubber gasket, (J) copper cooling coils, (K) removable top, (L) cooling coils, (M) 2-inch condenser, (N) thermocouple well, (O) vacuum outlet, (P) charge, (Q) baffles and (R) sublimed ZrF_4.

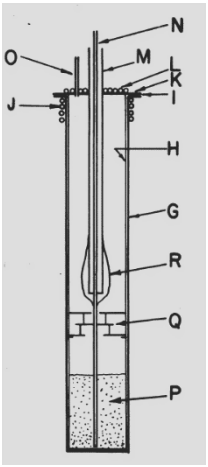

Figure 2-2: Sublimation apparatus used by Abate and Wilhelm for the purification of ZrF_4

The sublimation system used by Yeatts and Rainey (Figure 2-3) is similar to that of Abate and Wilhelm. It consists of a 3-inch nickel pipe, with the impure ZrF_4 loaded into the bottom part of the pipe and covered with a loosely fitting top with nickel sheet baffles and an aperture at the top. Above this section is a hair-pin type water-cooled ¼-inch nickel tube that serves as the condenser (Yeatts & Rainey, 1965).

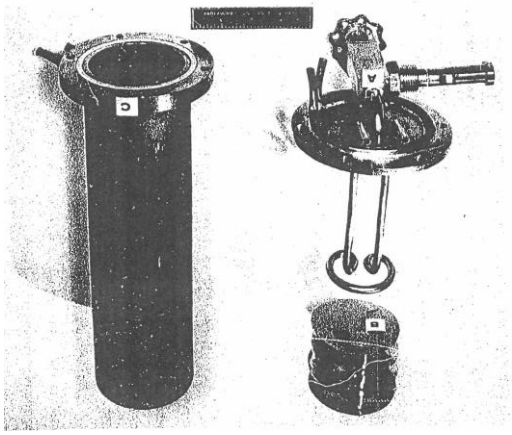

Figure 2-3: Sublimation and desublimation system with baffles for the purification of ZrF_4

Kotsar *et al.* used a metallic nickel sublimer able to take a charge weight of 1 kg to 3 kg. It consists of an evaporating barrel 8.5 cm in diameter, a filter, a vapour delivery line and a condenser (Figure 2-4). The heated zone consists of two temperature zones: the sublimation zone kept at temperatures of 700 °C to 850 °C and the upper zone kept at temperatures of 458 °C to 600 °C. The internal parts of the equipment are labelled as follows: (1) mounting, (2) heater, (3) evaporating barrel, (4) material to be sublimed), (5) shields, (6) thermocouples, (7) filter, (8) current leads, (9) condenser, (10) sublimed ZrF_4, (11) lid and (12) vacuum chamber (Kotsar *et al.,* 2001).

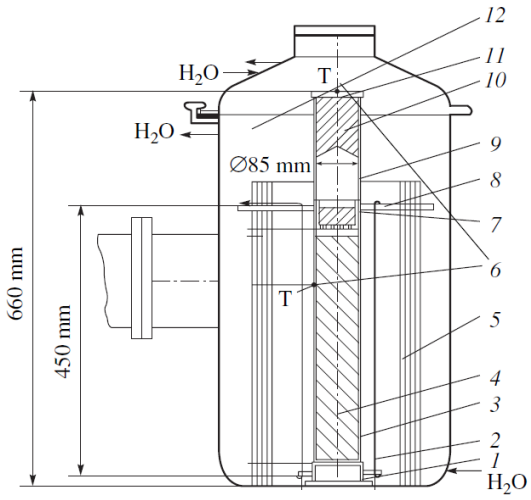

Figure 2-4: Sublimation apparatus used by Kotsar *et al.* for the purification of ZrF_4

It is evident from the literature that several authors use a particular setup for vacuum sublimation, as reported in the work done by Abate and Wilhelm, Yeatts *et al.* and Kotsar *et al.* The principle is the same in each case, i.e. the use of a vertical sublimer with added baffles to reduce impurities entrained in the sublimated product and a condenser just above the baffles for collection of the purified product. The authors merely made changes to the operating temperatures, pressures and size of equipment. These setups were, however, only used for the purification of ZrF_4 and not for the removal of Hf.

2.4.2 Vacuum sublimation purification (separation of Zr and Hf)

Setups similar to those discussed above have also been used for the separation of Zr and Hf. Monnahela *et al.* used a similar setup (Figure 2-5) for multistage sublimation to purify ZrF_4 by reducing Hf levels to below 100 ppm, but without the use of baffles (Monnahela *et al.,* 2013).

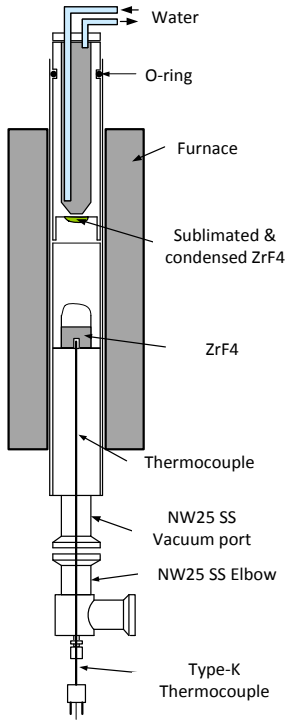

Figure 2-5: Vacuum sublimation apparatus used by Monnahela *et al.* for the separation of ZrF_4 and HfF_4

Solov'ev and Malyutina used a somewhat different experimental setup (Figure 2-6) in kinetic studies for the sublimation of ZrF_4. The equipment is labelled as follows: (1) current supply, (2) cover, (3) casing, (4) desublimer, (5) trays with purified material and (6) electric heater (Solov'ev & Malyutina, 2002a).

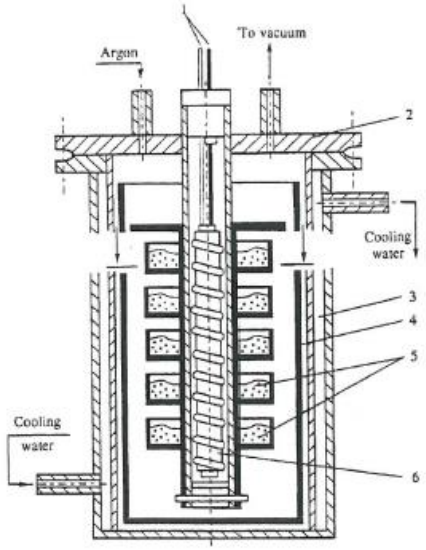

Figure 2-6: Vacuum sublimation apparatus (Solov'ev & Malyutina, 2002a)

Solov'ev and Malyutina also studied the separation of Zr and Hf in a vacuum with the addition of NiF_2, but no mention was made of the equipment that was used (Solov'ev & Malyutina, 2002b).

2.4.3 Sublimation purification in an inert atmosphere (excluding Hf)

Dai *et al.* purified ZrF_4 from impurities in a resistance furnace (Figure 2-7) operating at high temperature and in an argon atmosphere of 200 Pa. The furnace is divided into two zones: the first zone was for the sublimation of the ZrF_4 along with the volatile impurities at temperatures exceeding 800 °C and the second zone was for the desublimation of the ZrF_4 at a lower temperature of between 500 °C and 700 °C, thereby separating the ZrF_4 from the volatile impurities (Dai *et al.,* 1992).

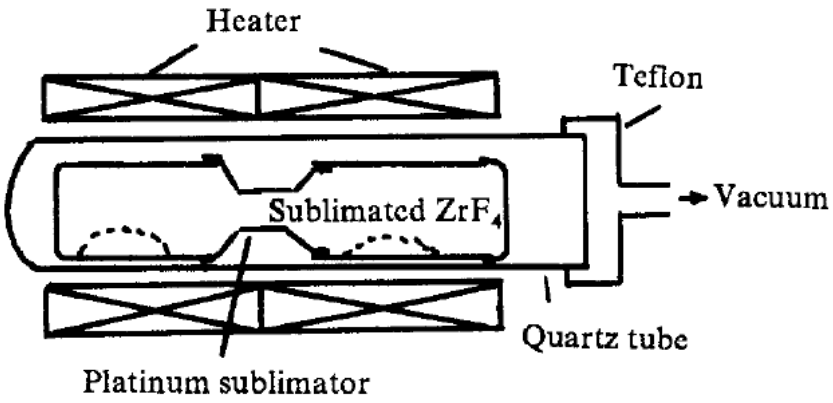

Figure 2-7: Sublimation apparatus for the purification of ZrF_4 used by Dai *et al.*

Fujuira *et al.* prepared $ZrBr_4$ by reacting Zr metal with Br_2 (Figure 2-8). The $ZrBr_4$ was carried to the reaction zone (7) where it was reacted with HF in an argon atmosphere. The resulting purified ZrF_4 product was collected in the deposition zone (8). Other labels include: (1) electric furnace, (2) electric furnace, (3) Pt tube, (4) Pt. sheet, (5) Zr metal, (6) Pt. tube, (7) reaction zone, (8) deposition zone and (9) thermocouple (Fujiura *et al.,* 1989).

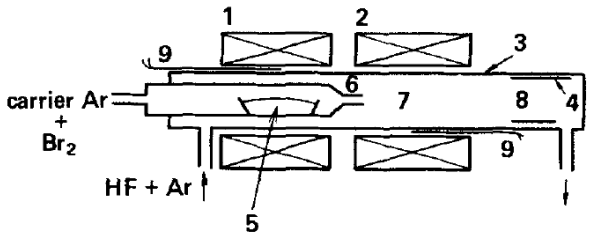

Figure 2-8: Chemical vapour deposition apparatus used by Fujiura *et al.* for the synthesis of high-purity ZrF_4

It seems as if the equipment used for sublimation in an inert atmosphere is for all practical purposes identical, as seen in the work done by Dai *et al.* and Fujiura *et al.* (Dai *et al.,* 1992; Fujiura *et al.,* 1989).

MacFarlane *et al.* used a setup (Figure 2-9) similar to that used in vacuum sublimation, where the apparatus consists of a lower crucible to sublime the ZrF_4 and an upper crucible for desublimation. The crucible was made of vitreous carbon heated by an induction heater. A single coil of the induction heater was positioned so as to heat the lower crucible, thereby establishing a temperature gradient across the upper crucible that is substantially lower than the temperature in the lower crucible. The authors make no mention of the temperature of the top crucible (MacFarlane *et al.,* 2002).

Figure 2-9: Sublimation setup used for the purification of ZrF_4

Other techniques for sublimation purification (not specifically of ZrF_4) are also discussed. Jeon *et al.* describe equipment for general sublimation purification using baffles with orifices. The apparatus (Figure 2-10) consists of a long tube with two heaters, one for sublimation and another for desublimation, thereby achieving separation of impurities that are both more and less volatile than the required component. Baffles with orifices are introduced and it is claimed that this addition results in an increase in the effective yield as well as a higher purity (Jeon *et al.,* 2010).

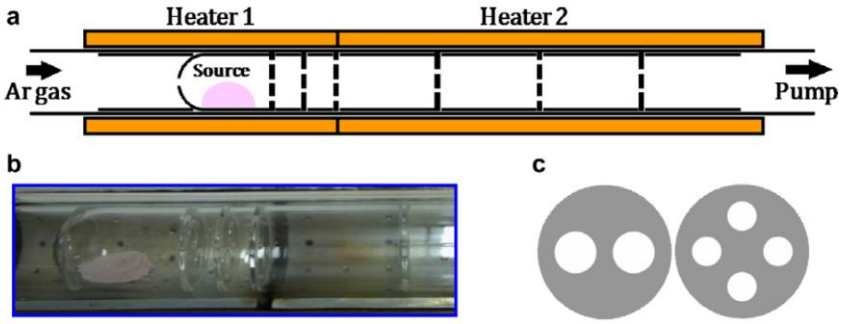

Figure 2-10: A highly efficient sublimation purification system using baffles with orifices

2.5 Typical sublimation rates of ZrF_4 and HfF_4

Typical sublimation rates for ZrF_4 and/or HfF_4 listed in the literature are discussed below.

2.5.1 Vacuum sublimation

Abate and Wilhelm investigated the purification of ZrF_4 by means of vacuum sublimation and found sublimation rates of 480 $g \cdot h^{-1}$, 650 $g \cdot h^{-1}$ and 954 $g \cdot h^{-1}$ at temperatures of 750 °C, 800 °C and 900 °C respectively (Abate & Wilhelm, 1951). The area available for sublimation was approximately 127 cm^2 and the sublimer could accept a 2 kg charge of ZrF_4. The total time required to sublime the entire 2 kg of ZrF_4 at 750 °C and 900 °C was found to be 360 minutes and 150 minutes respectively.

Kotsar *et al.* purified ZrF_4 and HfF_4 and obtained the product of the sublimation rate and degree of sublimation for ZrF_4. Values of 0.5 $g \cdot cm^{-2} \cdot h^{-1}$ to 0.9 $g \cdot cm^{-2} \cdot h^{-1}$ ZrF_4 in the temperature range 700 °C to 750 °C were obtained for ZrF_4. The pressures reported were in the range of 10^{-2} Pa to 10^{-4} Pa (Kotsar *et al.,* 2001). The maximum bed height according to Figure 2-4 is approximately 37 cm, with a sublimation area of approximately 56.7 cm^2.

Yeatts and Rainey reported, in accordance with the literature data, that a sublimation rate of 1 $g \cdot h^{-1}$ to 10 $g \cdot h^{-1}$ (which they considered a reasonable rate) could be produced at temperatures in the range of 700 °C to 800 °C. Their work revealed a sublimation rate of 4 $g \cdot h^{-1}$ at 750 °C to 800 °C with approximately 46 cm^2 available as a sublimation area and a system pressure never greater than 53 Pa. They also found that the sublimation rate depended more on the size of the aperture between the top and the boat than on the temperature, which might explain the low sublimation rates that resulted from their work. See Section 2.4.1 for more detail on the equipment used (Yeatts & Rainey, 1965).

In a study to investigate the dependence of the sublimation rate on the process pressure at laboratory scale, the authors used a three-section vacuum setup which consisted of evaporation, condensation and cooling zones. The sublimer could take a 10 g charge and had a sublimation area of approximately 10 cm^2. Experiments were done on both industrial ZrF_4 and pure ZrF_4 obtained from the double sublimation of the industrial sample (Ti *et al.,* 1990a). Sublimation rates were calculated per unit surface area in the temperature range of 650 °C to 850 °C and in the pressure range of 13.3 Pa up to 13 360 Pa.

Sublimation rate of ZrF_4

Effect of temperature under vacuum

Table 2-1 gives a summary of the above discussion (Section 2.5.1) of the sublimation rates as well as the sublimation conditions obtained for ZrF_4.

Table 2-1: Summary of the sublimation rates obtained for ZrF_4 from the literature data

Reference	Pressure [Pa]	Temperature [°C]	Sublimation rate [$g \cdot h^{-1}$]
(Abate & Wilhelm, 1951)	40	750	333
(Abate & Wilhelm, 1951)	40	900	800
(Abate & Wilhelm, 1951)	40	980	985
(Abate & Wilhelm, 1951)	40	1100	1327
(Yeatts & Rainey, 1965)	< 53	750-800 (775)	4
(Kotsar *et al.,* 2001)	10^{-2} to 10^{-4}	700	28
(Kotsar *et al.,* 2001)	10^{-2} to 10^{-4}	750	51
(Ti *et al.,* 1990a)	13.3	800	63
(Ti *et al.,* 1990a)	13.3	850	114

The dependence of the sublimation rate on temperature from literature sources (Table 2-1) is presented in Figure 2-11. A linear line was fitted through the respective data points and it seems as though the sublimation rate has a linear dependence on the temperature in the temperature range investigated. Deviations might be due to surface area, heat transfer sample purity, pressure or other factors.

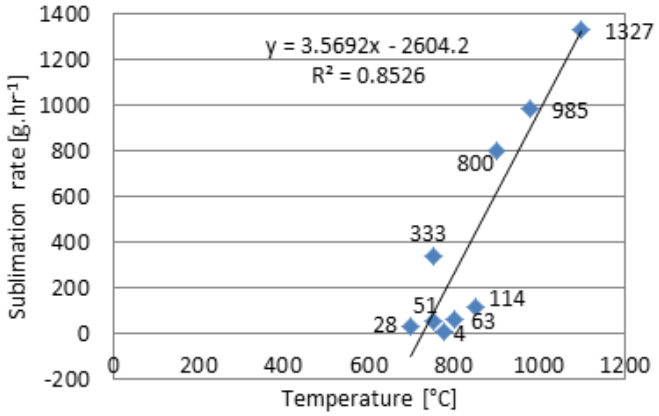

Figure 2-11: Influence of temperature on the sublimation rate under vacuum conditions

Ti *et al.* stated that sublimation under vacuum conditions is a pure surface phenomenon (Ti *et al.,* 1990b). The area-dependent sublimation rates were calculated based on the available information in the respective literature sources. The information is illustrated in Table 2-2. (Abate & Wilhelm, 1951; Yeatts & Rainey, 1965; Kotsar *et al.,* 2001; Ti *et al.,* 1990a).

Table 2-2: Area-dependent sublimation rates

Reference	Area [cm^2]	Temperature [°C]	Area-dependent sublimation rate [$g \cdot cm^{-2} \cdot h^{-1}$]
(Abate & Wilhelm, 1951)	127.2	750	2.62
(Abate & Wilhelm, 1951)	127.2	900	6.29
(Abate & Wilhelm, 1951)	127.2	980	7.74
(Abate & Wilhelm, 1951)	127.2	1100	10.43
(Yeatts & Rainey, 1965)	45.8	750-800 (775)	0.087
(Kotsar *et al.,* 2001)	56.7	700	0.5
(Kotsar *et al.,* 2001)	56.7	750	0.9
(Ti *et al.,* 1990a)	10	800	6.3
(Ti *et al.,* 1990a)	10	850	11.4

The area-dependent sublimation rates as a function of the temperature (as calculated from literature sources) are shown in Figure 2-12.

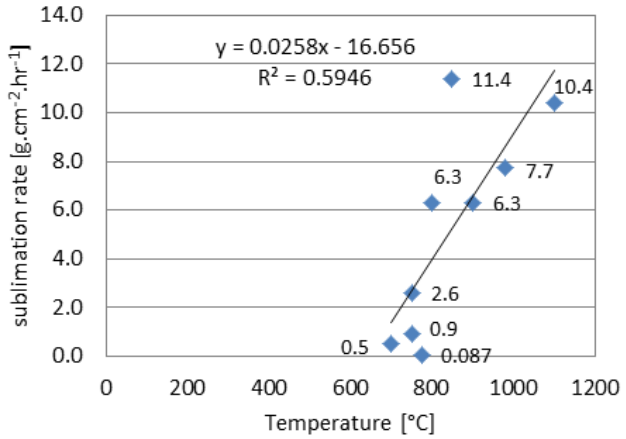

Figure 2-12: Area-dependent rate as a function of temperature

The R^2 value of 0.59 is relatively low and additional dependencies of the sublimation rate need to be investigated (e.g. heat transfer and pressure).

A study was made of the dependence of vacuum sublimation rates on the process temperature by using pure ZrF_4 (a product obtained from the double vacuum sublimation of industrial ZrF_4). A correlation which relates the sublimation rate ($g \cdot cm^{-2} \cdot min^{-1}$) to the temperature (K), i.e. the well-known Langmuir equation, is reported (Ti*et et al.,* 1990b):

$$logW = 5.293 - 6565/T \qquad (1)$$

Where W is the sublimation rate in $g \cdot cm^{-2} \cdot min^{-1}$ and T is the temperature in K. A linear relationship with an R^2 value greater than 0.99 was obtained for the pure ZrF_4. A logarithmic plot of the area-dependent sublimation rates (under vacuum conditions) obtained from Table 2-2 (impure ZrF_4) is presented as a function of the inverse temperature in Figure 2-13.

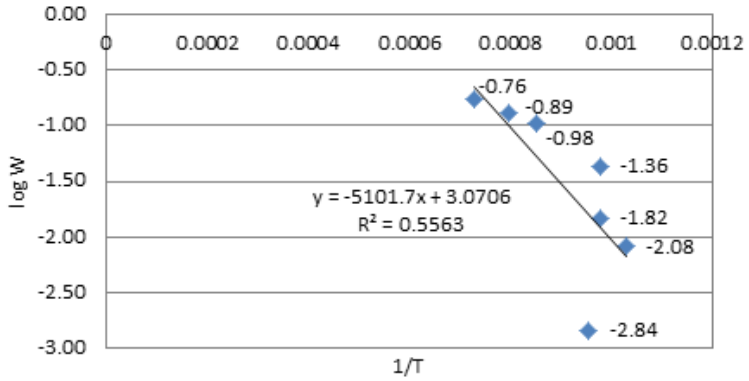

Figure 2-13: Langmuir expression for the sublimation of ZrF_4 under vacuum conditions

From the trend line equation obtained in Figure 2-13 it is evident that the values of A and B nearly correspond to those in Equation 1 obtained by the work of Ti *et al.* (Ti *et al.,* 1990c) on pure ZrF_4. The R^2 value of 0.56 may be attributable to several other factors (e.g. the effect of sample purity, pressure and heat transfer).

Effect of pressure

Since the Langmuir equation only holds under deep vacuum conditions, it is necessary to investigate the effect of pressure on the sublimation rate at low vacuum conditions. Ti *et al.* studied the effect of an increase in pressure on the vacuum sublimation rate and found a gradual decline in the sublimation rate (Ti *et al.,* 1990a). The effect of pressure on the sublimation rate at low vacuum pressure can be described by the correlation in Equation 2 (Ti *et al.,* 1990a):

$$y = a - b \cdot x^n \tag{2}$$

where y and x are the sublimation rate and pressure and a, b and n are constants. More data are required in order to obtain the pressure dependency of the data in Table 2-2 as presented in Equation 2. Furthermore, no indication was given as to whether the pressures reported in Table 2-1 are absolute or gauge pressures. Therefore no correction could be made for the dependency on pressure of the sublimation rate.

Effect of product composition

Due to the significant differences of the vapour pressures of ZrF_4 compared to those of the metal fluoride impurities in the ZrF_4, it is often concluded that the impurities will remain in the residue after sublimation. Yeatts & Rainey stated that the difference in the sublimation rate does not indicate a significant effect upon the impurity levels of the elements investigated (Yeatts & Rainey, 1965).

With that said, Ti *et al.* found that pure ZrF_4 has a higher sublimation rate than industrial ZrF_4 which contains a certain degree of impurities. They concluded that this phenomenon might be due to the accumulation of low-volatile components in the near-surface layer of the sample, making diffusion and evaporation increasingly difficult, which results in a decreased sublimation intensity. At a specific temperature, the sublimation rate of pure ZrF_4 was found to be 20 % to 50 % higher than that of industrial ZrF_4, which contains a certain degree of impurities (Ti *et al.,* 1990c, 1990a).

Effect of layer height

In a study of the influence of layer height on the vacuum sublimation rate of ZrF_4, Ti *et al*. concluded that the sublimation rate does not necessarily depend on the height of the sample. The authors further concluded that the sublimation of ZrF_4 becomes increasingly difficult due to diffusion of the sublimated ZrF_4 through the layer of non-volatile impurities (Ti *et al.,* 1990b).

Effect of particle size

The sublimation efficiency of zinc particles indicated that a decrease in particle size does not necessarily indicate an increase in the sublimation efficiency. The authors of this study mentioned that sublimation becomes increasingly difficult with smaller particles due to sintering problems, which lead to a decrease in the number of molecules able to vaporize from the surface (Zhan *et al.,* 2009).

It is, however, expected that samples with greater surface areas, i.e. smaller particles, may sublime at different rates to those of larger particles with a smaller surface area. No information was found on the effect of particle size on the sublimation efficiency of ZrF_4 and/or HfF_4.

Other effects that may influence the sublimation rate

ZrF_4 has several crystal structures, which may have a drastic effect on its sublimation rate.

ZrF_4 is also quite hygroscopic and several forms of zirconium oxyfluorides may exist together. The presence of oxyfluorides may have a drastic effect on the efficiency and yield of sublimation and these needs to be investigated. The porosity of the particles may also play a significant role in the sublimation rate.

Sublimation rate of HfF_4

A 1 400 g HfF_4 sample was sublimed in a sublimer similar to the one shown in Figure 2-2. The authors reported that 10 hours was sufficient for complete sublimation of the HfF_4 at 675 °C at approximately 1.3 Pa (Williams *et al.,* 1956). This amounts to approximately 140 $g \cdot h^{-1}$. No indication was given of the sublimation area.

Kotsar *et al.* determined the sublimation rates of HfF_4 in the sublimer shown in Figure 2-4 and obtained values of 0.3 $g \cdot cm^{-2} \cdot h^{-1}$ and 0.6 $g \cdot cm^{-2} \cdot h^{-1}$ at 700 °C and 770 °C respectively (Kotsar *et al.,* 2001). The sublimation area was approximately 56.7 cm^2, which amounts to 17 $g \cdot h^{-1}$ at 700 °C.

2.5.2 Sublimation in an inert atmosphere

In the apparatus used by MacFarlane *et al.* (Figure 2-9), a 50 % yield was obtained when a 20 g sample was sublimed for 1 hour in the lower crucible with a volume of 67 ml and at temperatures of 850 °C to 875 °C. The same yield was obtained in a scaled-up system with a lower crucible volume of 116 ml with samples of as much as 100 g which were sublimed for 3 hours. Taking the yield into account, the sublimation rates obtained in the two crucibles were 10 $g \cdot h^{-1}$ and 10.7 $g \cdot h^{-1}$ respectively (MacFarlane *et al.,* 2002).

The bottom crucible dimensions are required in order to obtain a surface-dependent rate. The following were assumed in order to estimate the dimensions of the bottom crucible:

- The ZrF_4 load of 116 ml equals the volume of the bottom crucible
- The diameter of the top section of the crucible is assumed equal to the height of the crucible
- The crucible volume was divided into a cylinder (top section) and half a sphere (bottom part), of which the total volume should amount to 116 ml (Figure 2-14).

The value of the radius corresponding to a volume of 116 ml equals 0.028 m^3 and corresponds to an area-dependent rate of 1.87 $g \cdot m^{-2} \cdot s^{-1}$ at 850 °C to 875 °C.

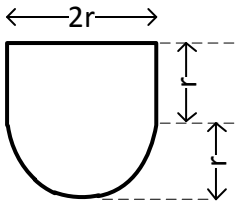

Figure 2-14: Approximate dimensions of the crucible used by MacFarlane (Figure 2-9)

This value can be compared to the area-dependent rate obtained from the sublimation rate model at the same temperature. It must be noted that the total time of 3 hours could be more than the actual time taken for complete sublimation of the 50 g sample. Furthermore, an explanation for the yield of only 50 % could be the presence of oxyfluorides in the sample.

2.5.3 Scaled-up sublimation processes

Typical sublimation capacities for scaled-up systems (not specifically for ZrF_4 sublimation) are 5 $kg \cdot m^{-2} \cdot h^{-1}$to 20 $kg \cdot m^{-2} \cdot h^{-1}$ and desublimation capacities of 10 $kg \cdot m^{-2} \cdot h^{-1}$ to 40 $kg \cdot m^{-2} \cdot h^{-1}$ (Raouzeos & Schwenk, 1996)**.**

Solov'ev and Malyutina stated that the technology of vacuum sublimation demonstrated positive results when evaluated on pilot plant equipment and that this technology has been introduced into industrial practices for producing reactor-purity Zr, but made no mention of the feasibility and economic viability of the process (Solov'ev & Malyutina, 2002a).

2.6 Nuclear specification for Zr

Table 2-3 lists the ASTM composition specifications for Zr sponge (Benedict *et al.,* 1981), ASTM grade R6001 and ASTM specification B349-73.

Table 2-3: Specification for nuclear grade Zr sponge

Element	Permissible impurities in Zr sponge max, ppm	Element	Permissible impurities in Zr sponge max, ppm
Aluminium	75	Iron	1 500
Boron	0.5	Manganese	50
Cadmium	0.5	Nickel	70
Carbon	250	Nitrogen	50
Chlorine	1300	Oxygen	1 400
Chromium	200	Silicon	120
Cobalt	20	Titanium	50
Copper	30	Tungsten	50
Hafnium	100	Uranium (total)	0.3

The mass fractions of permissible impurities in ZrF_4 were obtained by assuming that all tetrafluorides are in their highest oxidation state. These are listed in (Table 2-4).

Table 2-4: Permissible impurities in ZrF_4

Element	Permissible impurities in ZrF_4 max, ppm	Element	Permissible impurities in ZrF_4 max, ppm
Aluminium	41	Iron	819
Boron	0.27	Manganese	27
Cadmium	0.27	Nickel	38
Carbon	137	Nitrogen	n/a
Chlorine	710	Oxygen	n/a
Chromium	109	Silicon	66
Cobalt	11	Titanium	27
Copper	16	Tungsten	27
Hafnium	55	Uranium (total)	0.16

It would be a favourable outcome of this study if the final product adhered to the above specifications for ZrF_4, especially in the case of Hf.

Influences of some elements:

- A high nickel content in the alloys promotes the absorption of hydrogen, leading to reduction in ductility (Benedict *et al.,* 1981)
- A higher niobium content results in better mechanical properties (Benedict *et al.,* 1981)
- Uranium and thorium form fission products if present in Zr cladding (Benedict *et al.,* 1981)

Chapter 3: Experimental

3.1 Process description and concept discussion

The BFD for the sublimation system is shown in Figure 3-1. A pre-weighed amount of $Zr(Hf)F_4$ was placed in a sublimer and exposed to elevated temperatures for a set amount of time. The sublimed mass diffuses into a stream of nitrogen gas which is pre-heated and used as sweep gas during the sublimation of $Zr(Hf)F_4$. The gas then flows across a water-cooled desublimer annulus section so as to desublime the $Zr(Hf)F_4$ across the length of the desublimer. The remainder of the gas is then passed to a water scrubber.

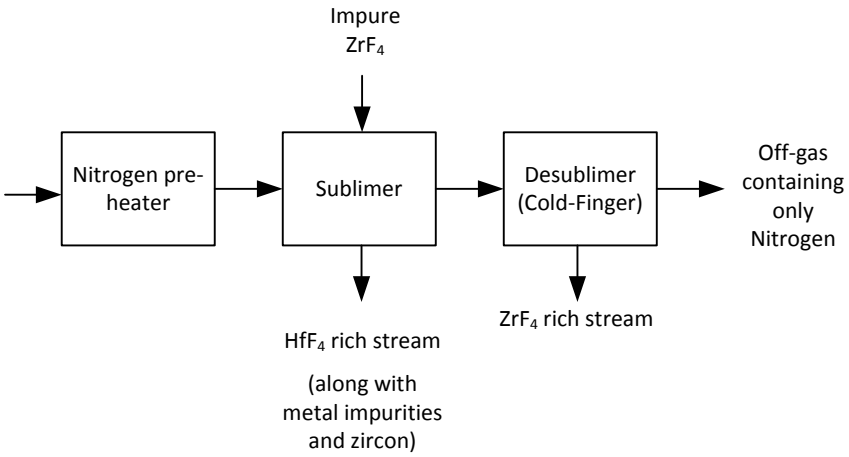

Figure 3-1: Block flow diagram (BFD) for the sublimation separation of ZrF_4 and HfF_4

The idea is to sublime a mass of $Zr(Hf)F_4$ at a pre-determined temperature for a pre-determined time and to stop sublimation after the time has elapsed. The sublimer residue as well as the desublimed mass are collected, weighed and analysed for Zr and Hf content. The ratio of Zr and Hf that remains in the sublimer as well as the ratio of Zr and Hf that desublimed over the length of the desublimer are determined. The aim was to establish the extent of separation within the sublimer and desublimer to achieve nuclear grade purity.

The nitrogen feed is controlled with a rotameter at a set regulated pressure. The rotameter was calibrated with the use of a bubble flow meter.

The sublimer is a reactor boat (Figure 3-2) 100 mm long and 20 mm deep which can take a maximum of 80 g $Zr(Hf)F_4$. The $Zr(Hf)F_4$ to be sublimed is placed in the boat which is placed in the tube furnace.

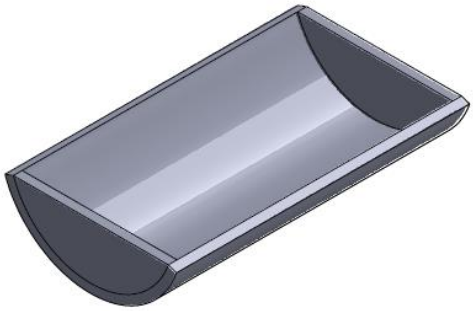

Figure 3-2: Schematic of the sublimer used

The desublimer is a long cylindrical pipe (cooled to ~ 30 °C) inside another insulated pipe which facilitates the carrying of the gas mixture. A simple geometry was selected for the desublimer to facilitate easy removal of the components at the end of the experiment. The desublimer temperature was much lower that the temperature of the outer pipe, the objective of which was not to desublime on the outer pipe which facilitates the hot gas. The spacing between the two pipes is minimal so as to reduce the diffusion path of the condensing particles.

Figure 3-3: gives a schematic of the sublimer and desublimer inside the tube furnace. The section above the sublimation pan facilitates the nitrogen gas, which reduces the partial pressure of the ZrF_4 and HfF_4 and carries the tetrafluorides to the desublimer space.

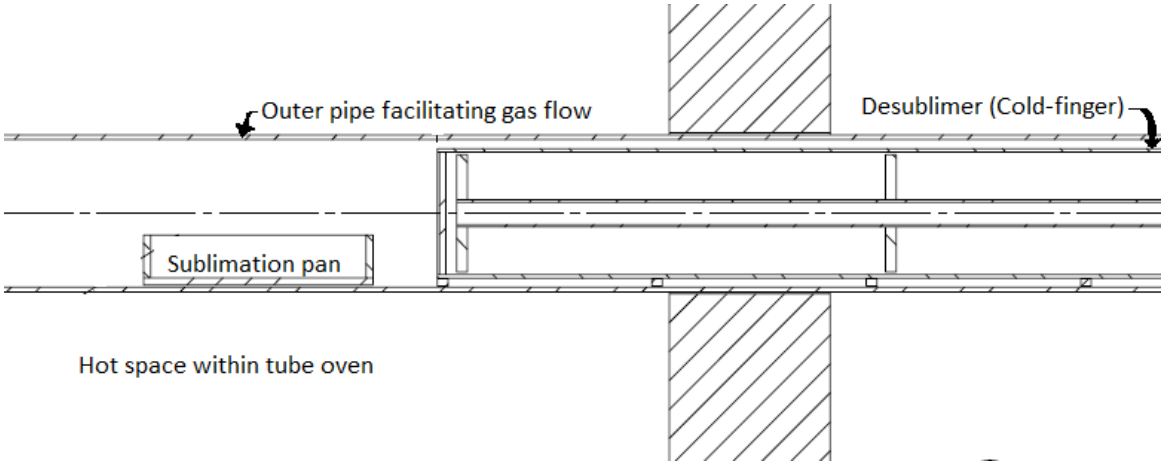

Figure 3-3: Schematic of sublimer and desublimer inside tube furnace

The experimental setup for the sublimation/desublimation system is shown in Figure 3-4 and Figure 3-5.

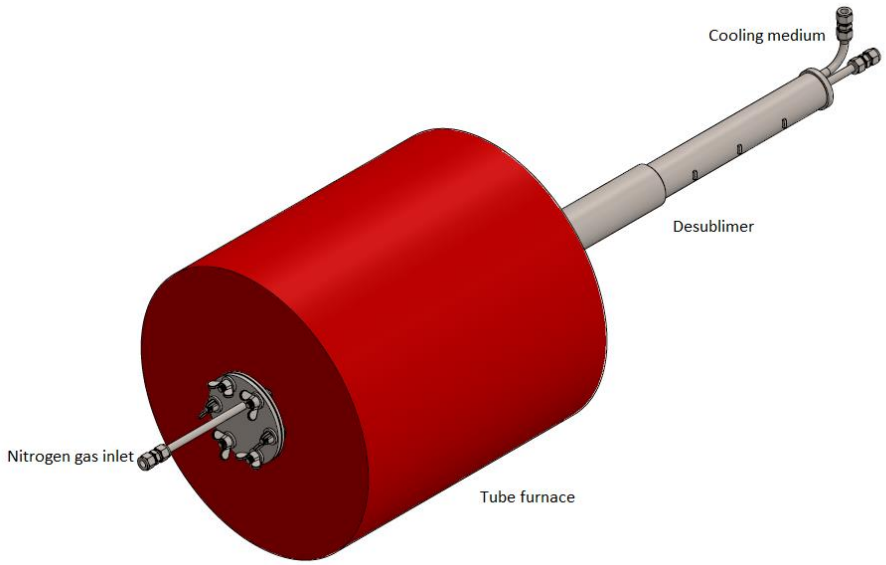

Figure 3-4: Experimental setup for the sublimation/desublimation separation of ZrF_4 and HfF_4

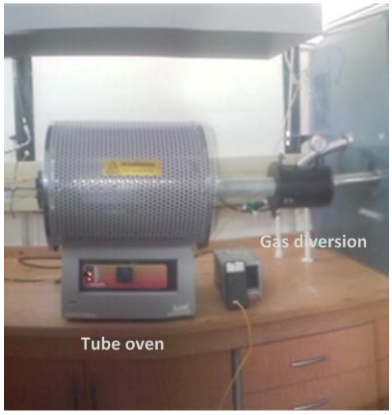

Figure 3-5: Illustration of the sublimation/desublimation setup

Figure 3-5 shows a gas diversion section which diverts the gas to a water scrubber which scrubs any desublimed $Zr(Hf)F_4$ entrained in the gas stream.

There is a difference between the temperature of the elements and the inside temperature of the furnace. The extent of the temperature difference depends on the nitrogen flow setting and the set temperature. Typical temperature differences range between 20 °C and 50 °C.

The sublimer is added to the oven once the required sublimation temperature has been reached. Figure 3-6 shows an image of the sublimer and desublimer inside the tube furnace at a set temperature of 850 °C.

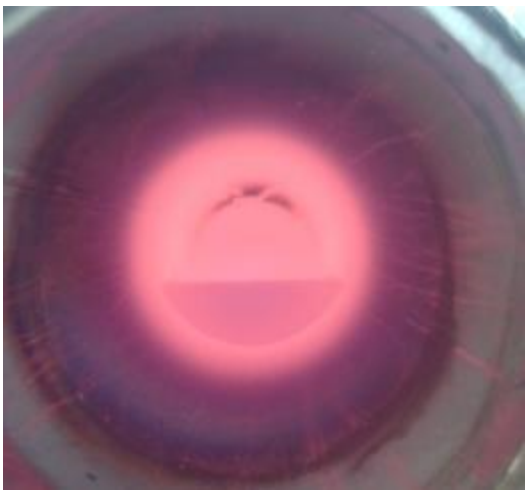

Figure 3-6: Image showing sublimer and desublimer in tube oven set at 850 °C.

The piping and instrumentation diagram of the system is shown in Figure 3-7.

3.2 Experimental procedure

Sublimation occurs as long as the vapour pressure is greater than the partial pressure in the bulk gas stream (Hanson & Corder, 2004). The use of a sweep gas constantly reduces the partial pressure and a higher sublimation rate will therefore result. In this work nitrogen was used as the sweep gas.

Two types of experiment were done. The tube oven was heated to the set temperature before sample loading. The first set of experiments was done to determine the rate of sublimation. Several sublimers containing 15 g sample mass were loaded one after the other into the tube furnace for different time intervals. The weight losses (mass sublimed) as well as the Zr/Hf mole ratios were determined for the sublimer residue. No desublimer was used for the determination of the rate of sublimation.

In the second set of experiments three sublimers containing 15 g ZrF_4 each were loaded into the tube furnace one after the other for 30 min. The idea here was to desublime as much as possible over the length of the desublimer to determine the Zr/Hf mole ratio as a function of the desublimer length. It was assumed that the sublimation conditions were the same for all the sublimer samples.

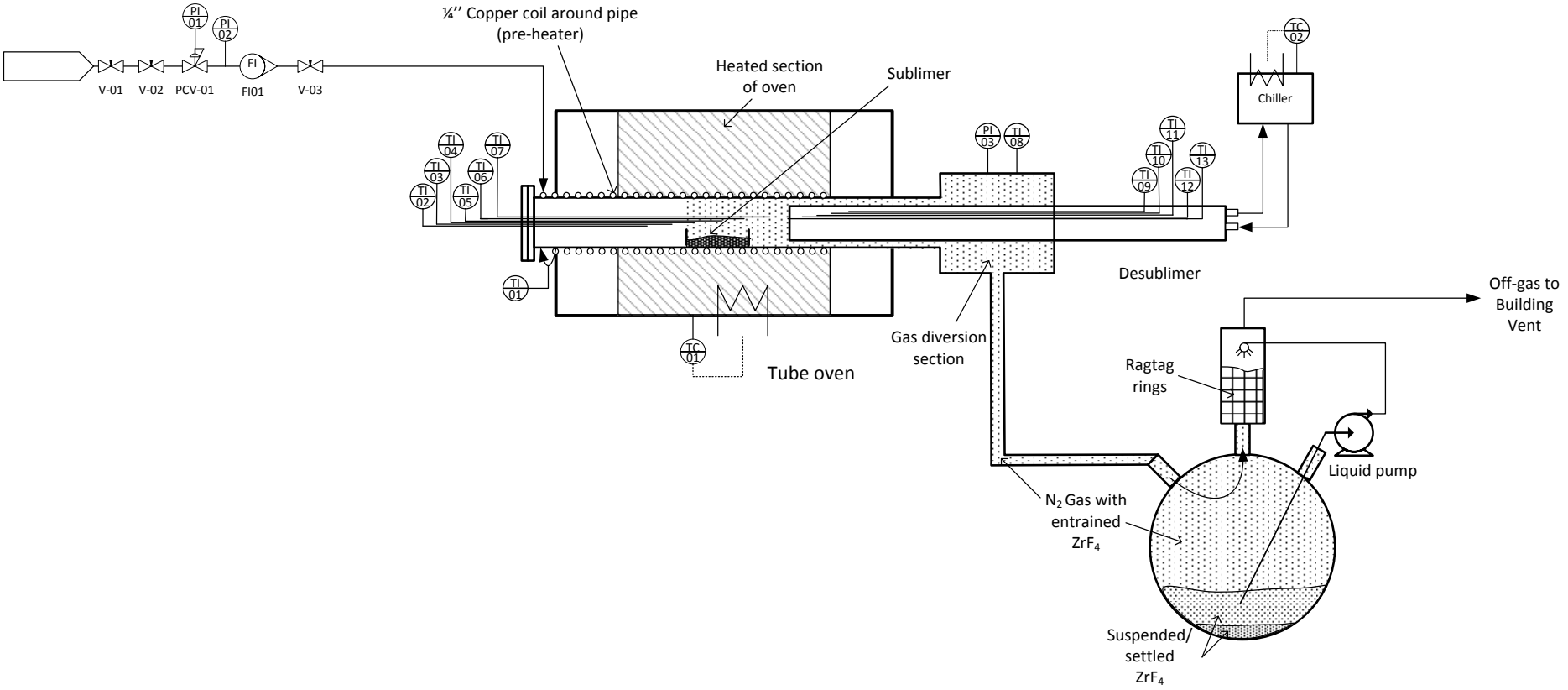

Figure 3-7: Piping and instrumentation diagram

Step-by-step procedure

1. Assemble the system.
2. If required, add the desublimer to the system.
3. Set the furnace to the required temperature.
4. Set the nitrogen flow to the required setting.
5. Weigh the correct amount of $Zr(Hf)F_4$ and place it in the sublimer pan.
6. Place the sublimer in the furnace once it has reached the required temperature.
7. Keep a constant flow of nitrogen during the sublimation experiment.
8. Keep the system at the set temperature for a pre-determined time, i.e. 15 minutes, 30 minutes and 45 minutes.
9. Once the time has elapsed, open the system and remove the sublimer while it is hot, place a lid on the sublimer and allow to cool.
10. Repeat steps 5 to 9 for the next experiment.
11. Once all the experiments at one temperature have been completed, switch off the furnace and allow it to cool completely.
12. If applicable, carefully remove the desublimer from the oven and take samples at different lengths of the desublimer.
13. Prepare samples for analysis.
14. Repeat for different temperatures.

The sublimation rate of ZrF_4 and HfF_4 are strongly dependent on the vapour pressures and the mole fractions of the respective components in the bulk mixture and therefore the sublimation rate of the ZrF_4 is much higher than that of the HfF_4. The sublimed mass then enters a desublimation zone in which the ZrF_4 and HfF_4 desublime at different rates. This implies that separation is achieved in both the sublimer and the desublimer.

The ultimate goal is to be able to provide experimental conditions, i.e. sublimation time, temperature and position on the desublimer which provide the best separation conditions. These conditions must, however, be in balance with the operation cost, as the cost will be higher at a higher temperature and for longer sublimation runs.

It is imperative to find the optimal temperature. Higher temperatures cause a lower degree of separation from impurities and lower temperatures increase the sublimation time drastically (Abate & Wilhelm, 1951; Solov'ev & Malyutina, 2002a).

It will be noted from the results discussed in the following sections that separation was achieved in both the sublimer and the desublimer.

Equipment used

The tube furnace was a Carbolyte Eurotherm, Type GHA 12/300 SR 20-802734, with a maximum temperature of 1 200 °C.

Chapter 4: Preparation and characterisation of $Zr(Hf)F_4$

4.1 Preparation of $Zr(Hf)F_4$

Zircon ($Zr(Hf)SiO_4$) is plasma treated at temperatures above 1 700 °C in order to dissociate the silicon from the zircon to produce plasma-dissociated zircon (PDZ or $Zr(Hf)O_2 \cdot SiO_2$).

$$Zr(Hf)SiO_4 \xrightarrow{\text{Plasma}} \rightarrow Zr(Hf)O_2 \cdot SiO_2 \quad (3)$$

The PDZ was then treated with HF in a fluidized bed at 110 °C to remove the silica from the matrix producing SiF_4 and H_2O as gaseous by-products and a bed of $Zr(Hf)O_2$ (DPDZ).

$$Zr(Hf)O_2 \cdot SiO_2 + HF(g) \xrightarrow{\text{Fluidized bed}} Zr(Hf)O_2 + SiF_4 \uparrow \quad (4)$$

The DPDZ was then reacted with ammonium bifluoride (ABF, i.e. $NH_4F \cdot HF$) bought in bulk from Minema Chemicals.

The DPDZ was pre-mixed with the ABF and introduced into the reactor (batch). The reaction mechanism to produce $Zr(Hf)F_4$ involved separate steps: the first step was the formation of the ammonium fluoride intermediate, i.e. $(NH_4)_3Zr(Hf)F_7$ at approximately 150 °C, while the remaining steps involved the decomposition of the intermediate, essentially decomposition of the $(NH_4)_3Zr(Hf)F_7$, to yield $Zr(Hf)F_4$, which ranged from temperatures of 200 °C to 410 °C, depending on the pressure (Haendler, Wheeler & Robinson, 1951).

$$Zr(Hf)O_2 + 4NH_4F \cdot HF \rightarrow (NH_4)_3Zr(Hf)F_7 + NH_4F + 2H_2O\uparrow \quad (5)$$

$$(NH_4)_3Zr(Hf)F_7 \rightarrow (NH_4)_2Zr(Hf)F_6 + NH_4F\uparrow \quad (6)$$

$$(NH_4)_2Zr(Hf)F_6 \rightarrow NH_4Zr(Hf)F_5 + NH_4F\uparrow \quad (7)$$

$$NH_4Zr(Hf)F_5 \rightarrow Zr(Hf)F_4 + NH_4F\uparrow \quad (8)$$

Sufficient detention times were required for each step to proceed to completion. It was found that approximately 90 minutes were required for the intermediates to form at a temperature of

approximately 150 °C and another 90 minutes above 400 °C were required for complete decomposition of the intermediates to $Zr(Hf)F_4$.

The same mechanism is assumed for the other metal oxide impurities contained in the DPDZ. The product therefore still contains HfF_4 along with other metal fluoride impurities, unreacted DPDZ and zircon. The formation of oxyfluorides and hydrides is very probable; therefore the entire fluorination process must be carried out in a leak-tight system to avoid contact with air and moisture.

4.1.1 Impurities in ZrF_4

The impurities in the ZrF_4 are mostly carried over from the impurities in the PDZ. The metal oxides present in the zircon (Namakwa Sands Zircon) before plasma treatment included ZrO_2, HfO_2, SiO_2, Fe_2O_3, TiO_2, Al_2O_3, Cr_2O_3, CaO, P_2O_5 and U and Th.

4.1.2 System description

The reactor was a 6'' stainless steel pipe equipped with flanges on the left for reagent addition. The flanges were equipped with a nitrogen inlet and a thermocouple fitting to measure the temperature of the reaction mixture to ensure that the temperatures were adequate for melting of the ABF but did not exceed the decomposition temperatures of the ABF. It was further necessary to exceed a temperature of 400 °C for decomposition of the $((NH_4)_3Zr(Hf)F_7$ but not to exceed 500 °C, at which point sublimation of the $Zr(Hf)F_4$ starts to become more evident.

The cold finger was a water-cooled copper coil inside a 6'' stainless steel pipe. The off-gases from the reaction are carried with the nitrogen stream to the cold finger where they are desublimed and collected on the copper coil. The gases exiting the cold finger should consist only of nitrogen and are passed to the outside scrubbing system, which consisted of a 1 % HF scrubber, an 18 % KOH scrubber and a fan which provided a vacuum of approximately -8 kPa.

The product remained in the reactor along with the unreacted DPDZ, PDZ and zircon. After removal, the product should be homogenized in an inert atmosphere for analysis. The piping and instrumentation diagram (P&ID) for the sublimation system is shown in Figure 4-1.

Should a blockage occur, the maximum partial pressure of the ABF in the nitrogen will not exceed 110 kPa (abs). The nitrogen supply line is regulated at 45 kPa (g), implying a total pressure of

45 kPa (g), which is 10 % lower than the total allowable pressure for the reactor not to be qualified as a pressure vessel. The partial pressure of the nitrogen in case of a blockage is then 22 kPa (g).

A pressure transmitter was also installed to monitor the pressure at the inlet of the nitrogen pre-heater. The transmitter was linked to the heaters to stop it from heating once the pressure reached 45 kPa (g). See interlock PH-I-01 on P&ID in Figure 4-1.

Thermal cut-outs were installed on the heater to prevent temperature run-away. See interlock TH-I-02 on P&ID in Figure 4-1.

From this it is evident that there are no statutory regulations applicable to the equipment used for the sublimation separation of Zr and Hf.

Mechanical engineering approval was obtained for the system and can be found in document AC-AMI01-ENN-16002.

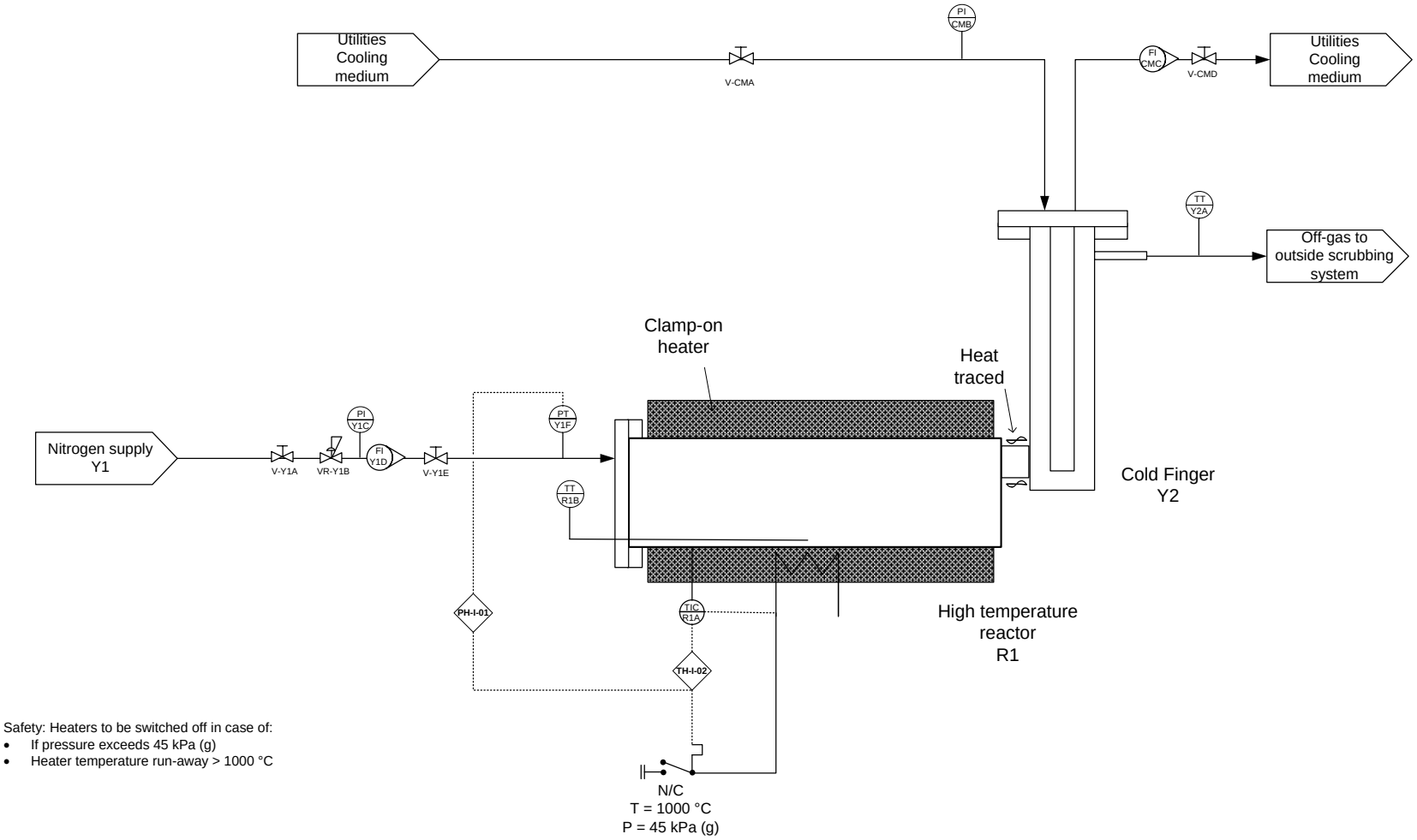

Figure 4-1: Batch reactor system for the production of $Zr(Hf)F_4$ from DPDZ and ABF

4.2 Characterisation of $Zr(Hf)F_4$ used in sublimation experiments

4.2.1 X-Ray diffraction

Identification of the ZrF_4 was done by means of X-Ray diffraction analysis to indicate the major components and to determine whether oxyfluorides and/or ammonium zirconium fluorides are present.

An XRD spectrum for $Zr(Hf)F_4$ product manufactured from DPDZ and ABF is shown in Figure 4-2, indicating that the major component present in the sample is ZrF_4.

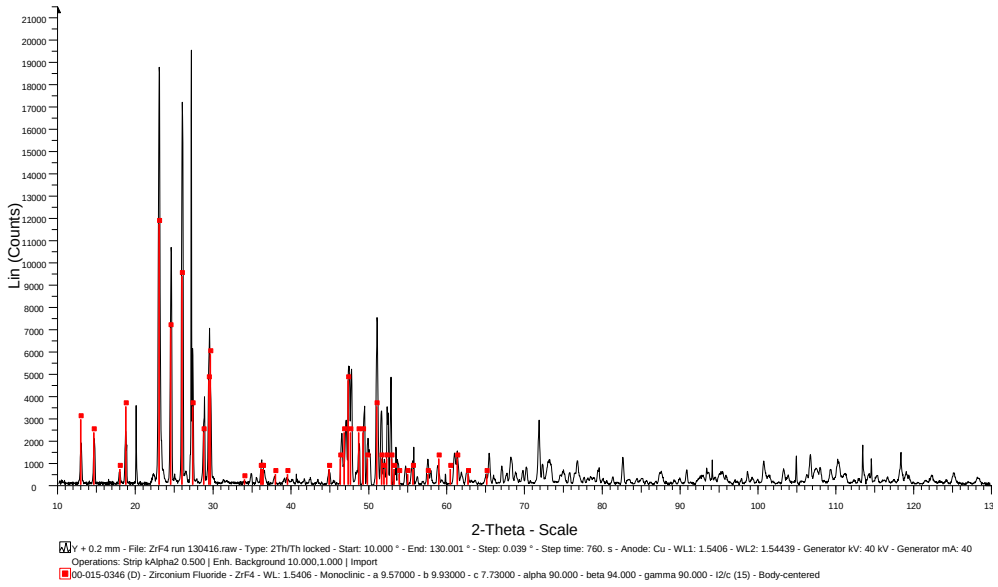

Figure 4-2: XRD pattern of $Zr(Hf)F_4$ overlaid with stick pattern of ZrF_4

Table 4-1 shows the quantitative XRD results obtained for three batches of $Zr(Hf)F_4$ prepared from DPDZ and ABF (run a, b and c).

Table 4-1: Quantitative XRD results for three batches $Zr(Hf)F_4$ prepared from DPDZ and ABF

Batch number	Weight % of respective components in samples		
	$Zr(Hf)F_4 \cdot H_2O$	$NH_4Zr(Hf)F_5$	$(NH_4)_2Zr(Hf)F_6$
Run a	9.55	37.99	0
Run b	0	39.6	1.62
Run c	0	39.93	6.02

The above results imply that there is a certain percentage of crystal water and NH_4F in the sample that will come off during heating of the samples. Table 4-2 lists the amounts of water and NH_4F in each batch.

Table 4-2: Calculated low-temperature volatiles in the three respective batches

Batch number	Weight % of low-temperature volatiles (LTV)		
	H_2O from $Zr(Hf)F_4 \cdot H_2O$	NH_4F from $NH_4Zr(Hf)F_5$	Total LTV
Run a	0.93	6.9	7.8
Run b	0	7.5	7.5
Run c	0	8.4	8.4

From the above results it is evident that the three batches contain approximately 8 % low-temperature volatiles.

4.2.2 Thermogravimetric analysis

Samples from the three batches were heated in a TGA from ambient temperature to 850 °C at a heating rate of 10 °C·min^{-1}. The TGA indicated the following:

- Amount of non-volatiles in the batch (i.e. total water and NH_4F or other species detected by XRD). This gives an indication of the extent of the decomposition reaction (reactions (5) to (8)
- The mass remaining at 850 °C is an indication of the quantity of zircon, oxyfluorides and unconverted oxides.

The TGA results of three batches $Zr(Hf)F_4$ of product prepared for the sublimation experiments are shown in Figure 4-3.

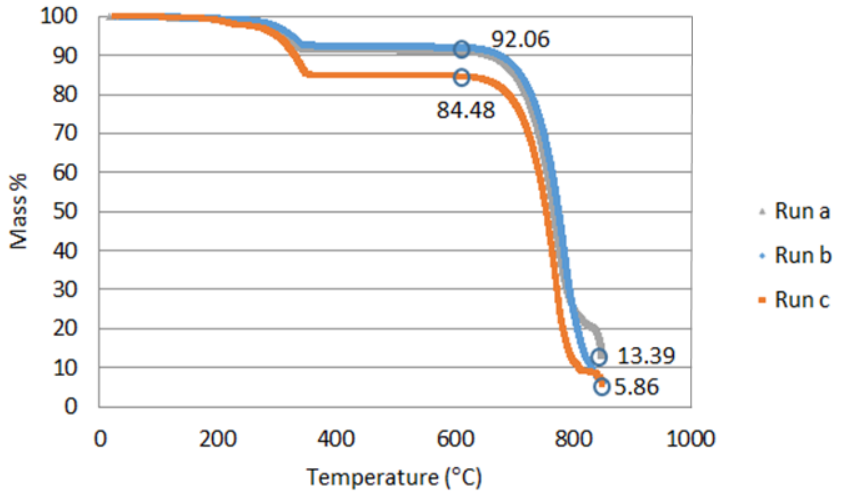

Figure 4-3: TGA result of three samples of $Zr(Hf)F_4$ prepared for sublimation experiments

The following observations were made:

- Runs a and b showed good repetition, with an 8 % decrease in the mass which is indicative of the presence of $Zr(Hf)F_4 \cdot H_2O$ and/or $(NH_4)ZrF_5$. This corresponds well to the results of the XRD analysis discussed in Section 3.3.2.
- Run c showed a mass decrease of 15.5 % prior to the sublimation temperature of 600 °C. Only 8.5 % low-temperature volatiles were detected by XRD and no explanation could be found as to what the content of the remaining 7 % could be. This batch was not used for sublimation experiments.
- The TGA for runs b and c indicates that approximately 6 % of the sample remains at a temperature of 850 °C. This corresponds to the approximate amount of zircon originally in the sample (6.7 %).
- The results obtained for "run a" indicates a residue of 13.4 % at 850 °C. This may imply that the conversion of the DPDZ was not successful. This does not, however, influence the results for the sublimation of the $Zr(Hf)F_4$.

Crystal structures

The tetragonal crystal structure (β-ZrF_4) and the unidentified crystal structure (γ-ZrF_4) transform irreversibly to the monoclinic structure at temperatures in excess of 400 °C. This is evident on the DTA curve of the ZrF_4 at approximately 440 °C (Brown *et al.,* 2005).

4.2.3 Scanning electron microscope

A scanning electron microscope (SEM) image indicated that the particles formed agglomerates and that no definite geometry was apparent for the respective particles (Figure 4-4). This implies that it

would be difficult to develop a sublimation model that is dependent on the particle geometry (Van der Merwe & Snyders, 2016).

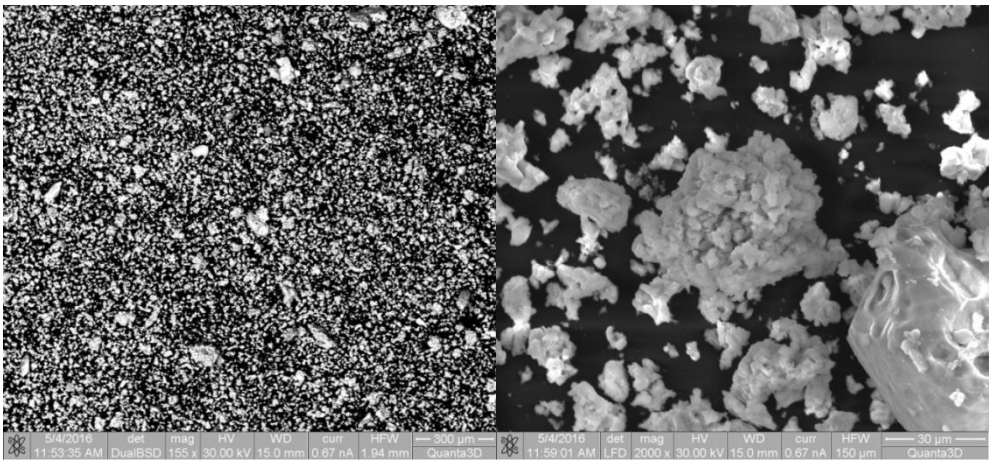

(a) (b)

Figure 4-4: (a) SEM image indicating very small $Zr(Hf)F_4$ particles along with the larger zircon and PDZ particles, (b) 30 µm magnification indicating agglomerates of small Zr(Hf) particles

4.2.4 Particle analysis

The absolute density of the $Zr(Hf)F_4$ was determined to be 4.487 $g \cdot cm^{-3}$. An AccuPyc II 1340 Gas Displacement Pyconemeter for volume measurements and density calculations was used. Table 4-3 shows the average particle size distributions of the $Zr(Hf)F_4$ sample determined with a Saturn DigiSizer II Analyzer. It was mentioned that the homogeneity of the sample could not be ensured prior to analysis and segregation of heavier particles into the sample container during storage could therefore be a relevant factor. Blending and sample splitting services prior to the analysis of bulk (larger samples) were carried out (Van der Merwe & Snyders, 2016).

Table 4-3: Average particle size distributions

Diameter	Average particle size (µm)
D_{10}	5.055
D_{50}	21.409
D_{90}	82.436

Chapter 5: Model development

5.1 Properties of ZrF_4, HfF_4 and N_2

This chapter discusses the vapour pressures of ZrF_4 and HfF_4, the physical properties of ZrF_4, HfF_4, metal fluoride impurities and N_2, the thermodynamic properties of ZrF_4 and HfF_4, the mass and thermal diffusion coefficients for ZrF_4 and HfF_4 in nitrogen, the flow properties and the heat and mass transfer correlations used in the sublimer and desublimer.

5.1.1 Vapour pressures

Vapour pressure of ZrF_4 and HfF_4

Figure 5-1 gives a range of vapour pressures from several sources in the literature for both ZrF_4 and HfF_4 at temperatures above 600 °C (Sense, Snyder & Clegg, 1953; Sense, Snyder & Filbert, 1954; Cantor *et al.,* 1958; Benedict *et al.,* 1981; and Koreneo *et al.,* 1972).

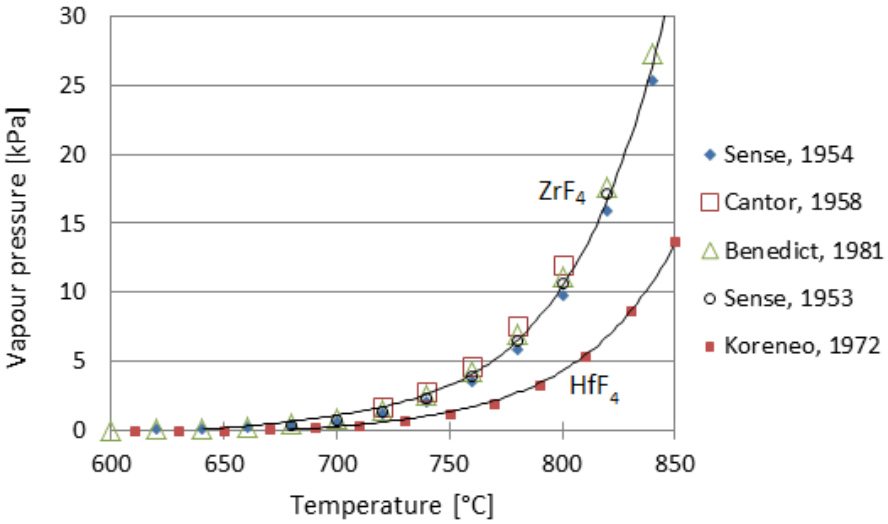

Figure 5-1: Vapour pressures for ZrF_4 and HfF_4 as reported in the literature

A higher temperature will result in a larger vapour pressure difference between ZrF_4 and HfF_4, which implies a larger difference in the partial pressures of the two tetrafluorides in the bulk nitrogen gas stream. A larger partial pressure difference results in a larger difference in the desublimation temperatures of the two respective components.

The data in Figure 5-1 were combined and can be expressed as Antoine constants for both ZrF_4 and HfF_4. These are illustrated by the correlations in Table 5-1.

Table 5-1: Combined vapour pressure correlations for ZrF_4 and HfF_4.

Component	Vapour pressure [kPa]	Temperature range [°C]
ZrF_4	$\log(P) = 12.096 - \frac{11879}{T}$	600 – 920
HfF_4	$\log(P) = 12.391 - \frac{12649}{T}$	600 – 950

Vapour pressures for these correlations also include those at temperatures below 600 °C (Brunetti *et al.,* 2011; Konings & Hildenbrand, 1994; Koreneo *et al.,* 1972; Nielsen, 2001).

The standard error for the correlation given for ZrF_4 was calculated for both constants using the LINEST function in Microsoft Excel. The standard error for the constants A and B was found to be 48.2 and 0.055 respectively. Since only one set of data was available for HfF_4 (taken in 1972) and since ZrF_4 and HfF_4 have many similarities, the assumption can be made that the data given for HfF_4 have a similar standard error.

Vapour pressures of some metal fluoride impurities

The vapour pressures of ZrF_4 and some metal impurities at 827 °C are listed in Table 5-2.

Table 5-2: Vapour pressures of metal fluoride impurities (Robinson, 1986: 189)

Metal fluoride	Vapour pressure (kPa)
ZrF_4	18.3
FeF_3	0.33
FeF_2	1.87E-03
CuF_2	3.47E-03
CuF	0.37
NiF_2	5.33E-04

These vapour pressures are required for the selection of the optimal sublimation temperature so as not to sublime the impurities along with the ZrF_4. It can be seen that the vapour pressures of FeF_3 and CuF are closest to that of ZrF_4 at 827 °C. This implies that Fe and Cu contribute most to impurity complications of the ZrF_4.

5.1.2 Physical properties of nitrogen

Equations 9 to 12 give temperature-dependent correlations for the dynamic viscosity, heat capacity and density of the nitrogen.

$$\mu_{N_2}(T) = 4.2606x10^{-6} + 4.75x10^{-8}T - 9.88x10^{-12}T^2 \quad (9)$$

$$Cp_{N_2}(T) = 1.08 - 1.26x10^{-4}T + 3.6x10^{-7}T^2 - 1.59x10^{-10}T^3 + 9.26x10^{-15}T^4 \quad (10)$$

$$\rho_{N_2}(T) = \frac{PMM_{N_2}}{RT} \quad (11)$$

$$k_{N_2}(T) = 3.09x10^{-3} + 7.59x10^{-5}T - 1.101x10^{-8}T^2 \quad (12)$$

Where T is the temperature in K, μ_{N_2} is the dynamic viscosity in kg·m^{-1}·s^{-1}, Cp_{N_2} is the heat capacity in kJ·kg^{-1}·K^{-1}, ρ_{N_2} is the density in kg·m^{-3}, P is the pressure in kPa, MM_{N_2} is the molar mass in kg·kmol^{-1}, R is the ideal gas constant (8.314 kPa·m^3·kmol^{-1}·K^{-1}) and k_{N_2} is the thermal conductivity in W·m^{-1}·K^{-1}. Values for these properties at several operating temperatures are listed in Table 5-3.

Table 5-3: Physical properties of nitrogen at several temperatures and at 100 kPa

Temperature [°C]	$\boldsymbol{\mu_{N_2}}$ [kg·m^{-1}·s^{-1}]	$\boldsymbol{Cp_{N_2}}$ [kJ·kg^{-1}·K^{-1}]	$\boldsymbol{k_{N_2}}$ [W·m^{-1}·K^{-1}]	$\boldsymbol{\rho_{N_2}}$ [kg·m^{-3}]
25	1.754 x 10^{-5}	1.038	0.025	1.131
650	3.969 x 10^{-5}	1.123	0.064	0.365
700	4.112 x 10^{-5}	1.132	0.067	0.346
750	4.251 x 10^{-5}	1.140	0.069	0.329

5.1.3 Physical properties of ZrF_4, HfF_4 and other metal fluoride impurities

An estimation was made of the metal fluoride impurities present in the ZrF_4 manufactured from the fluorination of plasma-dissociated zircon with ammonium bifluoride (Pretorius, 2013). Solov'ev *et al.* studied the vacuum sublimation separation of HfF_4 from ZrF_4, with ZrF_4 being produced from natural zircon. Impurities in addition to those in the study above that are mentioned to be present in zircon are CoF_2, NiF_2 and LaF_3 (Solov'ev & Malyutina, 2002b). The melting and boiling points of these impurities are listed in Table 5-4.

Table 5-4: Melting, boiling and/or sublimation temperatures of some metal fluorides

Metal fluoride	Melting point [°C]	Boiling point [°C]	Sublimation point [°C]
ZrF_4	841 – 892[*4]	906[*1]	912[*2]
HfF_4	-	974[*1] / 968[*3]	970[*2]
FeF_2	1 100[*1]	1 837[*1]	
TiF_3			950[*2] decompose
AlF_3	-	1 279[*1]	1 276[*2]
CrF_3	1 425[*2]		
MgF_2	1 263[*2]	2 227[*2]	
CaF_2	1 418[*2]	2 500[*2]	
UF_4	1 036[*2]	1 417[*2]	
ThF_4	1 110[*2]	1 680[*2]	
CoF_2	1 130[*1]	1 130[*1]	
NiF_2	1 283[*1]	1 474[*1]	
LaF_3	-	1 136[*1]	

[*1]Solov'ev & Malyutina, 2002b

[*2]*CRC handbook of chemistry and physics*, 2008

[*3]Nielsen, 2001

[*4]Brown *et al.,* 2005: 147

From Table 5-4 it is evident that the sublimation temperatures must not exceed 1 000 °C to ensure that impurities are not sublimed, thereby contaminating the sublimation product.

Density of ZrF_4

In the work done by Abate and Wilhelm, a 12.725 cm cylinder was used as the sublimation retort with a sublimation area of 127.2 cm^2. A 2 kg charge was fed into the reactor which was initially 15.27 cm deep. This results in a heap density of 1.03 $g \cdot cm^{-3}$ (Abate & Wilhelm, 1951). No mention was made as to whether the charge was pushed down the cylinder to form a slightly compressed pellet, or was only slightly tapped. Looking at the equipment used, it may be assumed that no compression of the powder took place, since the baffles are placed well above the charge (Figure 2-2). The crystal density of ZrF_4 is 4.43 $g \cdot cm^{-3}$ (Nielsen *et al.,* 2001).

Phases and structures of ZrF_4

Zirconium is found in different forms. There are an amorphous phase and three crystalline phases: α-ZrF_4, β-ZrF_4 and γ-ZrF_4. The β-ZrF_4 phase is known to be thermodynamically stable at room temperature and has a monoclinic structure. The α-ZrF_4 phase, however, has a tetragonal structure and is known to transform to the stable β-ZrF_4 at higher temperatures (Rivas *et al.,* 1997). The transformation of the α-ZrF_4 and γ-ZrF_4 phases to the β-ZrF_4 phase occurs at temperatures exceeding 400 °C (Brown *et al.,* 2005: 144).

Hygroscopicity of ZrF_4 and HfF_4

In a study on the hyperfine characterisation of β-ZrF_4, it was found that β-ZrF_4 is stable in dry N_2 atmosphere between 0 °C and 467 °C and an exposure to wet-air streams has no effects on the hyperfine interaction pattern at room temperature. α-ZrF_4 is moisture sensitive and forms stable hydrated varieties of ZrF_4, *e.g.* $ZrF_4{\cdot}3H_2O$ and $ZrF_4{\cdot}H_2O$ (Rivas *et al.,* 1997). The same should apply for HfF_4.

$HfF_4{\cdot}3H_2O$ begins its dehydration above 57 °C, where HfF_4 is the predominant dehydration product with approximately 30 % $HfF_4{\cdot}H_2O$ remaining (Martínez *et al.,* 1983; Caracoche *et al.,* 1985). Anhydrous HfF_4 can be achieved at 120 °C (Caracoche *et al.,* 1985). The same should apply for ZrF_4.

ZrF_4 form after sublimation

Vacuum sublimation of macroscopic crystals of ZrF_4, prepared by the hydrofluorination of ZrO_2 at 700 °C, yielded transparent crystals with an average dimension of several millimetres and faintly violet in colour (Westrum, 1965). In another study, ZrF_4 was prepared and sublimated in dry HF at 825 °C. 25 g of the resulting water-white needles were then loaded into a 5 cm diameter vitreous carbon crucible and heated to the growth temperature of 650 °C in a flowing atmosphere of diluted HF in He. After 3 days at 650 °C, the mass was cooled to room temperature over a one-day time period. The product formed one clear and transparent continuous uncracked cylindrical disk which underwent only minor cracking during cooldown. Figure 5-2 shows the crystals formed in this study (Robinson & Fuller, 1987).

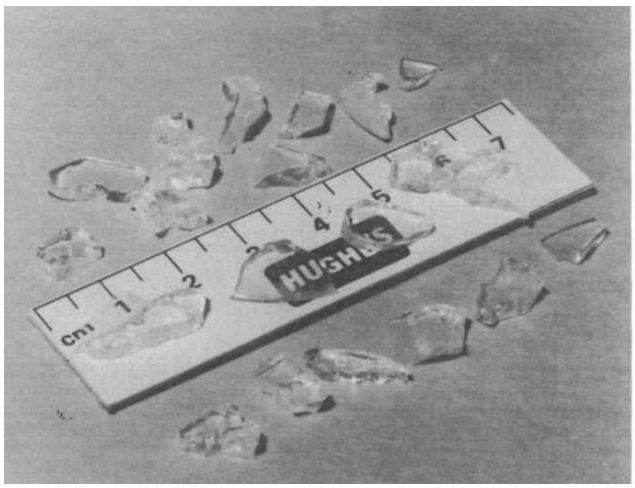

Figure 5-2: Transparent crystals formed by recrystallisation at 650 °C over a 3-day time period (Robinson & Fuller, 1987)

5.1.4 Thermodynamic properties of ZrF_4 and HfF_4

Melting of ZrF_4

The heat of fusion for ZrF_4 at the melting point given in Table 5-4 is -64.22 $kJ \cdot mol^{-1}$, with a liquid ZrF_4 formation enthalpy of -1 975.5 $kJ \cdot mol^{-1}$ (Brown *et al.,* 2005: 147).

Enthalpy and entropy of sublimation for ZrF_4

The heat of sublimation is a crucial parameter in determining the possibility of separating two components in a mixture (Green, 2000). For ZrF_4 and HfF_4 this is, however, more complicated due to their similarities. It can, however, be useful when determining the possibility of separating the metal impurities from the $Zr(Hf)F_4$ mixture. The enthalpy of sublimation for ZrF_4 is approximately 240 $kJ \cdot mol^{-1}$ (Brown *et al.,* 2005; van der Vis *et al.,* 1997; Sense *et al.,* 1954; Konings & Hildenbrand, 1994).

The entropy of sublimation for ZrF_4 is 125.6 $J \cdot mol^{-1} \cdot K^{-1}$ (Cantor *et al.,* 1958).

Enthalpy and entropy of formation

The free energies of formation for ZrF_4 and HfF_4 are listed in Table 5-5.

Table 5-5: Free energy of formation

Reference	Compound	ΔH_{form} [kJ·mol^{-1}]
(Benedict *et al.,* 1981)	ZrF_4 [*1]	-1 582.7
(Benedict *et al.,* 1981)	HfF_4 [*1]	-1 519.9

[*1]Energy of formation from elements at 1 000 K

Table 5-6 lists some chemical thermodynamic data for ZrF_4 in the solid and gaseous state (Brown *et al.,* 2005; Van der Vis *et al.,* 1997).

Table 5-6: Chemical thermodynamic data for ZrF_4 in the solid and gaseous state

Species	ΔG_f° [kJ·mol^{-1}]	ΔH_f° [kJ·mol^{-1}]	S° [J·mol^{-1}·K^{-1}]	C_p° [J·mol^{-1}·K^{-1}]
β-ZrF_4	-1 810.12	-1911.3	104.7-105.3	102.8
ZrF_4(g)	-1 634.58	-1671.1-1673.6	319.4-322.1	87.44

Figure 5-3 to Figure 5-5 give the heat capacity, standard enthalpy and entropy of both solid and gaseous ZrF_4 as a function of temperature.

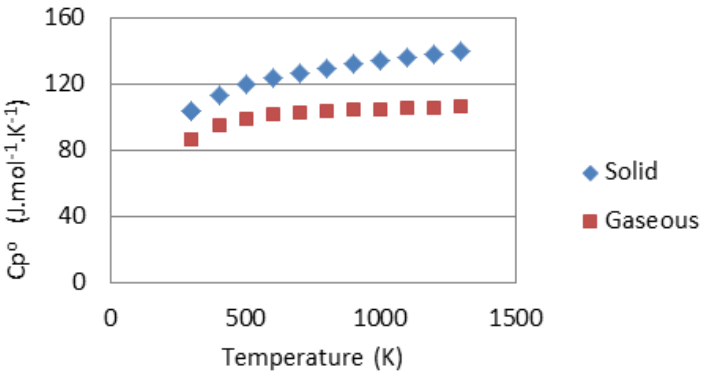

Figure 5-3: Heat capacity as a function of temperature

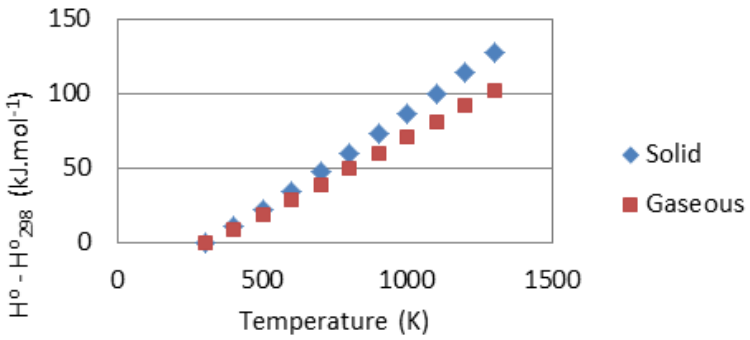

Figure 5-4: Enthalpy as a function of temperature

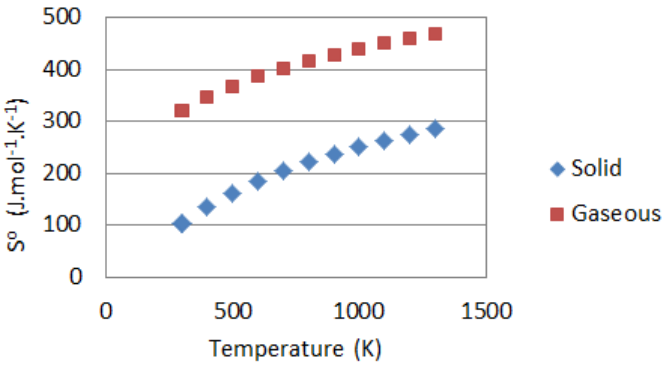

Figure 5-5: Entropy as a function of temperature

Dehydration of $Zr(OH)_4$ to ZrO_2(cr)

$Zr(OH)_4$ dehydration energies depend on several properties, i.e. aging, preparation method, etc. The energy of dehydration to the monoclinic form of ZrO_2 can be in the order of -15.8 $\pm$ 4.5 to 8.2 $\pm$ 4.4, depending on the type of $Zr(OH)_4$ (Brown *et al.,* 2005).

5.1.5 Diffusion coefficients

Thermal separation processes are mass transfer operations which are driven by molecular forces. At least two phases (the mixture phase as well as an auxiliary phase) are present wherein mass and often heat, exchange occurs. The required driving forces are concentration and temperature gradients (Sattler & Feindt, 1995).

Mass diffusion coefficients

In order to calculate the mass transfer coefficient which is required to estimate the sublimation rate, it is first necessary to determine the diffusion coefficients of both ZrF_4 and HfF_4 in nitrogen. The range for diffusivity of a gas at atmospheric pressure is 1 10^{-2} $cm^2 \cdot s^{-1}$ to 10^{-2} $cm^2 \cdot s^{-1}$ (Perry & Green,

1997). The diffusion coefficient can be expressed by the Lennard-Jones potential to evaluate the influence of the molecular forces between the molecules. This correlation, also known as the Chapman-Enskog equation, holds for binary gas mixtures of nonpolar, non-reacting species (Perry & Green, 1997; Welty, 2001), which is the case for ZrF_4 and HfF_4 in nitrogen.

$$D_{i,N2} = \frac{0.001858 \cdot T^{3/2} \cdot \left[\frac{1}{MM_i} + \frac{1}{MM_{N2}}\right]^{1/2}}{P{\sigma_{i,N2}}^2 \Omega_D} \tag{13}$$

Here i represents either ZrF_4 or HfF_4, T is the absolute temperature in K, P is the absolute pressure in atmospheres, MM is the molecular weight, $\sigma_{i,N2}$ is the collision diameter, a Lennard-Jones parameter in Å and Ω_D is the collision integral for molecular diffusion. If the molecular volume, critical temperatures or boiling temperatures of the components are known, then these values can be estimated with empirical relations.

Collision diameter ZrF_4

Equation 14 can be used to calculate the collision diameter of nitrogen with ZrF_4 ($\sigma_{N_2ZrF_4}$) and HfF_4 ($\sigma_{N_2HfF_4}$). An example is given for ZrF_4.

$$\sigma_{N_2ZrF_4} = \frac{\sigma_{N_2} + \sigma_{ZrF_4}}{2} \tag{14}$$

The value for σ_{N_2} is listed in the literature as 3.798 Å (Reid *et al.,* 1988), but these Lennard-Jones parameters are only available for a few pure gases and values for ZrF_4 and HfF_4 may be obtained using empirical correlations. These correlations are, however, dependent on the molecular volumes, the critical volumes and the critical temperatures and pressures, which are not attainable for ZrF_4 and HfF_4. Since σ is denoted as the Lennard-Jones diameter of the respective spherical molecule (Welty, 2001), an estimation will be made for the diameter of a ZrF_4 and HfF_4 molecule with the assumption of spherical molecules. Obtaining such data for both ZrF_4 and HfF_4 in the gas phase is difficult and it will therefore be assumed that a single ZrF_4 and HfF_4 molecule in the gas phase has the same dimensions as a molecule in the solid state.

Sizes of the respective molecules were calculated at room temperature with the use of Spartan software (’14 V1.1.4). The equilibrium geometry was calculated with the Hartree-Fock method with the 6-31* parameter set. Table 5-7 gives a summary of the respective values obtained.

The assumptions made are as follows (a similar approach was used for HfF_4):

- The ZrF_4 molecule approaches a spherical molecule and therefore the diameter approaches the distance between the centre of two opposite F atoms.
- The lengths between all Zr and F atoms are equal.

Table 5-7: Estimating the Lennard-Jones diameter using Spartan software

Description	Diameter element (Å)
Diameter of element F	1.5138
Distance between two F atoms in ZrF_4 molecule	3.098
Distance between two F atoms in HfF_4 molecule	3.059

Equation 14 can now be used to calculate an estimated value for the respective collision diameters. These are listed in Table 5-8.

Table 5-8: Estimating collision diameters for ZrF_4 and HfF_4 with N_2

Collision diameter	Diameter element (Å)
$\boldsymbol{\sigma_{N_2ZrF_4}}$	4.205
$\boldsymbol{\sigma_{N_2HfF_4}}$	4.185

Collision integral

The collision integral (Ω_D) is a dimensionless parameter and a function of the Boltzmann constant κ (1.38×10^{-16} ergs·K^{-1}), the temperature and the energy of molecular interaction $\epsilon_{i,N2}$. Equation 15 can be used to calculate the molecular interaction of nitrogen with ZrF_4 ($\epsilon_{N_2ZrF_4}$). A similar approach is used for the case of HfF_4.

$$\epsilon_{N_2ZrF_4} = \sqrt{\epsilon_{ZrF_4}\epsilon_{N_2}} \tag{15}$$

The value of $\epsilon_i/_{\mathrm{K}}$ for nitrogen gas equals 71.4 (Reid *et al.,* 1988). Values for ϵ_{ZrF_4} and ϵ_{HfF_4} may be obtained with the use of empirical correlations if the critical temperature (T_c) or the normal boiling temperature (T_b) of the components are known:

$$\epsilon_i/_{\mathrm{K}} = 0.77\, T_c \tag{16}$$

$$\epsilon_i/_{\mathrm{K}} = 1.15\, T_b \tag{17}$$

The boiling points for ZrF_4 (912 °C) and HfF_4 (970 °C) are available in the literature (Lide, 2007). These are also indicated as the respective sublimation points. It is common knowledge that ZrF_4 sublimes at temperatures around 600 °C, but for purposes of calculating the Lennard-Jones parameters, the values of 912 °C and 970 °C will be assumed to be satisfactory. Table 5-9 gives the values for the energy of molecular interaction which can be used to determine the collision integrals from the Lennard-Jones constants table (Welty, 2001).

Table 5-9: Collision integral parameters

Collision integral parameters	Value
$\boldsymbol{\epsilon_{ZrF_4}}$	1.881 x 10^{-13} erg
$\boldsymbol{\epsilon_{HfF_4}}$	1.973 x 10^{-13} erg
$\boldsymbol{\epsilon_{N_2ZrF_4}}$	4.305 x 10^{-14} erg
$\boldsymbol{\epsilon_{N_2HfF_4}}$	4.409 x 10^{-14} erg

The values of $^{\kappa T}/_{\epsilon_{N_2ZrF_4}}$ and $^{\kappa T}/_{\epsilon_{N_2HfF_4}}$ are calculated and used to determine the values of the collision integrals $\Omega_{D_{N_2ZrF_4}}$ and $\Omega_{D_{N_2HfF_4}}$. These are inputs to the diffusion coefficient calculation (Equation 13) for ZrF_4 and HfF_4 in nitrogen as a function of the sublimation temperature (Table 5-10).

Table 5-10: Diffusion coefficients for ZrF_4 and HfF_4 in nitrogen at 1 atmosphere

Temperature (°C)	$\boldsymbol{D_{N_2ZrF_4}}$ ($cm^2 \cdot s^{-1}$)	$\boldsymbol{D_{N_2HfF_4}}$ ($cm^2 \cdot s^{-1}$)
700	0.703	0.687
750	0.768	0.751
800	0.836	0.817
850	0.908	0.887

Testing the method for determining the diffusion coefficients

The Lennard-Jones parameters for the diffusion coefficient of SF_6 in nitrogen were calculated with the same method as that used for ZrF_4 and HfF_4 in nitrogen. Using Spartan software, the diameter of an SF_6 molecule was determined to be 3.108 Å, resulting in a collision diameter with nitrogen of 4.151 Å.

The collision integral was estimated with the use of the boiling temperature of SF_6, which is -64 °C.

Table 5-11 lists some calculated and literature values (Marrero & Mason, 1972) for the diffusion coefficient of SF_6 in nitrogen at several temperatures. Since the calculated values are very close to the literature values, the assumption will be made that the method is good enough for determination of the diffusion coefficients of ZrF_4 and HfF_4 in nitrogen.

Table 5-11: Comparison of calculated diffusivities with literature values

Temperature (°C)	Calculated value ($cm^2 \cdot s^{-1}$)	Literature value ($cm^2 \cdot s^{-1}$)
100	0.15309	0.14699
200	0.23240	0.23099
727	0.87951	0.86298

Thermal diffusion coefficients

Kim (2013) showed that the theoretical foundation of thermal diffusion is still Einstein's random walk and added the spatial heterogeneity of the random walk to reflect the temperature gradient of thermal diffusion. The thermal diffusivity and the Soret coefficient (S_T) was then determined theoretically. The walk speed S_w corresponds to the speed of the Brownian particles, which is a function of the temperature. The molecular description of the thermal diffusion coefficient is given by:

$$D_i{}^T = \frac{D_{i,N2}}{S_w}\frac{dS_w}{dT}. \tag{18}$$

The Soret coefficient therefore becomes:

$$S_T = \frac{1}{S_w}\frac{dS_w}{dT} \tag{19}$$

According to Einstein's equipartition theorem, the speed v satisfies:

$$\frac{1}{2}M_B v^2 = \frac{3}{2}\kappa T, \tag{20}$$

Where M_B is the mass of a Brownian particle, T is the temperature and κ is the Boltzman coefficient. Here T is defined by the mean of the kinetic energy of particles. The

velocity is understood as the average velocity in the root mean square sense and therefore it corresponds to the walk speed S_w of the random walk system. Therefore:

$$S_w \equiv v = \sqrt{\frac{3\,\kappa\,T}{M_B}} = c\sqrt{T}. \tag{21}$$

Integration of $\frac{1}{S}\frac{dS}{dT}$ yields:

$$\frac{1}{S_w}\frac{dS_w}{dT} = \frac{1}{c\sqrt{T}}\frac{d(c\sqrt{T})}{dT} = \frac{1}{2T} \tag{22}$$

and therefore

$$D_i{}^T = \frac{D_{i,N2}}{2T} \tag{23}$$

This equation is also used by Nakashima and Takeyama(1989). The Soret coefficient is described as follows:

$$S_T = \frac{1}{2T} \tag{24}$$

It is interesting to note that it is not necessary to know the actual particle speed of the Brownian particles in order to calculate $D_i{}^T$ and S_T.

5.1.6 Flow properties

The mol fractions of ZrF_4 and HfF_4 in the bulk nitrogen gas stream are relatively low due to the large partial pressure of the nitrogen. Most of the flow properties, i.e. Reynolds numbers, Prandtl numbers, etc. are calculated from properties of the nitrogen alone. The Reynolds number is given by Equation (14.

$$Re = \frac{u \cdot\ D_e \cdot \rho_{N_2}(T)}{\mu_{N_2}(T)} \tag{25}$$

Where u is the linear velocity in m·s^{-1} and $D_e = \frac{4\,A_{flow}}{perimeter}$ is the equivalent flow diameter in m and A_{flow} is the flow area in m^2.

5.1.7 Heat transfer

The Prandtl number (Equation 15) for gases should range between 0.7 and 1, which indicates both momentum and heat dissipated through the fluid at about the same time (Çengel & Klein, 2007). The Prandtl number for the current system was calculated as 0.7.

$$Pr = \frac{Cp_{N_2}(T) \cdot \ \mu_{N_2}(T)}{k_{N_2}(T)} \tag{26}$$

Tip of the desublimer

Convective heat transfer for forced convection over a flat plate (in this case the tip of the desublimer) for laminar flow conditions with Reynolds number < 5×10^5 and Prandtl number > 0.6 can be calculated as follows for ZrF_4 and HfF_4 respectively (Çengel, 2006).

$$Nu = 0.664 Re^{0.5} Pr^{1/3} \tag{27}$$

Since the flow in the case of the desublimer tip is not parallel to the plate, but is a cross-flow, a correlation was required to estimate the Nusselt number for cross-flow. The correlation proposed by Churchill and Bernstein for cross-flow over a cylinder was used and the result compared to that obtained for flow over a flat plate (Hewitt *et al.,* 1994):

$$Nu = \ 0.3 + \frac{0.62\ Re^{1/2} Pr^{1/3}}{[1 + (\frac{0.4}{\mathrm{Pr}})^{2/3}]^{1/4}} [1 + \left(\frac{Re}{28\ 200}\right)^{5/8}]^{4/5} \tag{28}$$

Annulus section of the desublimer

Nusselt numbers for laminar flow in annuli may be predicted by the following correlation (Perry & Green, 1997: 5-15):

$$Nu = 1.02 \cdot Re^{0.45} \ \cdot \ Pr^{0.5} \left(\frac{D_e}{L_{c,desub}}\right)^{0.4} \cdot \left(\frac{D_2}{D_1}\right)^{0.8} \cdot \left(\frac{\mu_b}{\mu_w}\right)^{0.14} \cdot Gr^{0.05} \tag{29}$$

Where Re is the Reynolds number calculated using the equivalent diameter of heat transfer, Pr is the Prandtl number, $L_{c,desub} = D_2 - D_1$ is the characteristic length of the annulus section of the

desublimer, where D_2 and D_1 are the outer and inner diameters of the annulus. $D_e = \frac{4 \cdot Flow\ Area}{\pi\ (D_2+D_1)}$ is the equivalent diameter, μ_b is the viscosity at the bulk temperature, μ_w is the viscosity at the wall temperature and Gr is the Grashof number given by Equation (30):

$$Gr = \frac{g\ \cdot \beta \cdot \rho^2\ \cdot \Delta T \cdot\ {L_{c,desub}}^3}{\mu^2} \tag{30}$$

Where $\beta = 1/T_{film}$ is the gas expansion coefficient and ΔT is the difference between the bulk temperature and the desublimer temperature.

All properties are determined at the film temperature which is the average between the bulk gas and desublimer wall temperature.

Convective heat transfer coefficient

The convective heat transfer coefficient can be calculated as follows:

$$\mathrm{h}_{conv} = \frac{Nu.\, k_{N_2}(T)}{D_{eH}} \tag{31}$$

Where D_{eH} is the equivalent diameter of heat transfer, which at the tip of the desublimer was taken as half that of the desublimer diameter. At the annulus section of the desublimer $D_{eH} = \frac{4 \cdot Flow\ Area}{\pi\ D_1}$, where $D_1$is the diameter of the annulus.

5.1.8 Mass transfer

Schmidt numbers are dependent on the diffusion coefficient and are therefore calculated for both ZrF_4 and HfF_4.

$$Sc_{\mathrm{i}} = \frac{\mu_{N_2}(T)}{D_{\mathrm{i}N_2}(P,T)\ \cdot\ \rho_{N_2}(T)} \tag{32}$$

Annulus section

The Sherwood number could not be found for an annulus section. However, these correlations are the mass transfer analogues to heat transfer correlations of the Nusselt number. For a given

geometry, a heat transfer correlation for the Nusselt number in terms of the Reynolds number and the Prandtl number can be used as a mass transfer correlation by replacing the Prandtl number with the analogous dimensionless number for mass transfer, the Schmidt number and replacing the Nusselt number with the analogous dimensionless number for mass transfer, the Sherwood number.

The mass transfer analogue to Equation 29, which is the Sherwood number, can therefore be expressed as follows:

$$Sh_i = 1.02 \cdot Re^{0.45} \cdot {Sc_i}^{0.5} \left(\frac{D_e}{L_{c,desub}}\right)^{0.4} \cdot \left(\frac{D_2}{D_1}\right)^{0.8} \cdot \left(\frac{\mu_b}{\mu_w}\right)^{0.14} \cdot Gr^{0.05} \quad (33)$$

Tip of the desublimer

The mass transfer analogue to heat transfer at the tip of the desublimer for laminar flow conditions with Reynolds number < 5 x 10^5 and Schmidt number > 0.6, the Sherwood number is given by Equation (34) (Çengel, 2006: 817):

$$Sh_i = 0.664 Re^{0.5} {Sc_i}^{1/3} \quad (34)$$

The analogue of the Churchill and Bernstein correlation for cross-flow over a cylinder was also used and the result compared to that obtained for flow over a flat plate (Hewitt *et al.,* 1994):

$$Sh_i = 0.3 + \frac{0.62\, {Re}^{1/2} {Sc_i}^{1/3}}{[1 + (\frac{0.4}{Sc_i})^{2/3}]^{1/4}} [1 + \left(\frac{Re}{28\,200}\right)^{5/8}]^{4/5} \quad (35)$$

Mass transfer coefficient

The mass transfer coefficient is a function of the Sherwood number, diffusion coefficient and characteristic length. In the sublimer, the characteristic length ($L_{c,sub}$) was taken as the width of the bed at any given time increment.

$$k_i = \frac{Sh_i \,.\, D_{i,N2}(P,T)}{L_{c,sub}} \quad (36)$$

In the desublimer, the characteristic length is the equivalent flow diameter in the annulus section and half the outer pipe diameter at the tip of the desublimer.

$$k_i{}^{\omega} = \frac{Sh_i \,.\, D_{i,N2}(P,T)}{D_e} \tag{37}$$

It is interesting to note that $k_i{}^{\omega}$ will differ quite significantly between the front tip section of the desublimer and the annulus section, due to its dependence on D_e and since $Sh_i = f(Re, Sc, duct\ geometry)$.

5.1.9 Lewis number

The Lewis number is a dimensionless number defined as the ratio of thermal diffusivity to mass diffusivity. It is used to characterize a fluid governed by both mass and heat transfer.

$$Le_i = \frac{Sc_i}{Pr} \tag{38}$$

In the case where Le >1, the process is governed by thermal diffusion. This implies that there is not enough time for the desublimating product to be delivered to the desublimator surface in the form of vapour and the process of volumetric desublimation is the dominant one. Volumetric desublimation occurs where the desublimate will transfer from the surface into the volume of gas-vapour mixture (Smolkin *et al.,* 2007).

5.2 Development of a model for the pre-heating of the nitrogen

Nitrogen used as a sweep gas during the sublimation of Zr(Hf)F_4. Pre-heating of the nitrogen is required before the nitrogen enters the section where sublimation takes place. It must be noted that nitrogen does not participate in radiation exchange as with other gases such as CO_2 and water (Çengel, 2006: 746). It is therefore assumed that the nitrogen is only heated by convection.

5.2.1 Model of pre-heating

Figure 5-6 gives an illustration of a 15 m length of ¼'' copper tubing spiralled around the tube furnace pipe which facilitates sublimation. The purpose is to pre-heat the nitrogen used as a sweep gas.

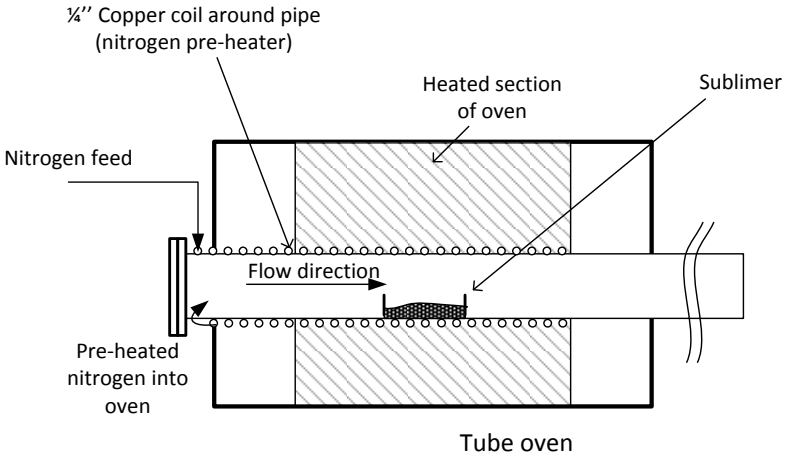

Figure 5-6: Pre-heating of nitrogen featuring ¼'' copper tubing spiralled around the pipe for sublimation in a tube oven

The nitrogen enters one side of the copper tubing and exits into the tube furnace. The nitrogen, now inside the pipe, is then further heated up to the space just before the sublimer.

The following assumptions were made for modelling the pre-heating of the nitrogen:

- Constant wall temperature
- Length of heating zone = 220 mm
- Negligible pressure drop
- Fully developed flow
- Properties are determined with length
- Homogeneous temperature distribution within control volume assumed
- The nitrogen velocity is determined from the set velocity in the desublimer. The velocity of the nitrogen in desublimer is approximately 0·1 $m \cdot s^{-1}$, which is the maximum velocity for the design of desublimers (Niemand, 2012). This amounts to approximately 0·3 $kg \cdot h^{-1}$ of nitrogen.

For fully developed flow under laminar flow conditions, the Nusselt and Sherwood numbers are equal to 3.66 (Çengel, 2006: 817) and only applies for Graetz numbers < 4 (Perry & Green, 1997: 5-15). For horizontal circular tubes and constant wall temperature, where 0.1 < Graetz number < 10^4, the following correlation for the Nusselt number can be used (Perry & Green, 1997: 5-15):

$$Nu = 3.66 + \frac{0.19\,Gz^{0.8}}{1+0.117Gz^{0.467}}\left(\frac{\mu_b}{\mu_w}\right)^{0.14}; \quad (39)$$

Where Gz is the Graetz number, μ_b is the viscosity at the bulk temperature and μ_w is the viscosity at the wall temperature. The Graetz number is calculated as follows:

$$Gz = Re \cdot \mathrm{Pr} \cdot \frac{d}{L}; \tag{40}$$

Where Pr is the Prandtl number, d is the diameter and L is the length of heat transfer.

The temperature of the gas film is the average between the bulk gas temperature and the wall temperature. All properties are calculated at the film temperature.

The average bulk temperature changes along the length of the tube according to Equation 41 (Çengel, 2006: 461).

$$T_{k+1} = T_w - (T_w - T_k) \cdot e^{-\left(\frac{h_{conv} \cdot A_{pipe}}{\dot{m} \cdot C_p}\right)} \tag{41}$$

Where T_k is the temperature at the k^{th} increment, T_w is the temperature of the wall, h_{pipe} is the convective heat transfer coefficient of an empty pipe, A_{pipe} is the surface area of the empty pipe, $\dot{m}$ is the mass flow of the nitrogen gas and C_p is the heat capacity of the nitrogen.

5.3 Development of a sublimation rate model

5.3.1 Predicting sublimation rates

Smith predicted evaporation rates for liquid spills of chemical mixtures (Smith, 2001). These rates are based on the transport of components across a vapour-liquid interface.

The assumptions of this model applicable to sublimation are as follows:

- There are no concentration gradients in the solid phase.
- At the interface, the solid and vapour phases are in equilibrium. This implies that vapour pressure data can be used directly to determine the rate of transfer from the solid phase into the vapour phase.
- Mass transfer is described by a binary diffusion coefficient approximated from the properties of the individual components. These properties include temperature, pressure, molecular weight and the Lennard-Jones constants.

- It is assumed that a thin film of nitrogen separates the vapour-solid interface from the bulk, which has a lower concentration of the chemical. Mass transfer develops quickly in a thin film, therefore it can be assumed that the concentration profile across the film is linear. This allows one to calculate the flux of the material (together with the associated diffusion coefficient). In other words, the evaporation rates of the components can be calculated.

Smith calculated the evaporation time of a liquid by using the vapour-liquid equilibrium relationship given in Equation 42.

$$\frac{dN_i}{dt} = \frac{-Ak_i(P_i^* - p_i')\gamma_i x_i}{RT} = r_{\mathrm{i}} \tag{42}$$

Where N_i is the number of moles of component i; A is the area of the spill; k_i is the film theory average mass transfer coefficient; P_i^* is the vapour pressure of component i; p_i' is the partial pressure of component i in the bulk gas; γ_i is the activity coefficient of component i, which depends on both the temperature and the liquid phase mole fraction; x_i is the mole fraction of component i in the liquid phase; R is the universal gas constant; T is the temperature, t stands for time; and r_{i} is the sublimation rate. It is assumed that the activity coefficients of ZrF_4 and HfF_4 approach unity and can therefore be ignored. The same correlation is used to determine the sublimation rate of both ZrF_4 and HfF_4.

5.3.2 Sublimation mode

The sublimer is a reactor boat (Figure 3-2) 100 mm long and 20 mm deep which can take a maximum of 85 g Zr(Hf)F_4. The Zr(Hf)F_4 to be sublimed is placed in the boat which is placed in a pipe inside the tube furnace (see Figure 3-2, Figure 3-3 and Figure 3-6). Nitrogen is used as the carrier gas. The ZrF_4 and HfF_4 sublime and diffuse into the nitrogen stream. Figure 5-7 illustrates the sublimation mode, whereby the nitrogen enters the sublimer and mixes with a sublimed mass of ZrF_4 and HfF_4. Here r_{ZrF4} is the sublimation rate, Δz is the length of the segment between positions j and $j+1$, $\dot{n}_j$ is the flux of either ZrF_4 (or HfF_4) at the j^{th} position in the sublimation pan and ΔH is the incremental height of the fraction of the bed that sublimed.

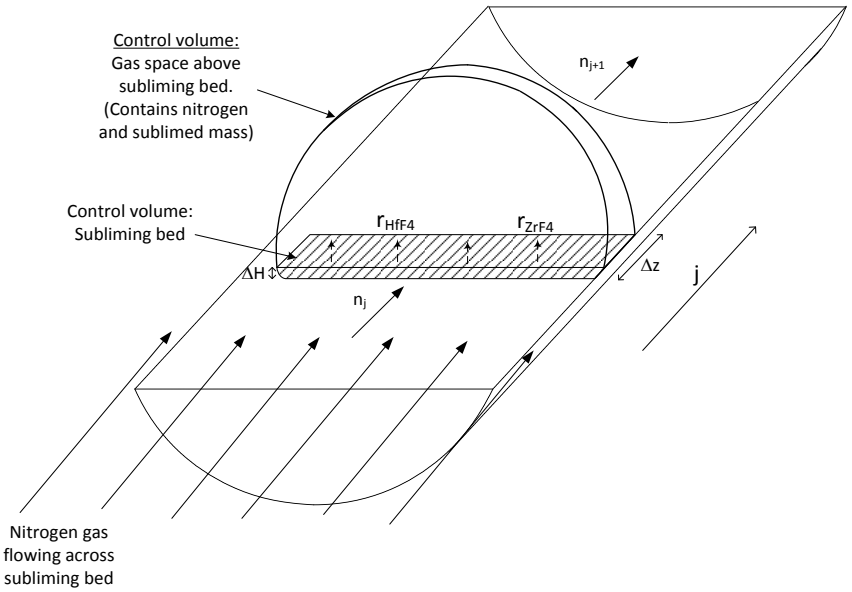

Figure 5-7: Illustration of the sublimation mode and definition of a control volume within the sublimation pan

The following must be taken into account:

- Due to the geometry of the sublimer, the area of sublimation decreases as time proceeds. This implies that the flow area of the gas space above the bed increases as sublimation proceeds.
- The partial pressure of the ZrF_4 and HfF_4 increases as the bulk gas flows across the length of the bed.

The partial pressures of ZrF_4 and HfF_4 exiting the bed are therefore dependent on the extent of sublimation and will therefore change as time proceeds. Figure 5-8 illustrates a cross-section of the sublimer in the tube oven.

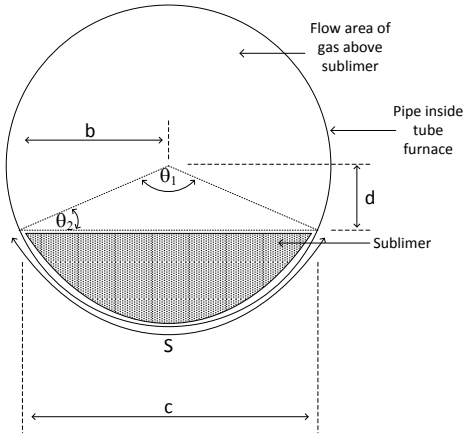

Figure 5-8: Cross-section of the sublimer in the tube oven

The cross-sectional bed area (A_{cross_S}) is calculated by dividing the volume of the bed (function of mass and bed density ρ_B = 800 kg·m^{-3}) by the length of the sublimation pan (100 mm). The value of θ_1 (in radians) is calculated by solving θ_1 in Equation 43.

$$A_{cross_S} = \frac{R^2}{2}(\theta_1 - \sin\theta_1) \tag{43}$$

Where R is the pipe radius with the wall thickness of the sublimer and the spacing between the sublimer and pipe wall subtracted. Now that θ_1 is known, the value of b can be calculated.

$$b = R\sin\frac{\theta_1}{2} \tag{44}$$

Where b is the base of the right-angle triangle θ_2. With the value of b known, the sublimation area ($A_{sub} = 2\,b\,\Delta z$), the time-dependent flow area of the gas above the sublimer ($A_{flow_S} = \frac{\pi\,{D_{pipe}}^2}{4} - A_{cross_S}$), the equivalent flow diameter ($D_{e_S} = \frac{4\,A_{flow_S}}{(\pi\,D_{pipe} - S + 2b)}$) and the arc length $S = \theta_1 R$ can be calculated. These are then used to calculate the velocity and Reynolds number.

The change in flow area (due to the sublimation area decreasing) implies that the new time increment has different properties, i.e. a new equivalent flow diameter, new Reynolds number, new Sherwood number, new mass transfer coefficient and ultimately a new sublimation rate. Furthermore, due to the different vapour pressures of the ZrF_4 and HfF_4 at the sublimation temperature, the rate of sublimation of the two respective fluorides also differs, which implies that the composition of the bed changes as time proceeds.

As more ZrF_4 and HfF_4 sublime and diffuse into the nitrogen stream along the length of the sublimation pan, the volume flow changes since the total pressure is assumed to remain constant. This implies a change in the velocity along the length of the sublimation pan, which has an influence on the Reynolds number and ultimately the rate of sublimation.

As time proceeds, the bed height and ultimately the sublimation area decrease with time, which implies that θ_1 and θ_2 are also functions of the extent of sublimation.

5.3.3 Continuity equation

The general relation for the mass balance may be stated as:

$$\begin{Bmatrix} Net\ rate\ of \\ accumulation\ within \\ control\ volume \end{Bmatrix} = \begin{Bmatrix} Net\ rate\ of\ mass \\ efflux\ from \\ control\ volume \end{Bmatrix} + \begin{Bmatrix} Rate\ of\ generation \\ within\ control \\ volume \end{Bmatrix} \quad (45)$$

which is the continuity equation and can be demonstrated in differential form according to Equation 46:

$$\frac{\mathrm{d}\rho}{\mathrm{dt}} = -\nabla \cdot \mathrm{j} + \mathrm{S} \quad (46)$$

Where ρ is the mol per unit volume (or area) and $\mathrm{j} = (\rho\bar{\mathrm{u}})$ is the flux where $\bar{\mathrm{u}}$ is the flow velocity vector field. S is the "source" or "sink" term which is the generation per unit volume (or area) per unit time. In this case the source term (S) is the sublimation rate (r_i).

The system is operated in such a way that no accumulation of mass occurs within the control volume ($\frac{\mathrm{d}\rho}{\mathrm{dt}} = 0$), which implies that the net rate of mass efflux from the control volume equals the rate of sublimation. The continuity equation becomes:

$$\nabla \cdot (\rho_i \bar{\mathrm{u}}) = r_i \quad (47)$$

Where i denotes ZrF_4 and HfF_4 respectively and r_i is the sublimation rate of ZrF_4 (or HfF_4) in mol per unit sublimation area per unit time (Equation 48).

$$r_{\mathrm{i}} = \frac{k_i(P_{\mathrm{i}}^* - p_{\mathrm{i}}')\, x_{\mathrm{i}}}{RT}, \quad (48)$$

Where k_i is the mass transfer coefficient in $m \cdot s^{-1}$ at time t, P_i^* is the vapour pressure in kPa, p_i' is the partial pressure in the bulk gas, x_i is the mol fraction of the ZrF_4 (or HfF_4) in the unsublimed bulk mass, R is the ideal gas constant (8.314 $kPa \cdot m^3 \cdot kmol^{-1} \cdot K^{-1}$) and T is the temperature in K.

5.3.4 Sublimation rate model

Assuming that the gas flowing above the bed is homogenously mixed within each control volume, the net rate of mass efflux from the control volume can be written as follows:

$$\nabla \cdot (\rho_i \bar{u}) = \frac{1}{r}\frac{d}{dr}(r\,\rho_i\,u_r) + \frac{1}{r}\frac{d}{d\theta}(\rho_i\,u_\theta) + \frac{d}{dz}(\rho_i.u_z) = \frac{d}{dz}(\,\rho_i\,u_z) \tag{49}$$

The net rate of mass efflux from the control volume therefore reduces to:

$$\frac{d}{dz}(\,\rho_i\,u_z) = \dot{n}_{j+1} - \dot{n}_j \tag{50}$$

In order to calculate the change in total flux along the length of the sublimation pan, the pan is divided into segments of length Δz and the flux in each following segment is calculated by adding the flux in the previous segment to the sublimed masses of ZrF_4 and HfF_4 in segment j of length Δz. The continuity equation therefore becomes:

$$\dot{m}_{i,j+1,t_g} = \dot{m}_{i,j,t_g} + \frac{k_{i,j,t_s}(P_i^* - p'_{i,j,t_s})\;x_{i,t}}{RT} MM_i\;\Delta z 2\;b \tag{51}$$

Where $\dot{m}_{i,j,t_g}$ is the total mass flow at time $t$of species i in the gas phase at the j^{th} position.

Time dependency

The mass left in the sublimation pan reduces as sublimation continues and can be approximated by subtracting the total mass sublimed at time t from the mass in the bed at time t:

$$M_{i,t+1_s} = M_{i,t_s} - \frac{\sum_{j=1|t}^{n}(k_{i,j,t_s}(P_i^* - p'_{i,j,t_s})\;x_{i,t}}{RT} MM_i\;\Delta z 2\;b\;\Delta t \tag{52}$$

Where M_{i,t_s} is the mass of ZrF_4 or HfF_4 at time t and Δt is the time increment.

5.3.5 Flow diagram for calculations of the sublimation process

Nitrogen enters the sublimation section where both ZrF_4 and HfF_4 sublime and diffuse into the bulk. The partial pressures of both ZrF_4 and HfF_4 increase as the bulk gas moves across the sublimer. The area of sublimation, flow area and bed composition changes with time, which implies that the sublimation rates change as sublimation proceeds as do the desublimation of the respective compounds. Should the mass left be equal to zero (or a set minimum) then the loop will stop and sublimation is complete. Figure 5-9 shows the process flow calculations diagram for the sublimation process.

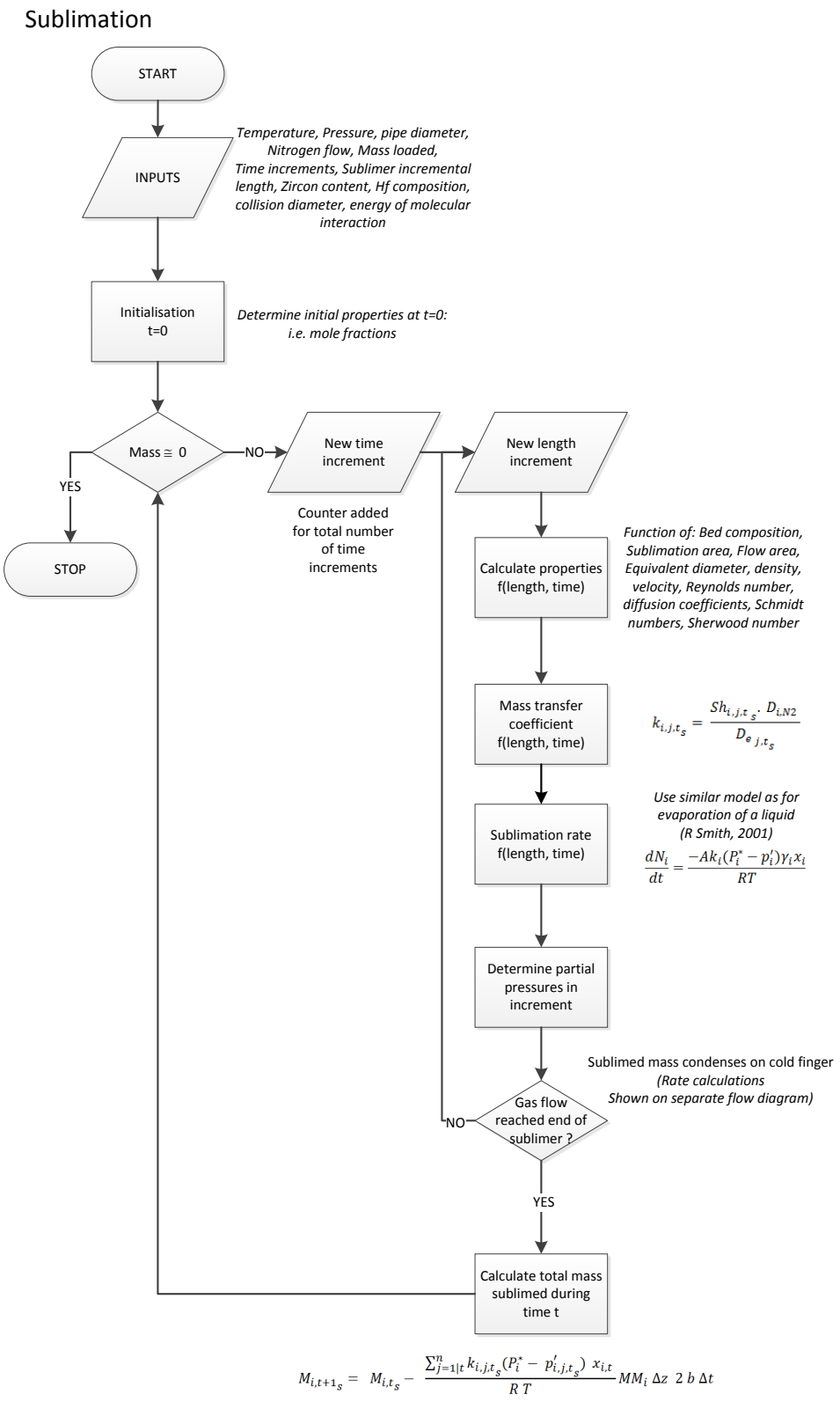

Figure 5-9: Flow calculations for the sublimation of ZrF_4 and HfF_4 as a function of the sublimation time and the length of the bed

5.4 Development of a desublimation rate model

In a multicomponent system, there are fluxes of momentum, energy and mass, each resulting from a different driving force (Table 5-12).

Table 5-12: Relationships between fluxes and driving forces

	Driving forces		
Flux	Velocity gradients	Temperature	Concentration Pressure External force
Momentum	Newton's law $[\mu, k]$		
Energy		Fourier's law $[k]$	Dufour effect $[D_i{}^T]$
Mass		Soret effect $[D_i{}^T]$	Fick's law $[D_{iN2}]$

There are three "mechanical driving forces" that tend to produce movement of a species with respect to the mean fluid motion. These are concentration gradient, pressure gradient and external forces acting on the species. For purposes of this study, it will be assumed that the effects of pressure gradient and external forces are negligible (Bird *et al.,* 1960: 564-565). Therefore the diffusion currents are made up of both density (Fick's law) and temperature gradients (Ludwig-Soret effect). This macroscopic description of thermodiffusion dates back to the 19th century and was developed in the context of standard kinetic theory and therefore applies to dilute gas mixtures only (Debbasch &Rivet, 2011).

5.4.1 Concentration and thermal diffusion contributions to the mass flux

Since the diffusion currents are made up of density (Fick's law) and temperature gradients (Ludwig-Soret effect), the mass flux can therefore be defined by two terms: (a) the concentration gradient, i.e. the concentration contribution to mass flux:

$$J_i{}^{\omega} = - D_{i,N2}\rho\nabla\omega_i \tag{53}$$

and (b) the temperature gradient, i.e. the thermal diffusion contribution to mass flux:

$$J_i^T = -D_i^T \rho \omega_i \nabla T \tag{54}$$

$D_{i,N2}$ is the mass diffusion constant ($m^2 \cdot s^{-1}$) of the diffusing species i in nitrogen, ρ is the density of the bulk gas ($kg \cdot m^{-3}$), ω_i is the mass fraction of the diffusion species, D_i^T is the thermal diffusion coefficient (a measure of the mass diffusion process due to temperature) and T is the temperature (Bird *et al.,* 1960: 502; Dominguez *et al.,* 2011; Kim, 2013).

The thermal diffusion term (J_i^T) describes the tendency for species to diffuse under the influence of a temperature gradient. The species move toward colder regions and a concentration gradient is formed. The effect is small, but separations of mixtures can be effected with steep temperature gradients (Bird *et al.,* 1960: 567; Kim, 2013).

The total mass flux is obtained by adding the concentration and temperature contributions together:

$$J_i = J_i^{\omega} + J_i^T \tag{55}$$

In preceding sections it was shown that $D_i^T = \frac{D_{i,N2}}{2T}$ and therefore the total mass flux equation can now be written as:

$$J_i = -D_{i,N2} \rho \nabla \omega_i - \rho \omega_i \frac{D_{i,N2}}{2T} \nabla T \tag{56}$$

5.4.2 Desublimation mode

The desublimer is situated inside a bigger pipe, which facilitates the sublimation. The coordinates z, r and θ are defined in Figure 5-10.

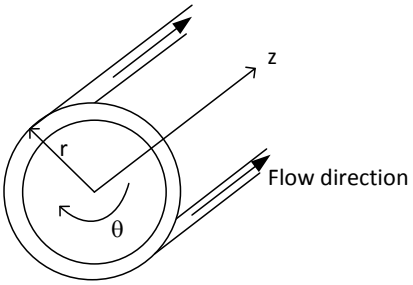

Figure 5-10: Definition of coordinates in annulus section of the desublimer

Figure 5-11 gives an illustration of the two driving forces leading to mass transport to the surface. Here $\omega_{i,w}$ and $\omega_{i,b}$ are the mass fractions of the diffusion species at the wall and in the bulk gas respectively. T_w and T_b are the temperatures at the wall and in the bulk gas.

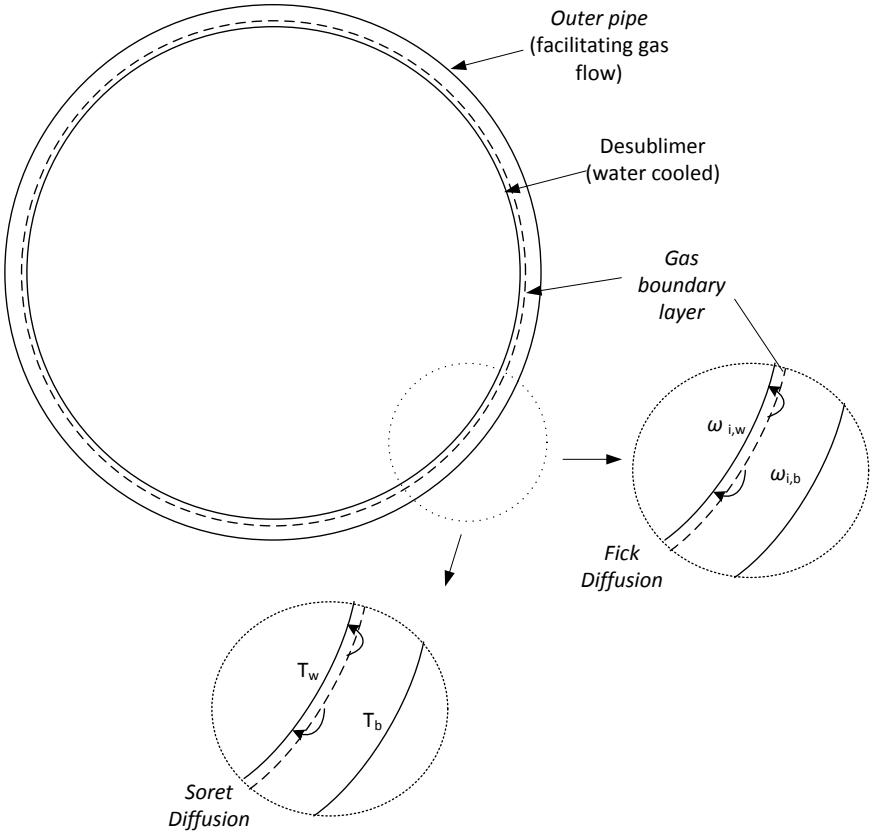

Figure 5-11: Cross-section of annular probe indicating the driving forces resulting in mass transport to the surface

It is assumed that $\frac{d\omega_i}{d\theta} = 0$ and that $\frac{d\omega_i}{dr} \ggg \frac{d\omega_i}{dz}$ and therefore:

$$\nabla\omega_i = \frac{d\omega_i}{dz} + \frac{d\omega_i}{dr} + \frac{d\omega_i}{d\theta} = \frac{d\omega_i}{dr} \tag{57}$$

The same assumption applies for the temperature change, where it is assumed that $= \frac{dT}{dr}$.

The total mass flux equation now reduces to:

$$J_i = -D_{i,N2}\rho\frac{d\omega_i}{dr} - \rho\,\omega_i\frac{D_{i,N2}}{2T}\frac{dT}{dr} \tag{58}$$

The concentration contribution to mass flux (${J_i}^{\omega}$) can therefore be written as:

$$ {J_i}^{\omega} = - D_{i,N2}\, \rho \frac{d\omega_i}{dr} \equiv \frac{{k_i}^{\omega} \cdot MM_g \cdot \left(p'_{\mathrm{i,b}} - p^*_{\mathrm{i,w}}\right)}{R\, T_f} \tag{59} $$

Where ${k_i}^{\omega}$ is the mass transfer coefficient in the desublimer which is a function of the mass diffusivity and the film thickness; $p'_{\mathrm{i,b}}$ is the partial pressure of species A in the bulk gas; $p^*_{i,w}$ is the vapour pressure at the wall temperature; and T_f is the film temperature which is the average of the bulk and wall temperature. The temperature contribution to mass flux can therefore also be written as a function of the mass transfer coefficient, where T_f is the film temperature.

$$ {J_i}^{T} = -\rho\, \omega_i \frac{D_{i,N2}}{2T} \frac{dT}{dr} \equiv \frac{{k_i}^{\omega} \cdot MM_g \cdot p'_i \cdot (\mathrm{T}_b - \mathrm{T}_w)}{2\, R\, {T_f}^2} \tag{60} $$

5.4.3 Desublimation rate model

In order to calculate the change in total flux along the length of the desublimer (annulus), the length is divided into segments of length Δz and the flux in each following segment is calculated by subtracting the desublimed masses of ZrF_4 and HfF_4 in the segment from the flux in the previous segment. The incremental mass balance in the desublimer along the length of the annulus can therefore be expressed by the following equation:

$$ \dot{m}_{i,j+1,t_g} = \dot{m}_{i,j,t_g} - \frac{{k_i}^{\omega} MM_g \Delta z\ 2\,\pi\, D_1}{R\, T_f} \left[\left(p'_{i,b} - P^*_{i,w}\right) + \frac{p'_{i,b} \cdot (T_b - T_w)}{2\, T_f} \right] \tag{61} $$

5.4.4 Flow calculations for the desublimation rate model

The flow calculations for the desublimation rate model are shown in Figure 5-12. The sublimed mass with calculated partial pressures for both the ZrF_4 and HfF_4 in the gas mixture enters the desublimer space. These are dependent on time and change as sublimation proceeds. Both heat and mass transfer play a role as the ZrF_4 and HfF_4 desublime. The bulk gas first desublimes on the tip of the desublimer, which is closest to the sublimation space. As the gas passes along the length of the desublimer, both the ZrF_4 and HfF_4 desublime, resulting in an increase in gas enthalpy due to the exothermic nature of desublimation. The gas is also cooled by the desublimer as it passes along the length of the desublimer. Therefore the gas enthalpy is a function of the convection cooling and the rate of desublimation along the length of the desublimer. The calculated gas enthalpy is used to

obtain a gas temperature (assumed N_2 only), which is done by interpolating enthalpy data (Boulos *et al.,* 1994). The new temperature at the next increment is now used to calculate the properties and the desublimation rate in the next increment.

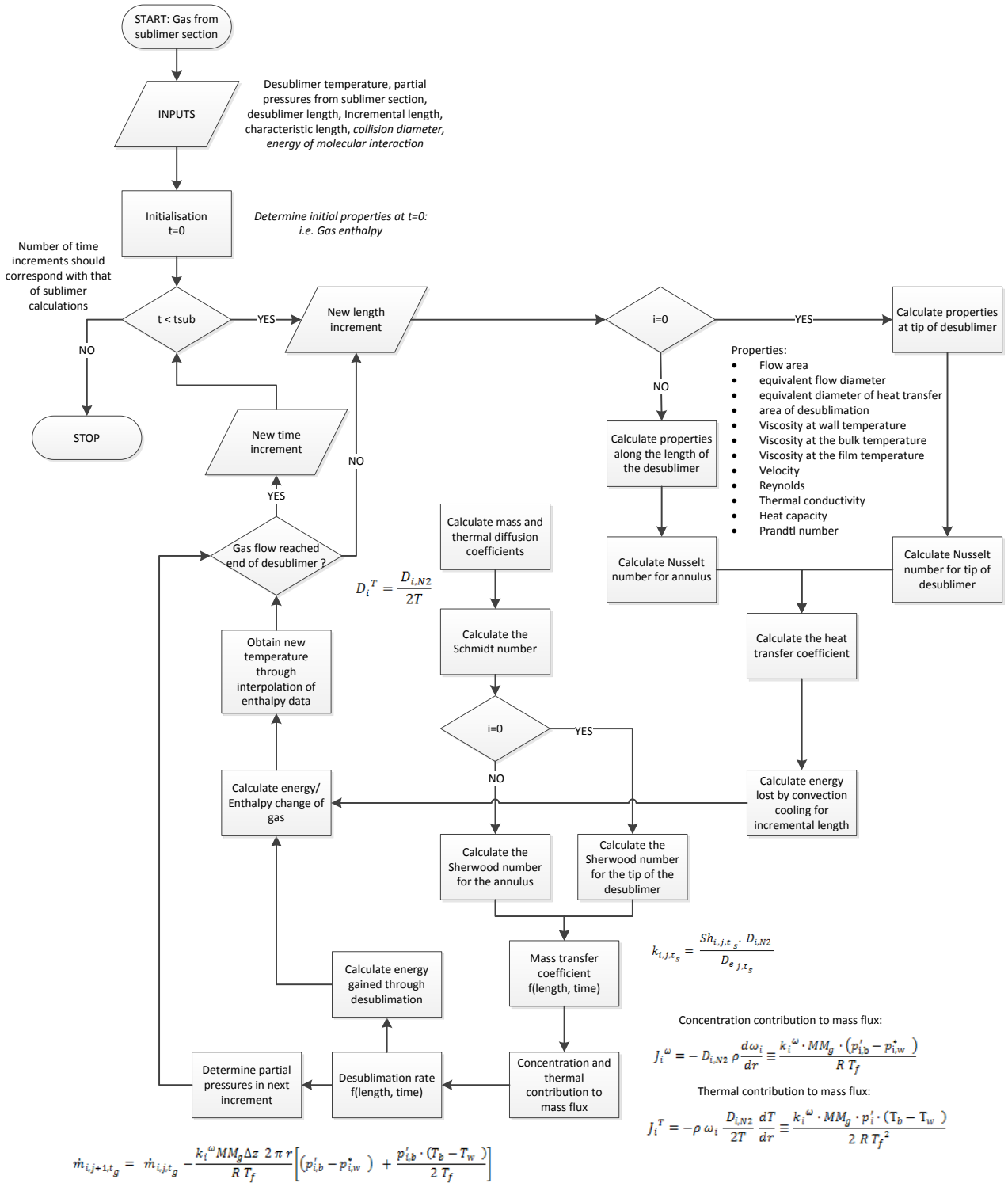

Figure 5-12: Flow calculations for desublimation of ZrF_4 and HfF_4 as a function of length of time

Chapter 6: Results and discussion

6.1 Model parameters

6.1.1 Variables

Sublimation temperature – The temperatures studied included 740 °C, 760 °C and 790 °C.

6.1.2 Constants

Pressure – An absolute pressure of 87 kPa was used and kept constant (open system).

Nitrogen feed – The nitrogen velocity was determined from the set velocity in the desublimer. The velocity of the nitrogen in the desublimer was approximately 0.1 $m \cdot s^{-1}$, which is a maximum velocity for the design of desublimers (Niemand, 2012). This amounts to approximately 0.3 $kg \cdot h^{-1}$ of nitrogen at room temperature.

With a nitrogen flow of 0.3 $kg \cdot h^{-1}$, the molar fractions of ZrF_4 and HfF_4 in the bulk gas stream at 740, 760 °C and 790 °C were below 0.01 %. This implies that the properties are relatively constant and independent of the contributing properties of the ZrF_4 and HfF_4. It is therefore assumed that the properties of nitrogen can be used as an estimate of the bulk gas properties.

Initial HfF_4 in bulk unsublimed material

The initial HfF_4 in bulk unsublimed material was calculated, assuming 1.32 % HfO_2 in PDZ (analysed by Pelindaba Analytical Laboratory on 6 July 2004) and 94 % dissociation of the zircon. The calculated initial HfF_4 content was 1.67 %.

6.2 Nitrogen preheating

Previous preheating of the nitrogen was achieved by flowing nitrogen over copper shavings at 700 °C in a separate muffle furnace. The outlet temperature of the nitrogen was 400 °C. The outlet of the muffle furnace was connected to the inlet of the tube furnace with one metre length of ½-inch copper tubing insulated with glass wool and tape. The nitrogen temperature measured at the entrance of the tube furnace was 30 °C, emphasising how quickly the nitrogen cools down. It is therefore assumed that the nitrogen heats up just as rapidly as it cools down.

With the oven at a set temperature and the additional preheating with ¼-inch copper coil on the outside of the pipe (Figure 5-6) and with the additional heating zone within the tube furnace, the temperature of the nitrogen gas at the sublimer point was assumed to be at the sublimation temperature, which was typically 30 °C lower than the set temperature of the oven.

6.3 Sublimation rate

The nomenclature $Zr(Hf)F_4$ defines a ZrF_4 crystal structure in which a percentage of the Hf is substituted for Zr. ZrF_4 and HfF_4 behave differently in the vapour phase as a function of temperature, i.e. due to the differences in vapour pressures. This implies that HfF_4 is thermodynamically less stable than ZrF_4. It is therefore assumed that the ZrF_4 will sublime separately from the HfF_4 due to the differences in thermodynamic stability of the two compounds.

The rate is dependent on the vapour pressure as well as the concentration of the components in the bulk mass to be sublimed. This implies that ZrF_4 will sublime at a much higher rate than the HfF_4 due to the higher vapour pressure at the temperature of the sublimer. The sublimation rate was determined at different temperatures and is shown in Figure 6-1. Here α is the ratio of the actual mass sublimed to the maximum potential sublimate (i.e. zircon subtracted).

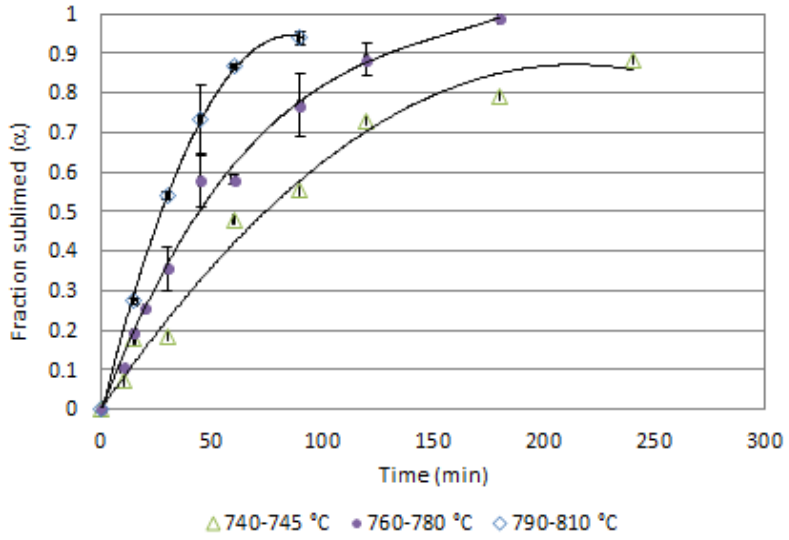

Figure 6-1: Sublimation rate of $Zr(Hf)F_4$ as a function of the sublimation temperature

One explanation for the sublimation rate forming a plateau before complete sublimation has been achieved (Figure 6-1) is the formation of a crust-like surface or sintered cake (Figure 6-2) which prevents further sublimation from occurring. This may be due to the presence of impurities

originating from the zircon. The sublimation temperature stays the same, but sintering of the cake negatively influences the sublimation kinetics.

Figure 6-2: Sublimer residue indicating cake formation

Figure 6-3 illustrates the formation of humps in the sublimer residue which may be an indication that the $Zr(Hf)F_4$ also sublimes from the bulk mass and not only from the surface. The hump formation may also be an indication that sublimation is taking place within the bulk volume, but it is not necessarily precise to assume that these sublimed masses actually escaped. For purposes of this study, the experimental rates obtained are compared to the modelled rates obtained for dependency on surface area only.

Figure 6-3: Sublimer residue indicative of hump formation

The linear section in Figure 6-1 (experimental results) is most importance for purposes of determining the rate and is shown in Figure 6-4.

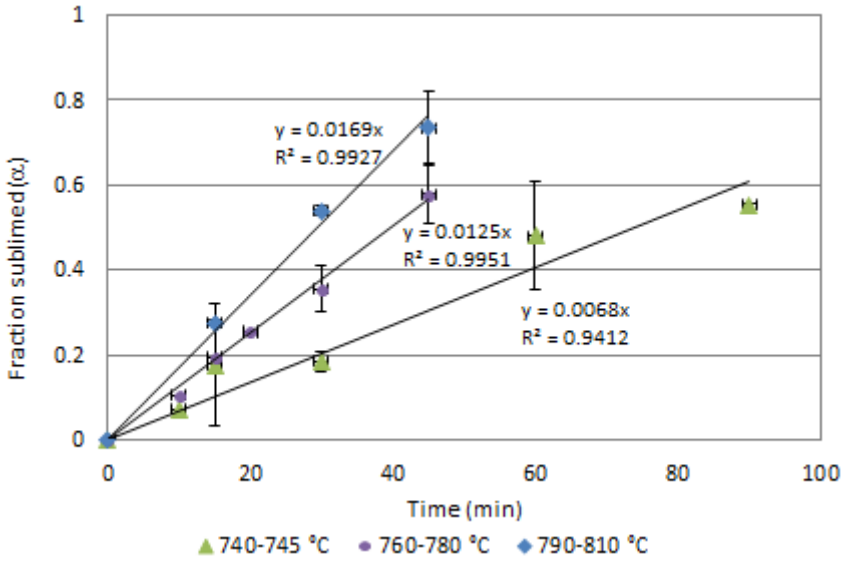

Figure 6-4: Linear section of the sublimation rate as a function of the temperature

The linear sections of the modelled rates are shown in Figure 6-5 and compared to the experimental results obtained. The model accurately predicts the rates of sublimation at the lower temperatures, but seems to over-predict at the higher temperatures.

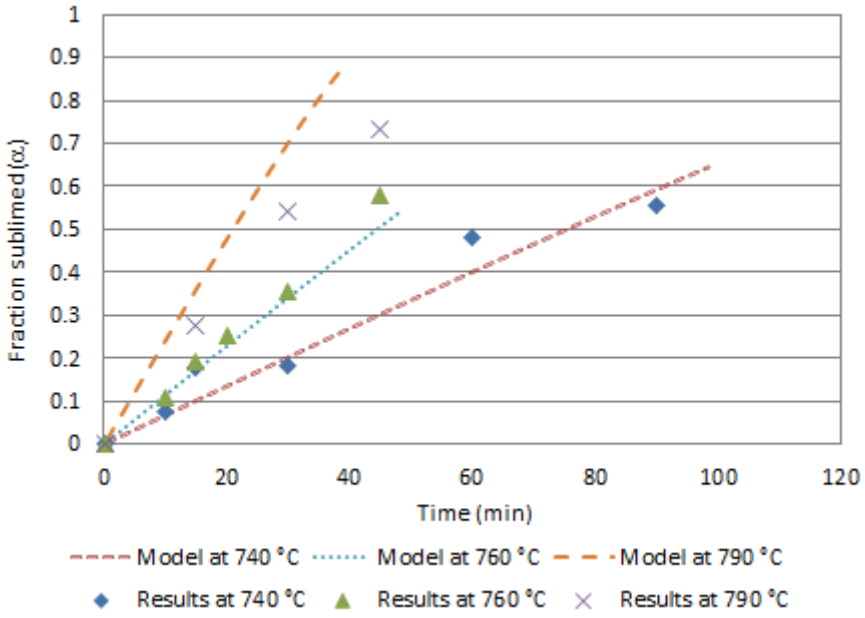

Figure 6-5: Modelled sublimation rates compared with experimental results

The slope of the fraction sublimed versus time (dα/dt inFigure 6-5) was plotted as a function of the temperature (Figure 6-6). These are shown for both the experimental and modelled results.

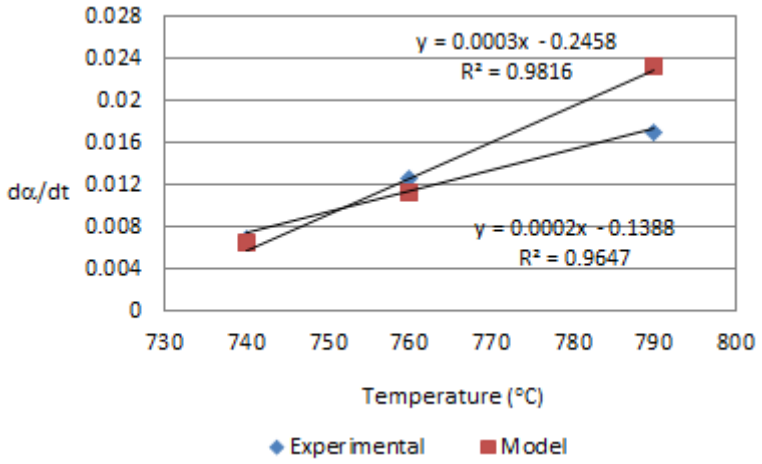

Figure 6-6: Slope of the fraction sublimed vs. time as a function of the sublimation temperature

It must be noted that the rate ($\frac{d\alpha}{dt}$) depends on the initial mass loaded (~15 g) as well as the sublimation area, with the sublimation area being a function of time.

This over-prediction of the sublimation rate at 790 °C may be even worse at even higher temperatures. For instance, the model predicts an average total flux of 7.34 $g \cdot m^{-2} \cdot s^{-1}$ for ZrF_4 and HfF_4 subliming at 850 °C. This predicted value is 3.9 times higher than the value estimated from literature data (1.87 $g \cdot m^{-2} \cdot s^{-1}$). The flux at 850 °C could not be determined experimentally due to equipment and material constraints. One reason for this might be because of the impurities present in the sample used by MacFarlane *et al.* (2002), since the presence of impurities can have a direct influence on the sublimation rate (Ti *et al.,* 1990c). Ti *et al.* found that the sublimation rates were 13 % to 20 % lower when industrial $Zr(Hf)F_4$ samples were used compared to pure $Zr(Hf)F_4$. This implies that the modelled values are allowed to differ from the experimental results obtained. It is assumed that these differences may be even higher at higher sublimation temperatures. However, under vacuum conditions, the flux was estimated from the literature to have an approximate value of 13.8 $g \cdot m^{-2} \cdot s^{-1}$ at this temperature, which emphasizes the statement made by Abate and Wilhelm (1951) that the use of vacuum increases the movement of vapour.

To indicate the extreme effect of the temperature on the total sublimation time, the modelled result for the total sublimation time of 15 g $Zr(Hf)F_4$ as a function of the sublimation temperature is shown in Figure 6-7. This is based on no crust formation and/or sintering of the cake.

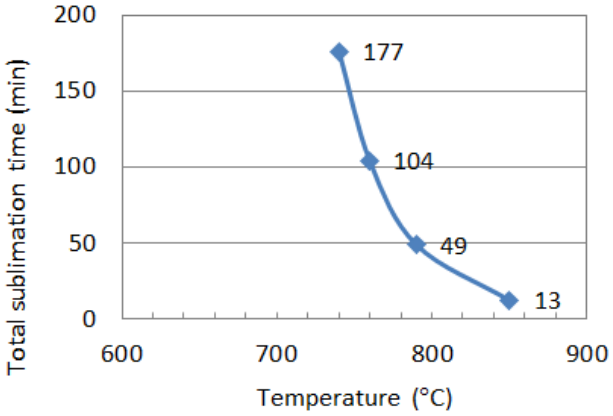

Figure 6-7: Modelled result for the total sublimation time as a function of the sublimation temperature

6.4 Separation within the sublimer

The ZrF_4 and HfF_4 masses remaining in the sublimer are shown in Figure 6-8. These are for a sublimation temperature of 790 °C. The model times out when the ZrF_4 or HfF_4 is less than 1/100th of the initial mass. From this figure it is seen that, should the sublimer be removed from the oven at a time when most of the sample has sublimed, the sublimer residue will be rich in Hf.

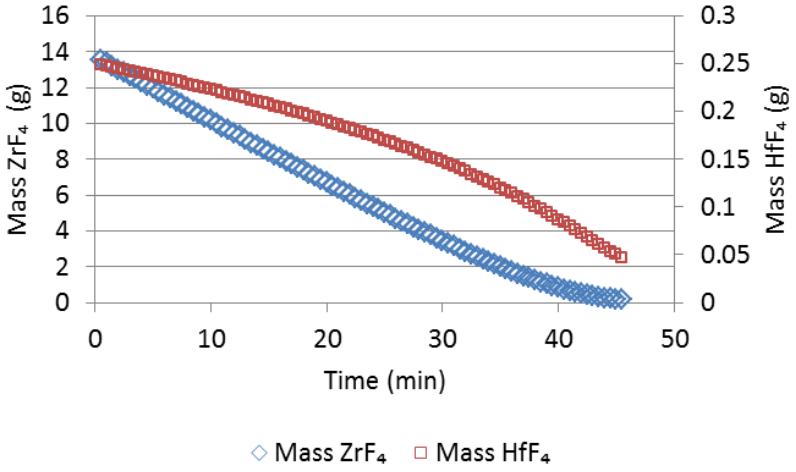

Figure 6-8: ZrF_4 and HfF_4 sublimer residue as a function of sublimation time at 790 °C

Zr/Hf mole ratios for the sublimer residue ranged between 86 (raw ZrF_4) and 30, depending on the sublimation temperature and duration. From Figure 6-9 it is evident that the sublimer residue becomes "Hf rich" with time due to the fact that HfF_4 sublimes at a lower rate than ZrF_4. It is important to note that separation between Zr and Hf is achieved within the sublimer. A lower ratio is indicative of a higher Hf content in the residue, which implies that the sublimer must be left in the oven for as long as possible, but must be removed once most of the ZrF_4 has sublimed.

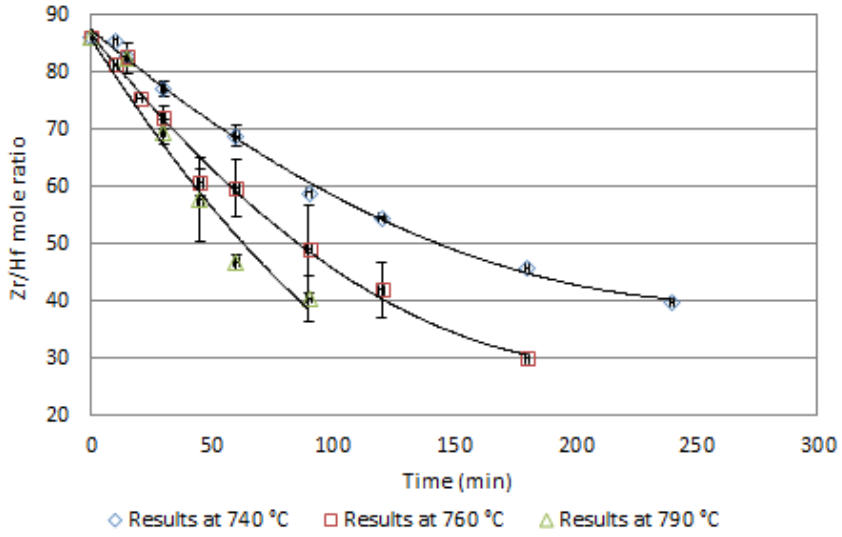

Figure 6-9: Zr/Hf mole ratio of the sublimer residue as a function of time and temperature

Comparing the linear section of the Zr/Hf mole ratio data in Figure 6-9 with that obtained from the model indicates that the model predicts too high a sublimation rate for the HfF_4, resulting in a lower Zr/Hf mole ratio. Model predictions were out by a factor of 1.6 at 740 °C, 1.7 at 760 °C and 2.8 at 790 °C. The slope of the linear section of the Zr/Hf mole ratio versus time (Figure 6-9) was plotted as a function of the sublimation temperature. These are shown for both the experimental and modelled results (Figure 6-10).

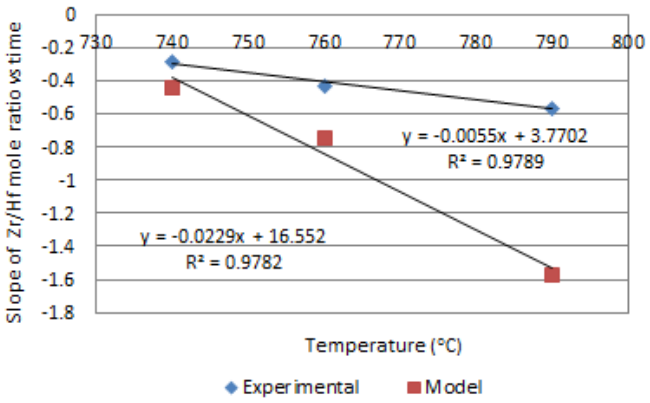

Figure 6-10: Slope of Zr/Hf mole ratio vs. time as a function of the sublimation temperature

From this figure it is seen that the model predictions are even worse at higher temperatures. The vapour pressure data for ZrF_4 was taken from four sources with a standard error of 48.2 and 0.055 for the constants A and B respectively. One explanation for the modelled Zr/Hf being lower may be that the vapour pressure data (single literature source) are possibly wrong, which can be true due to the strong dependency of the vapour pressure on temperature.

6.5 Separation within the desublimer

It is assumed that the sublimed ZrF_4 and HfF_4 desublimes into a crystal structure in which the Zr and Hf occur in identical crystallographic positions as with the starting material.

Desublimation has the disadvantage of low product yield, which is caused by the formation of aerosols at a high super-cooling level of the source vapour. Due to this, the decision was made to take triplicate sublimer masses of 15 g each, once the others had been exposed to the sublimation temperature for 30 minutes each, thereby to increase the total mass sublimed and also the total mass desublimed. The mass desublimed on the desublimer was sampled at several intervals to determine whether there was a difference in the Zr/Hf ratio with the length of the desublimer. Figure 6-11 illustrates the desublimer with desublimed $Zr(Hf)F_4$ and the respective sampling point.

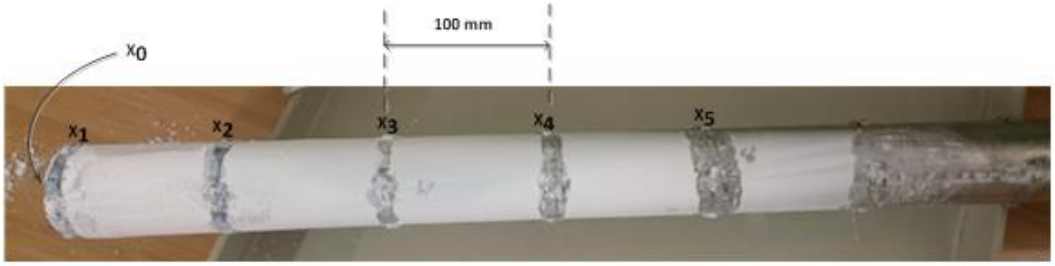

Figure 6-11: Sample positions on the desublimer

Here X_0 is the tip of the desublimer closest to the heating zone and along the length of the desublimer are X_1 through to X_5 which are 100 mm apart, with X_1 being the first 10 millimetres on the desublimer. The sublimation temperatures investigated were 700 °C, 740 °C and 790 °C.

6.5.1 Experimental results

Figure 6-12 gives the Zr/Hf mole ratio of the collective mass obtained throughout on the desublimer.

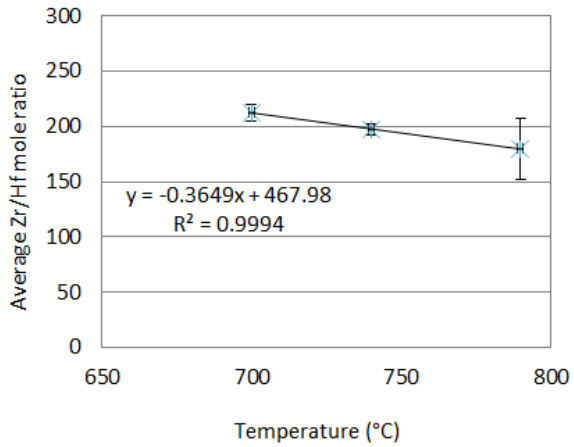

Figure 6-12: Zr/Hf mole ratio across the length of the desublimer

It is clear that the sublimation temperature does have an effect on the separation achieved in the desublimer. A lower sublimation temperature will result in a higher mole ratio (better separation) of the collective desublimed mass.

The Zr/Hf mole ratios atX_0 differed from experiment to experiment with no repeatable results and are therefore not shown. No results are shown for the Zr/Hf mole ratios from X_4 onward since there were not enough data collected for analysis due to the amount of desublimed product which varied from experiment to experiment. The Zr/Hf mole ratios at X_1, X_2 and X_3 at the respective temperatures are shown in Figure 6-13. Again it is shown that there is a definite relationship between the mole ratio and the temperature, where a lower temperature gives better separation.

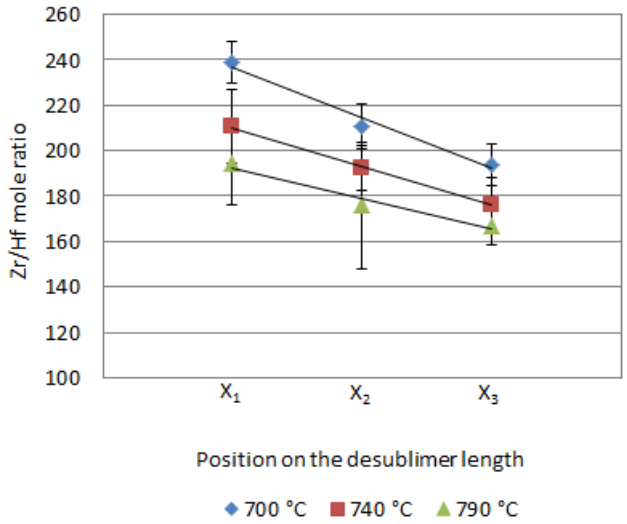

Figure 6-13: Temperature-dependent mole ratios as a function of desublimer position

The mole ratio range (span) at lower temperatures is also larger, indicating better separation across the length of the desublimer. The mole ratio at 700 °C ranges from 239 at X_1 up to 194 at X_3 giving a

range of 45, whereas at 790 °C the mole ratio range is approximately 27 between X_1 and X_3, indicating that better separation is achieved across the length of the desublimer at lower temperatures.

A plot of the slopes (in Figure 6-13) versus temperature for X_1 to X_3 is shown in Figure 6-14. This may be used to predict the mole ratios at different positions on the desulbimer with the assumption of linearity.

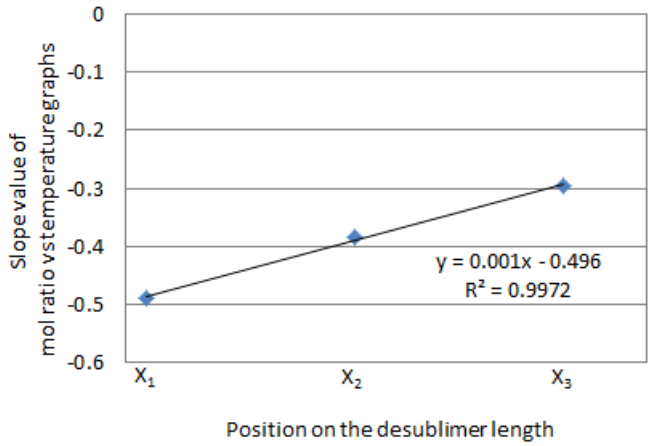

Figure 6-14: Linear relationship for the slope of the Zr/Hf mole ratio versus temperature graphs as a function of the position on the desublimer

These results may be used to predict separation further along the length of the desublimer.

Approximately 50 % of the sublimed mass desublimes at a sublimation temperature of 700 °C and 740 °C, whereas 70 % of the sublimed mass desublimes at 790 °C. The desublimed mass as a function of the sublimation temperature is shown in Figure 6-15.

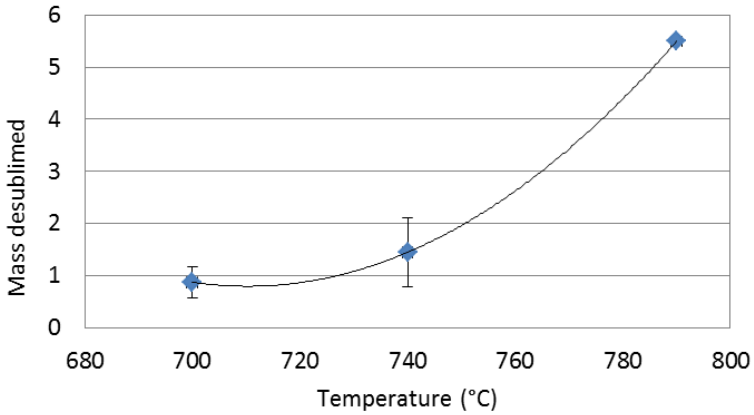

Figure 6-15: The amount of mass that desublimes is a function of the sublimation temperature

6.5.2 Model predictions

Figure 6-16 shows the experimental and model results obtained for separation along the length of the desublimer. Model predictions indicate better separation with mole ratios typically higher by a factor of 1.5 at 700 °C and 740 °C and 1.2 at 790 °C.

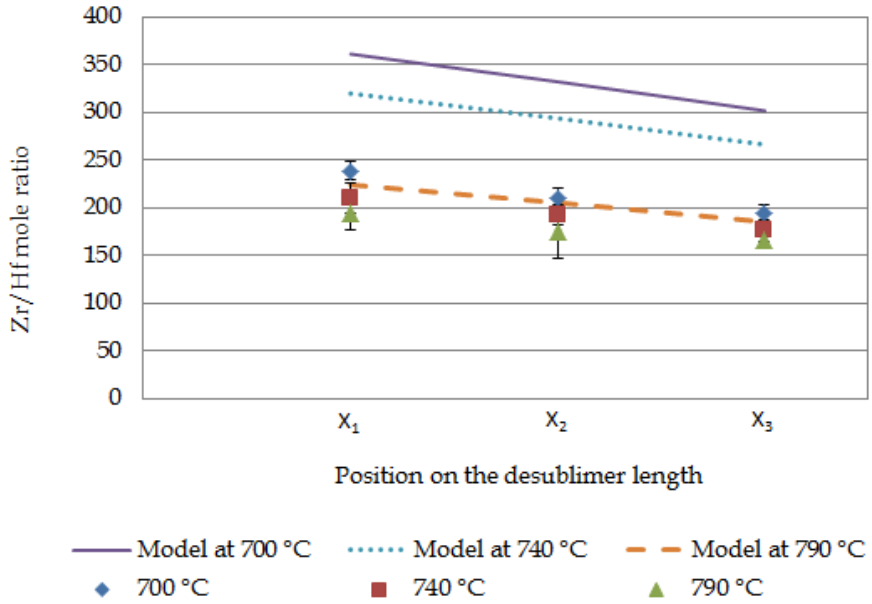

Figure 6-16: Experimental and model results obtained for separation along the length of the desublimer

Model predictions indicated that approximately 55 % of the sublimed mass desublimes over the 300 mm length, irrespective of the temperature.

6.5.3 Bulk gas temperature

The bulk gas temperature measured was 500 °C at X_1 (Figure 6-17) at a sublimation temperature of 790 °C.

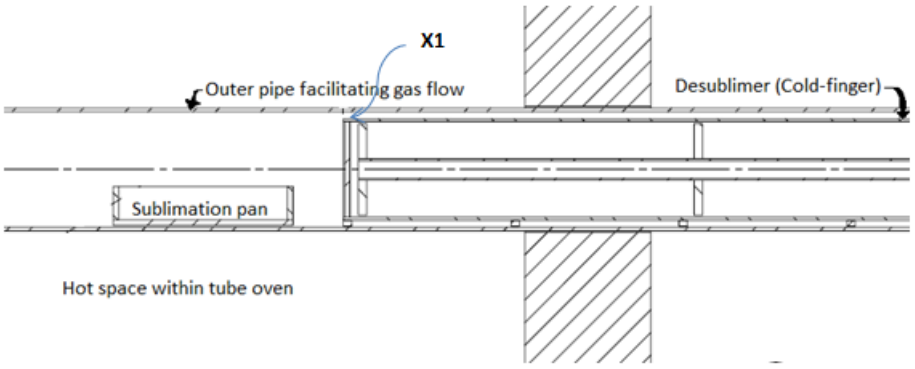

Figure 6-17: Schematic of sublimer and desublimer inside tube furnace

The modelled result for the cooling of the bulk gas in the annulus section is shown in Figure 6-18. Here the modelled result indicates that the bulk temperature decreases quite drastically over the length on the annulus section of the desublimer.

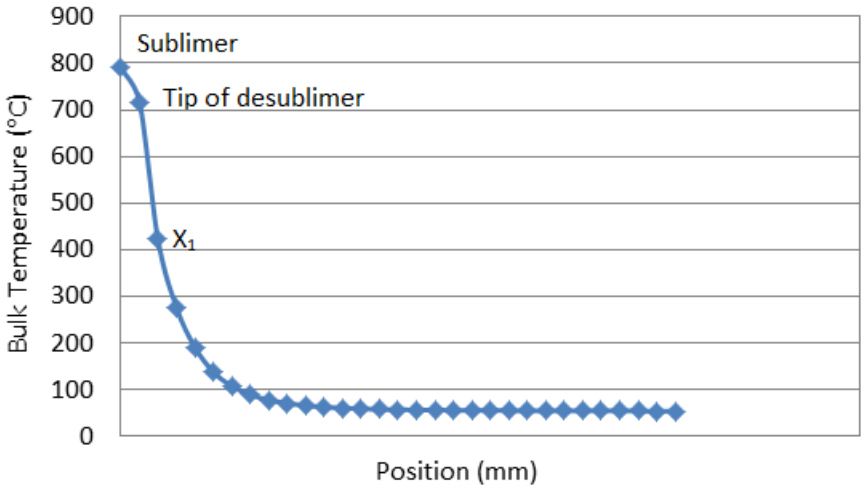

Figure 6-18: Modelled result for cooling of the bulk gas after exiting the sublimer section with the sublimation temperature set at 790 °C

Comparing the modelled versus the experimentally measured temperature at X_1, it is seen that the modelled value is out by less than 17 %. At X_2 the measured value was, however, ~100 °C, which is well below the modelled values obtained. This implies that there are other factors that need to be included in the model to account for these temperature differences, which may have a huge or a minute effect on the Zr/Hf mole ratios obtained.

6.6 Modelled partial pressures

6.6.1 Partial pressures of ZrF_4 and HfF_4across the sublimer and desublimer section

The partial pressure of the ZrF_4 in the sublimer and desublimer changes with both length and time as shown in Figure 6-19 for ZrF_4 and in Figure 6-20 for HfF_4. The partial pressures of the ZrF_4 and HfF_4 in the bulk gas increase in the sublimer section, after which they decrease as desublimation proceeds along the length of the desublimer. It is further shown that the partial pressures decrease as time proceeds. These pressures are shown for a sublimation temperature of 790 °C.

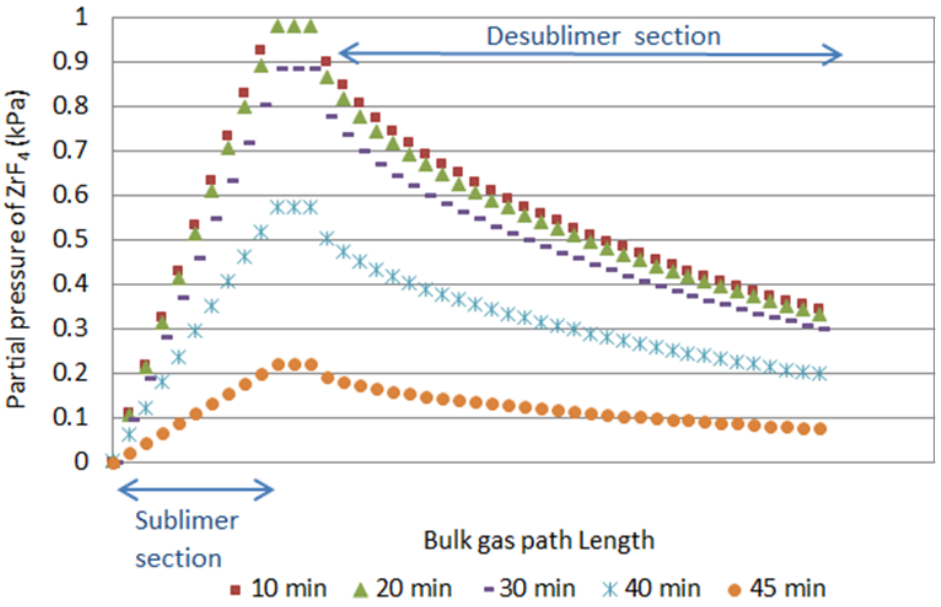

Figure 6-19: Partial pressures of ZrF_4 within the sublimer and desublimer

As with ZrF_4, the same is shown for HfF_4, but the reciprocal is true, namely where the partial pressure increases with time.

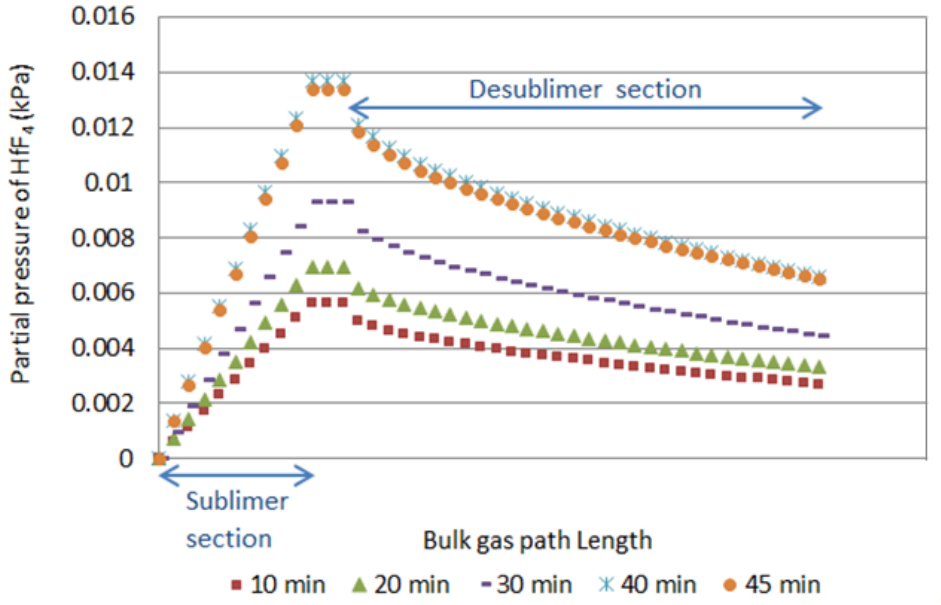

Figure 6-20: Partial pressures of HfF_4 within the sublimer and desublimer

6.6.2 Partial pressures exiting the sublimer section

The partial pressures at which ZrF_4 and HfF_4 exit the sublimer section and enter the desublimation section are shown as a function of time at 790 °C in Figure 6-21 and at 760 °C in Figure 6-22.

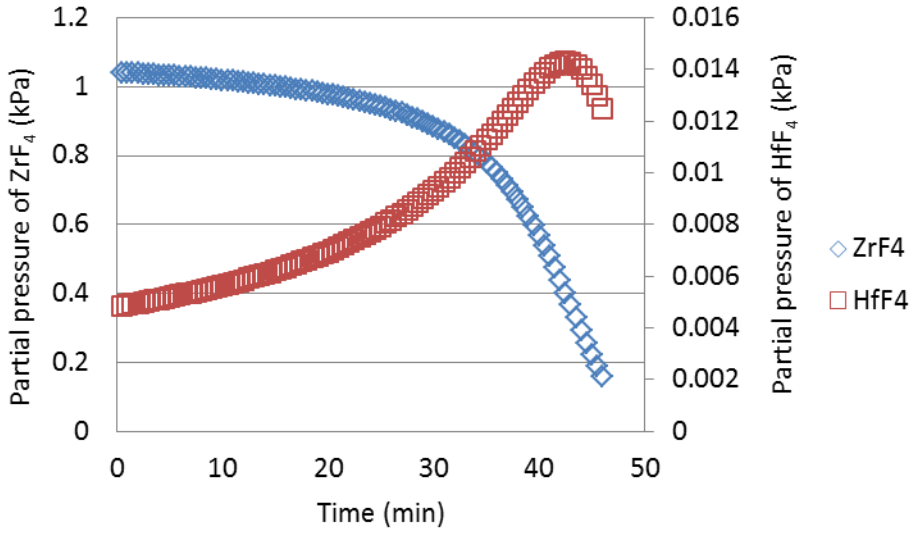

Figure 6-21: Partial pressures of ZrF_4 and HfF_4 exiting the sublimer section at 790 °C

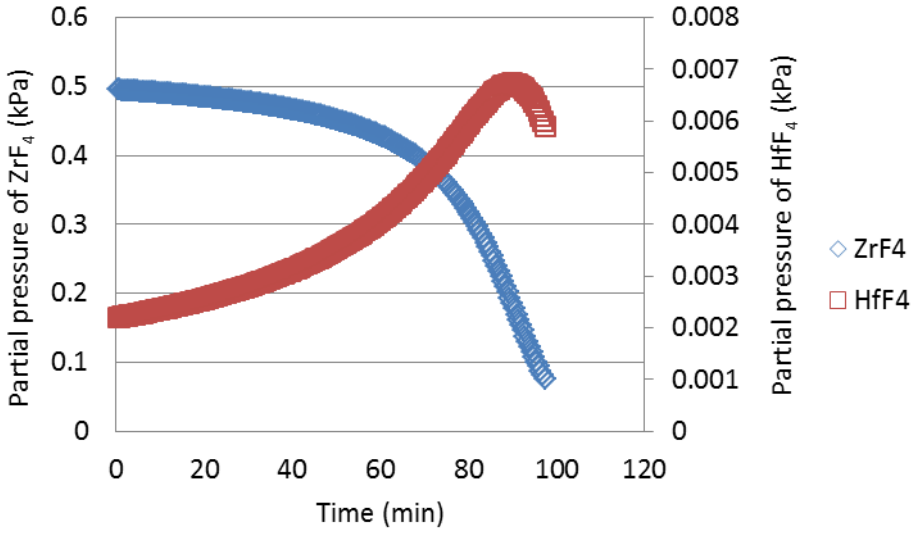

Figure 6-22: Partial pressures of ZrF_4 and HfF_4 exiting the sublimer section at 760 °C

From Figure 6-21 and Figure 6-22 it can be seen that the sublimation temperature has a big influence on the partial pressures obtained in the sublimer. To achieve better separation it would be advantageous to remove the sublimer from the heating zone before the partial pressure of the ZrF_4 becomes too low and that of the HfF_4 becomes too high. For example, looking at a partial pressure change of 20 % implies that at 790 °C the partial pressure change is ~ 20 % within the first 30 minutes, whereas at 760 °C the change is 20 % after 60 minutes.

Noting these differences may be valuable in determining the optimal temperature and residence time for the sublimation process.

6.7 Number of sublimation steps determined by the model

The starting Hf concentration in the $Zr(Hf)F_4$ bulk material is 1.27 % (1.67 % HfF_4) with a zircon content of 6.7 %. After the first sublimation step, the model result for the collective bulk mass obtained from the desublimer contains no zircon and the Hf concentration decreases to a certain extent.

It was shown that lower temperatures give better separation but require a longer sublimation time to achieve the same degree of sublimation. The number of steps required to obtain < 100 ppm Hf were determined at both 790 and 760 °C with a sublimation time of 30 minutes.

From Figure 6-1 it can be seen that the fraction sublimed for 30 minutes at 790 °C is the same as that sublimed for 60 minutes at 760 °C. The number of steps required to obtain a Hf content of less than 100 ppm were calculated for a 60 minutes' residence time at 760 °C and the three scenarios compared.

Note that the calculations were based on the results obtained from a single sublimation step. This implies that the mass collected from the desublimer was not sublimed to account for a second or third step. The masses collected were simply too small to enable us to do second, third and more sublimation steps. The results collected from this first sublimation step were compared to the results of the model and these comparisons were used to estimate the extent of separation for second, third and more sublimation steps. This was therefore a theoretical study to determine the number of sublimation steps required to obtain < 100 ppm Hf in the product.

There are many other factors that can influence the results, for example the particle surface area before and after sublimation and the amount of oxyfluorides present after collection from the desublimer.

6.7.1 Model run at 790 °C sublimation temperature and 30 minutes' sublimation time

The model was run at a sublimation temperature of 790 °C for several repetitive times. Each time a new value was entered for the Hf concentration (i.e. HfF_4) in the bulk material with the assumption of removal of the sublimer after 30 minutes. This was done to determine the number of steps required.

Assuming that the modelled Zr/Hf mole ratio is 1.2 times that of the actual mole ratio at 790 °C, the implication is that the Hf result after each step needs to be multiplied by 1.2 before feeding this input to the next step. The results obtained (Figure 6-23) indicated that 8 steps would be required to reduce the Hf concentration to less than 100 ppm.

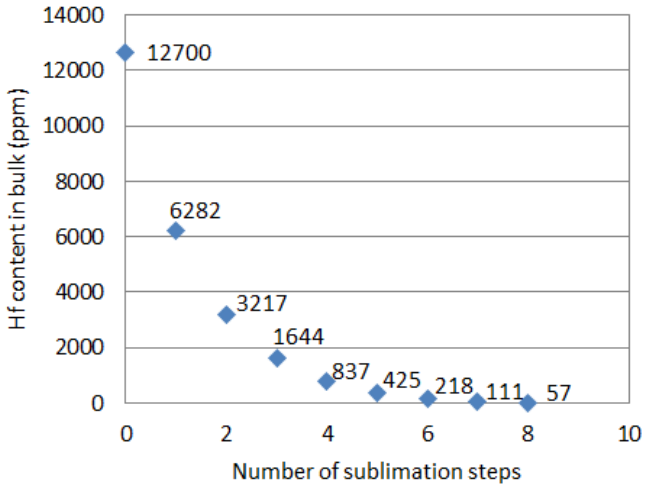

Figure 6-23: Number of calculated sublimation steps required to obtain < 100 ppm Hf at a sublimation temperature of 790 °C and removal of the sublimer after 30 minutes

At 790 °C it was found that approximately 70 % of the sublimed mass could be collected in the desublimer. This implies that 18.5 kg would be required to produce 1 kg of nuclear grade (< 10 ppm Hf) ZrF_4.

6.7.2 Model run at 760 °C sublimation temperature and 30 minutes' sublimation time

At a sublimation temperature of 760 °C and removal of the sublimer after 30 minutes with the assumption that the modelled Zr/Hf mole ratio is 1.5 times that of the actual mole ratio at 760 °C, 7 steps are required to reduce the Hf concentration to less than 100 ppm (Figure 6-24).

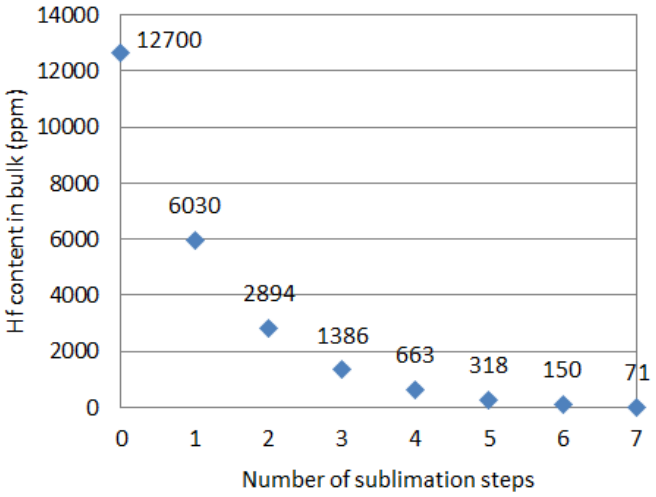

Figure 6-24: Number of calculated sublimation steps required to obtain < 100 ppm Hf at a sublimation temperature of 760 °C and removal of the sublimer after 30 minutes

Note that lower sublimation temperatures give better separation but require longer sublimation times to obtain the same amount of sublimed material.

6.7.3 Model run at 760 °C sublimation temperature and 60 minutes' sublimation time

At a sublimation temperature of 760 °C and removal of the sublimer after 60 minutes with the assumption that the modelled Zr/Hf mole ratio is 1.5 times that of the actual mole ratio at 760 °C, 10 steps are required to reduce the Hf concentration to less than 100 ppm (Figure 6-25).

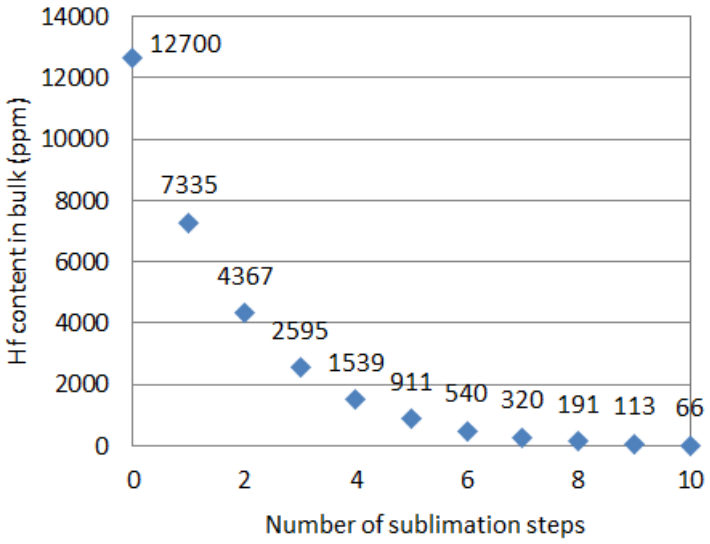

Figure 6-25: Number of sublimation steps required to obtain < 100 ppm Hf with a sublimation temperature of 760 °C and removal of the sublimer after 60 minutes

It must, however, be kept in mind that less mass was desublimed at the lower temperature, which may influence the yield if a lower operating temperature is chosen (Figure 6-15).

From the above results it is clear that fewer steps are required to obtain < 100 ppm Hf at lower temperatures with removal of the sublimer after 30 minutes.

However, at 760 °C the area-dependent rate is 0.873 $g \cdot m^{-2} \cdot s^{-1}$, whereas at 790 °C the rate is 1.85 $g \cdot m^{-2} \cdot s^{-1}$, which implies that the sublimation reactor (and desublimer) must be 2.1 times larger to achieve the same rate as at 790 °C to benefit from using one sublimation step fewer at 760 °C.

Chapter 7: Conclusions and recommendations

7.1 Conclusions

Sublimation provides a dry process for separation which has the added advantage of producing much less waste, especially liquid wastes, which have undesirable environmental effects. Little information is available on the sublimation separation of Zr and Hf, especially in the fluoride form and most studies in the literature involve sublimation under vacuum conditions.

Experimental results indicate that separation is achieved in both the sublimer and across the length of the desublimer. A downside to the sublimation was sintering of the cake which negatively influences the sublimation kinetics.

A sublimation and desublimation model was developed. The model was used to calculate the sublimation and desublimation rates of both the ZrF_4 and HfF_4, which enabled the calculation of Zr/Hf mole ratios within the sublimer residue and across the length of the desublimer.

The data from the model were compared to the experimental results. Good comparisons of the sublimation rates were shown at temperatures of 740 °C and 760 °C, but the sublimation rates at temperatures of 790 °C were over-predicted. These could be due to the non-equilibrium nature of the $Zr(Hf)F_4$ sublimation process and the interaction of impurities at higher temperatures.

The over-prediction of the sublimation rates were used as input to the desubliming stage and therefore modelled results were worse for the desublimation when compared to experimental results obtained.

In both the experimental and modelled results for the separation in the desublimer, it was found that a lower sublimation temperature would result in a higher mole ratio (better separation), both within the sublimer residue and across the length of the desublimer. Optimal temperature selection is therefore imperative with respect to operational cost and material of construction.

Further optimisation of the sublimation process in an inert atmosphere may be considered based purely on the extent of separation achieved in both the sublimer and desublimer. Literature indicated that pure $Zr(Hf)F_4$ gives higher rates of sublimation and therefore it would be interesting to test the efficiency of a second step.

7.2 Recommendations

From this work it was shown that lower sublimation temperatures resulted in better separation but with lower sublimation rates. Vacuum sublimation, however, gives higher fluxes and requires lower temperatures. It is therefore recommended that this study be repeated under vacuum conditions to determine the extent of separation that can be achieved along the length of the desublimer. To stress the importance of this the recommendation, it must be noted that sublimation provides dry methods with no liquid waste. It may require fewer steps, which is less labour intensive and lower capital costs than other commercial technologies. The major drawbacks are the high energy requirements to obtain the high separation temperatures, resulting in expensive construction materials.

For the current system, the following recommendations are made:

- Due to the sintering of the cake, it is recommended that a mixer be added in the sublimation step.
- To ensure adequate heat transfer in the desublimer, it is recommended that a continuous scraper be installed to scrape the desublimed product from the surface of the desublimer.
- Due to the separation achieved along the length of the desublimer, it is recommended that the desublimed product be removed at predetermined positions along the length of the desublimer.
- Due to the differences in separation achieved at different sublimation temperatures, residence times and along the length of the desublimer, it is recommended that a cascade of sublimer/desublimer systems be developed, each at different operating conditions. Figure 7-1 shows such a system.

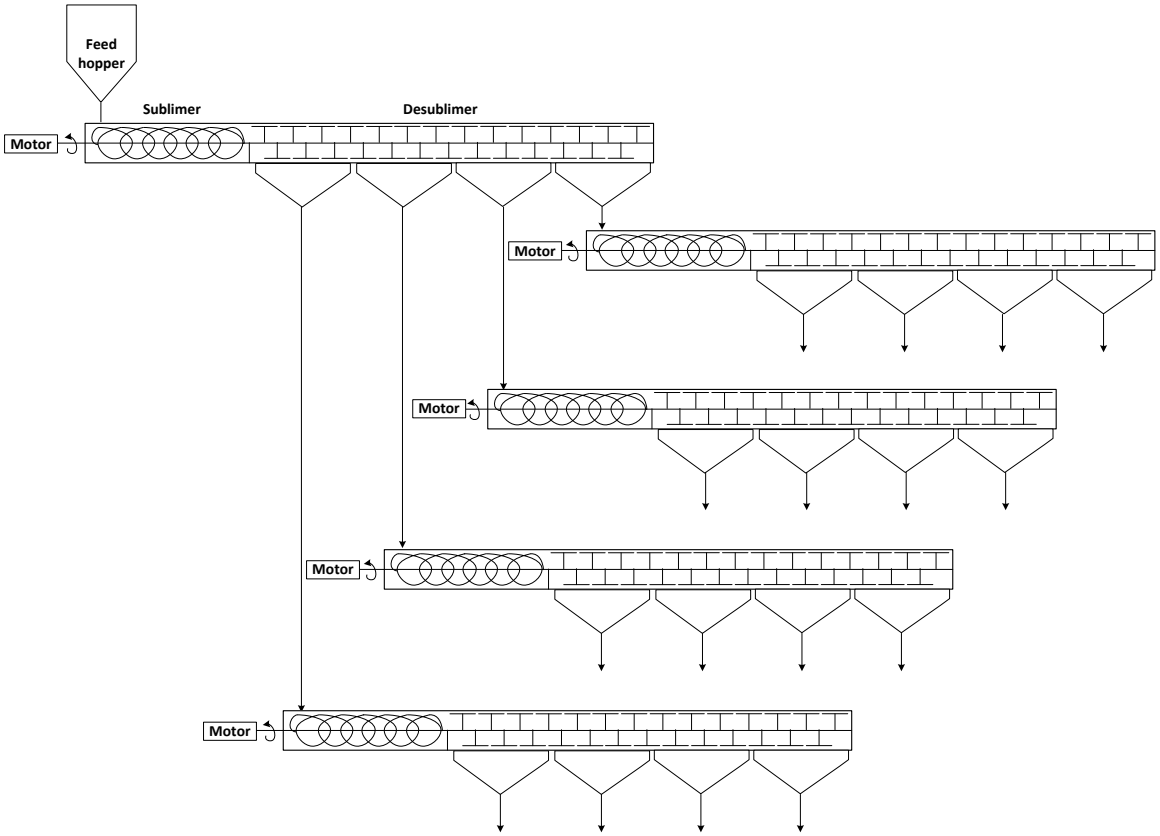

Figure 7-1: Cascade of sublimer/desublimer systems for the separation of Zr and Hf

Recommended alterations and/or additions to increase the purity of the samples as well as the rate of sublimation:

- A pre-dry step of the salt is necessary to avoid the formation of metal oxides and metal oxyfluorides (Yeatts and Rainey, 1965).
- The sweep gas could be replaced by fluorine gas, but this would add complications.
- A slow temperature increase up to 500 °C under vacuum (Yeatts and Rainey, 1965) would ensure homogeneous heating. One reason for doing this is due to possible heat transfer problems, which would keep the temperature gradient in the sample as low as possible.
- A system can be developed in which baffles could be added to prevent the entrainment of ZrO_2 and $ZrOF_2$ during sublimation of ZrF_4 (Yeatts and Rainey, 1965).
- Compounds could be added to provide a "gettering" activity in order to reduce the number of steps required to obtain reactor-grade ZrF_4 (Solov'ev & Malyutina, 2002b). The details are described in Section 2.3.1.
- The addition of pulverized metallic scrap to the ZrF_4 mixtures can give a higher rate of sublimation (Solov'ev and Malyutina, 2002).

Inadequate information was found on the sublimation rate of ZrF_4 or HfF_4 in an inert atmosphere. The sublimation rate is assumed to be dependent on several factors, including temperature, available

sublimation area, pressure, composition, particle size, surface area of the sample, crystal structure, hygroscopic nature of the sample and the type of equipment used. No information was available on the effect of particle size, the surface area of the sample, the crystal structure and the hygroscopic nature of the sample would have on the desired separation. It is therefore recommended that these parameters and their effect on the sublimation rate be studied.

Chapter 8: References

Abate, LJ and Wilhelm, HA (1951) Sublimation of zirconium tetrafluoride, United States Atomic Energy Commission, Ames Laboratory.

Banda, R, Lee, HY and Lee, MS (2012) Separation of Zr from Hf in hydrochloric acid solution using amine-based extractants, *Ind. Eng. Chem. Res*., *51* (28), 9652–9660.

Banda, R, Min, SH and Lee, MS (2013) Selective extraction of Hf(IV) over Zr(IV) from aqueous H_2SO_4 solutions by solvent extraction with acidic organophosphorous based extractants, *J. Chem. Technol. Biotechnol*., 89 (11), 1712–1719.

Barberis, P (2008) Metallurgy and properties of Zr alloys for nuclear applications. Processing and forming of industrial components, Presentation at international training session, INSTN - CEA Saclay, France.

Begovich, JM and Sisson, WG (1983) Continuous ion exchange separation of zirconium and hafnium using an annular chromatograph, *Hydrometallurgy, 10* (1), 11–20.

Benedict, JT, Schumb, WC and Coryell, CD (1954) Distribution of zirconium and hafnium between cation-exchange resin and acid solutions. The column separation with nitric acid-citric acid mixture, *J. Am. Chem. Soc*., *76* (8), 2036–2040.

Benedict, M, Pigford, TH and Levi, HW (1981) *Nuclear Chemical Engineering*, McGraw-Hill, New York.

Besson, P, Guerin, J, Brun, P and Bakes, M (1977) Process for the separation of zirconium and hafnium tetrachlorides from mixtures thereof, *US Patent 4,021,531,* assigned to Ugine Aciers, US.

Bird, RB, Stewart, WE and Lightfoot, EN (1960) *Transport Phenomena,* John Wiley & Sons, Inc.

Boulos, MI, Fauchais, P and Pfender, E (1994) *Thermal Plasmas: Fundamentals and Applications*, Springer, US.

Branken, DJ, Lachmann, G, Krieg, HM and Bruinsma, DSL (2010) Influence of KF and HF on the selectivity of Zr and Hf separation by fractional crystallisation of $K_2Zr(Hf)F_6$, *Ind. Eng. Chem. Res.*, *49* (2), 797–808.

Branken, DJ (2009) Separation of Zr and Hf via fractional crystallisation of $K_2Zr(Hf)F_6$: a theoretical and experimental study, PhD Thesis, North-West University, Potchefstroom.

Brown, PL, Curti, E and Grambow, B (2005) *Chemical Thermodynamics of Zirconium,* Elsevier, The Netherlands.

Brown, AEP and Healy, TV (1978) Separation of zirconium from hafnium in nitric acid solutions by solvent extraction using dibutyl butylphosphonate: Part 1. Chemistry of the separation, *Hydrometallurgy, 3* (3), 265–274.

Brown, AEP and Wain, AG (1978) Separation of zirconium from hafnium in nitric acid solutions by solvent extraction using dibutyl butylphosphonate: Part 2. Mixer-settler runs, *Hydrometallurgy,3* (3), 275-282.

Brunetti, B, Piacente, V and Scardala, P (2011) Vapor pressure of zirconium tetrafluoride *J. Chem. Eng. Data*, *56* (5), 1970–1973.

Byers, CH, Sisson, WG, Snyder, TS, Beleski, RJ, Francis, TL and Nayak, UP (1998) Zirconium and hafnium separation in chloride solutions using continuous ion exchange chromatography, *US Patent 5,762,890,* assigned to Westinghouse Electric Corporation, US.

Byers, CH, Sisson, WG, Snyder, TS, Beleski, RJ, Nayak, UP and Francis, TL (1997) Zirconium and hafnium separation in sulfate solutions using continuous ion exchange chromatography, *US Patent 5,618,502,* assigned to Westinghouse Electric Corporation, US.

Cantor, S, Newton, R, Grimes, W and Blankenship, F (1958) Vapor pressures and derived thermodynamic information for the system RbF-ZrF_4, *J. Phys. Chem.,* 62 (1), 96–99.

Caracoche, MC, Martinez, JA, Rivas, PC and Lopez Garcia, AR (1985) TDPAC investigation on thermally related $HfF_4 \cdot 3H_2O$ and HfO_2,*Hyperfine Interactions, 23* (2), 221-229.

Çengel, YA and Klein, S (2007) *Heat and mass transfer: a practical approach*, McGraw-Hill, Singapore.

Corder, WC and Hanson, SP (2004) Other separation processes*,* In *The Electrical Engineering Handbook, Second Edition, ,* CRC Press.

Coster, D and Hevesy, G (1927) Process of separating zirconium from hafnium, *US Patent 1,618,96*0, assigned to Philips Nv, US.

Cox, RP, Peterson, HC and Beyer, GH (1958) Separating hafnium from zirconium. Solvent extraction with tributyl phosphate, *Ind. Eng. Chem.*, *50* (2), 141–143.

Lide, DR (2008) *CRC handbook of chemistry and physics: a ready-reference book of chemical and physical data,* CRC, London.

Da Silva, ABV and Distin, PA (1998) Zirconium and hafnium separation without waste generation, *CIM Bulletin, 91* (1018), 221–224.

Dai, G, Huang, J, Cheng, J, Zhang, C, Dong, G and Wang, K (1992) A New preparation route for high-purity ZrF_4, *J. Non-Cryst. Solids, 140* (1-3), 229–232.

De Boer, JH (1927) Zirconium, *Ind. Eng. Chem., 19* (11), 1256–1259.

Debbasch, F and Rivet, JP (2011) The Ludwig–Soret effect and stochastic processes, *J. Chem. Thermodyn., 43* (3), 300–306.

Delons, L, Lagarde, S, Favre-reguillon, A, Pellet-Rostaing, S, Lemaire, M and Poriel, L (2010) Process for the separation and purification of hafnium and zirconium, *US Patent 7,708,962 B2,* assigned to Compagnie Europeenne du Zirconium-Cezus.

Deorkar, NV and Khopkar, SM (1991) Liquid-liquid extraction of zirconium from hafnium and other elements with dicyclohexyl-18-crown-6, *Analytica Chimica Acta, 245*, 27–33.

Dominguez, G, Wilkins, G and Thiemens, MH (2011) The Soret effect and isotopic fractionation in high-temperature silicate melts, *Nature, 473* (7345), 70–73.

Favre-Réguillon, A, Fiaty, K, Laurent, P, Poriel, L, Pellet-Rostaing, S and Lemaire, M (2007) Solid/liquid extraction of zirconium and hafnium in hydrochloric acid aqueous solution with anion exchange resin – kinetic study and equilibrium analyses, *Ind. Eng. Chem. Res., 46* (4), 1286–1291.

Folweiler, RC (1987) Chemical vapor purification of fluorides, *US Patent 4,652,438 A,* assigned to GTE Laboratories Incorporated.

Fujiura, K, Ohishi, Y, Sakaguchi, S and Terunuma, Y (1989) Synthesis of high-purity zirconium fluoride for fluoride glass fibers by chemical vapor deposition, *J. Am. Ceram. Soc.* 72 (8), 1368–1372.

Gillot, J and Goldberger, WM (1969) Separation methods for volatile solids, *US Patent 3,457,049* A, assigned to The Battelley Dev Corp.

Gosling, K and Bowen, RE (1973) Efficient vacuum fractional-sublimation apparatus, *Anal. Chem., 45* (8), 1574–1575.

Green, JD (2000) II / Distillation /sublimation, in *Encyclopedia of Separation Science (2nd Ed.),* Wilson, I.D. (Ed.), Academic Press, Oxford.

Gruen, DM and Katz, JJ (1949) Separation of hafnium and zirconium by a fractional distillational procedure, *J. Am. Chem. Soc., 71* (11), 3843–3844.

Hansen, RS, Gunnar, K, Jacobs, A and Simmons, CR (1950) The adsorption separation of zirconium and hafnium, *J. Am. Chem. Soc., 72* (11), 5043–5045.

Hanson, SP and Corder, WC (2004) *Other separation processes* in The Engineering Handbook, Second Edition, CRC Press.

Hevesy, G (1925) The discovery and properties of hafnium, *Chem. Rev., 2* (1), 1–41.

Hevesy, G and Kimura, K (1925) The solubilities of the phosphates of zirconium and hafnium, *J. Am. Chem. Soc., 47* (10), 2540–2544.

Huffman, EH and Lilly, RC (1951) Anion exchange of complex ions of hafnium and zirconium in HCl–HF mixtures, *J. Am. Chem. Soc., 73* (2), 2902–2905.

Hurst, FJ (1983) Separation of hafnium from zirconium in sulfuric acid solutions using pressurized ion exchange, *Hydrometallurgy, 10*(1), 1–10.

Ishizuka, H (1974) Process for refining zirconium tetrachloride containing hafnium tetrachloride, *US Patent 3,856,477,* assigned to Ishizuka, H.

Jacque, L and Dumez, P (1960) Process for the separation of substances by vaporisation, *US Patent 2,944,878(A),* assigned to Pechiney Prod Chimiques SA.

Jang, SM, Yang, S, Liou, BI, Chen, JY, Jean, LS, Tsai, CT and Huang, CT (2005) Apparatus and process for vacuum sublimation, *US Patent 0,047,979 A1*, assigned to Industrial Technology Research Institute.

Jeon, HG, Inoue, M, Hiramatsu, N, Ichikawa, M and Taniguchi, Y (2008) A modified sublimation purification system using arrays of partitions, *Organic Electronics*, *9*(5), 903–905.

Jeon, HG, Kondo, Y, Maki, S, Matsumoto, E, Taniguchi, Y and Ichikawa, M (2010) A highly efficient sublimation purification system using baffles with orifices, *Organic Electronics,* 11(5), 794–800.

Kawato, S, Hayashi, N, Sonoda, T and Inoue, S (2014) Vapor deposition device and vapor deposition method, *US Patent 8,628,620*, assigned to Sharp Kabushiki Kaisha (Osaka, JP).

Kim, YJ (2013) Einstein's random walk and thermal diffusion, https://arxiv.org/abs/1307.4460 *[2016, May12]*

Kodde, M and Mewes, D (1995) Generation of very fine solid particles by vapor desublimation in a gaseous mixture, *J. Aerosol Sci., 26* (1), S565–S566.

Konings, RJM, Allen, TR, Stoller, RE and Yamanaka, S (2012) *Comprehensive Nuclear Materials*, Elsevier.

Konings, RJM and Hildenbrand, DL (1994) The vapor pressure, infrared spectrum and thermodynamic properties of ZrF_4(g) *Journal of Chemical Thermodynamics 26*, 155–163.

Koreneo, Y, Sorokin, I, Chirina and Novoselo, N (1972) Vapor-pressure of hafnium tetrafluoride *Zhurnal Neorg. Khimii, 17* (5), 1195.

Kotsar, ML, Bateev, VB, Baskov, PB, Sakharov, VV, Fedorov, VD and Shatalov, VV (2001) Preparation of high-purity ZrF_4 and HfF_4 for optical fibers and radiation-resistant glasses, *Inorg. Mater.,* 37 (10), 1085–1091.

Kragh, H and Robertson, P (1979) On the discovery of element 72, *J.Chem.Educ.,* 56 (7), 456.

Kraus, KA and Moore, GE (1949) Separation of zirconium and hafnium with anion exchange resins, *J. Am. Chem. Soc., 71* (9), 3263–3263.

Lide, DR (2007) *CRC Handbook of Chemistry and Physics,* 88th Edition, CRC Press, London.

MacFarlane, DR, Newman, PJ and Voelkel, A (2002) Methods of purification of zirconium tetrafluoride for fluorozirconate glass, *J. Am. Ceram. Soc., 85* (6), 1610–1612.

Marrero, TR and Mason, EA (1972) Gaseous diffusion coefficients, *J. Phys. Chem. Ref. Data,* 1 (1), 3.

Martínez, JA, Caracoche, MC, Rodríguez, AM, Rivas, PC and García, ARL (1983) On the kinetics of chemical reactions in hafnium tetrafluorides using time differential-perturbed angular correlations, *Chemical Physics Letters, 102* (2–3), 277-280.

McLaughlin, DF and Stoltz, RA (1988) Zirconium and hafnium tetrachloride separation by extractive distillation with molten zinc chloride lead chloride solvent, *US Patent 4,737,244 A*, assigned to Westinghouse Electric Corp.

McLaughlin, DF and Stoltz, RA (1989) Molten salt extractive distillation process for zirconium-hafnium separation, *US Patent 4,874,475,* assigned to Westinghouse Electric Corp.

Megy, JA (1978) Method of separating hafnium from zirconium, *US Patent 4,072,506,* assigned to Teledyne Industries Inc., LA.

Monnahela, OS, Augustyn, WG, Nel, JT, Pretorius, CJ and Wagener, JB (2013) The vacuum sublimation separation of zirconium and hafnium tetrafluoride, paper presented at the *AMI-sponsored Precious Metals 2013 Conference*, 14–16 October, 2013, Protea Hotel, Cape Town.

Moulin, L, Thouvenin, P and Brun, P (1984) New process for zirconium and hafnium separation, in *Zirconium in the Nuclear Industry,* Franklin, D and Adamson, R (Eds.), ASTM International.

Murskii, GL, Garbar, AM, Loginov, AV, Rodchenkov, VI and Pimenov, VG (1989) Rectification of zirconium tetrafluoride by sublimation in the chlorine flow, *Vysokochist. Veshchestva,* 1, 91–94.

Nakashima, K and Takeyama, N (1989) Thermal diffusion in a lorentz gas, *J. Phys. Soc. Jpn.*, 58 (12), 4352–4357.

Nayl, AA, El-Nadi, YA and Daoud, JA (2009) Extraction and separation of Zr(IV) and Hf(IV) from nitrate medium by some CYANEX extractants, *Sep. Sci. Technol., 44* (12), 2956–2970.

Nel, JT, Havenga, JL, Du Plessis, W and Le Roux, JP (2013) Treatment of chemical feedstocks, *US Patent 9,468,975 B2*, assigned to the South African Nuclear Energy Corporation Limited.

Newnham, IE (1956) The separation of zirconium and hafnium by differential reduction of their tetrachlorides, *J. Am. Chem. Soc. 79* (20), 5415–5417.

Nielsen, RH (2001) Hafnium and hafnium compounds, in *Kirk-Othmer Encyclopedia of Chemical Technology*, Seidel, A (Editor-in-chief), John Wiley & Sons, Inc.

Nielsen, RH, Schlewitz, JH and Nielsen, H (2001) Zirconium and zirconium compounds in *Kirk-Othmer Encyclopedia of Chemical Technology*, Seidel, A (Editor-in-chief), John Wiley & Sons, Inc.

Niemand, HF (2012) UF_6 Desublimer Design Guide*,* NED-NFC-GLN-11001.

Niselson, LA, Egorov, EA, Chuvilina, EL, Arzhatkina, OA and Fedorov, VD (2009) Solid−liquid and liquid−vapor equilibria in the Zr(Hf)Cl_4−K$AlCl_4$ Systems: A basis for the extractive distillation separation of zirconium and hafnium tetrachlorides, *J. Chem. Eng. Data,* 54 (3), 726–729.

Pastor, RC and Robinson, M (1986) Method for preparing ultra-pure zirconium and hafnium tetrafluorides, *US Patent 4,578,252 A*, assigned to Hughes Aircraft Company

Perry, RH and Green, DW, (1997) *Perry's Chemical Engineers' Handbook* 7th Edition*,* McGraw-Hill, New York.

Poriel, L, Favre-Réguillon, A, Pellet-Rostaing, S and Lemaire, M (2006) Zirconium and hafnium separation, Part 1. Liquid/liquid extraction in hydrochloric acid aqueous solution with aliquat 336, *Sep. Sci. Technol., 41* (9), 1927–1940.

Pretorius, CJ (2013) *A theoretical approach to identify the metal fluoride impurities in ZrF_4*, Internal report AC-AMI02-REP-12006, Applied Chemistry, Necsa.

Qureshi, M and Husain, K (1971) Quantitative cation exchange separation of zirconium and hafnium in formic acid media, *Anal. Chem. 43* (3) 447–449.

Raouzeos, G and Schwenk, W (1996) Sublimation – A non-fluid thermal separation process, http://www.listdryprocessing.com/info-center/downloads.html#A2 [2014, June 12].

Reid, RC, Prausnitz, JM and Poling, BE (1988) *The properties of gases and liquids*, Mc Graw-Hill, New York.

Retief, WL, Nel, JT, du Plessis, W, Crouse, PL and Retief, ND (2011) Treatment of zirconia-based material with ammonium bifluoride, *US Patent 8,778,291 B2*, assigned to the South African Nuclear Energy Corporation Limited.

Reuter, K, Passing, G and Kirchmeyer, S (2009) Process for separating zirconium and hafnium, *US Patent 7,635,396,* assigned to H. C. Starck GmBH & Co.

Rivas, PC, Martinez, JA, Rodriguez, AM, Lopez Garcia, AR and Dejneka, M (1997) Hyperfine characterisation of beta-zirconium tetrafluoride, *Hyperfine Interactions, 110* (3/4), 195–198.

Robertson, GR (1932) Sublimation, *J. Chem. Educ.* 9, 1713

Robinson, M (1986) Processing and purification techniques of heavy metal fluoride glass (HMFG)*, J. Cryst. Growth, 75* (1), 184–194.

Robinson, M and Fuller, KC (1987) The recrystallisation of ZrF_4 and AlF_3, M*aterials Research Bulletin*, *22*, 1725–1732

Royston, D and Alfredson, PG (1970) *Review of processes for the production of hafnium-free zirconium*, Australian Atomic Energy Commission, Research Establishment, Lucas Heights.

Saleh, AS (2012) Solvent extraction of Zr(IV) and Hf(IV) with N,N,N′,N′-tetraoctyldiglycolamide, *J. Radioanal. Nucl. Chem., 292* (3), 1109–1114.

Sarbeck, LE, Lee, DR, Jacoby, LJ, Haygarth, JC, Goodwin, CT and Crocker, WA (1993) Zirconium-hafnium separation process, *US Patent 517,687,805*.

Sattler, K and Feindt, HJ (1995) *Thermal separation processes: principles and design*, Wiley-VCH, Weinheim, New York.

Sense, KA, Snyder, MJ and Clegg, JW (1953) *Vapor pressures of beryllium fluoride and zirconium fluoride*, US Atomic Energy Commission Technical Information Services, Oak Ridge, Tennessee.

Sense, KA, Snyder, MJ and Filbert, RBJ (1954) The vapor pressure of zirconium fluoride, *J. Phys. Chem., 58* (11), 995-996.

Skaggs, RL, Rogers, DT and Hunter, DB (1984) *Review of anhydrous zirconium-hafnium separation techniques*, US Dept. of the Interior, Bureau of Mines, United States.

Smith, RL (2001) Predicting evaporation rates and times for spills of chemical mixtures, *Ann Occup Hyg, 45,* 437–445.

Smolik, M, Jakóbik-Kolon, A and Porański, M (2009) Separation of zirconium and hafnium using Diphonix® chelating ion-exchange resin, *Hydrometallurgy, 95* (3-4), 350–353.

Smolkin, P, Buynovskiy, A, Lazarchuk, V, Matveev, A and Sofronov, V (2007) Mathematical model of desublimation process of volatile metal fluorides, *Bulletin of the Томск Polytechnic University, 310* (3), 69–71.

Solov'ev, AI and Malyutina, VM (2002a) Metallurgy of less-common and precious metals. Production of metallurgical semiproduct from zircon concentrate for use in production of plastic metallic zirconium, *Russ. J. Non-Ferrous Met., 43* (9), 9–13.

Solov'ev, AI and Malyutina, VM (2002b) Production of metallic zirconium tetrafluoride purified from hafnium to reactor purity, *Russ. J. Non-Ferrous Met.,43* (9), 14–18.

Štefan Schlosser, JM (2009) *Separation of mixtures by pertraction or membrane based solvent extraction and new extractants,* Institute of Chemical and Environmental Engineering, Slovak University of Technology, Slovakia.

Stephens, W (1984) Extractive metallurgy of zirconium – 1945 to the present, in *Zirconium in the Nuclear Industry*, Franklin, D and Adamson, R (Eds.), ASTM International.

Street, K and Seaborg, GT (1948) The ion-exchange separation of zirconium and hafnium, *J. Am. Chem. Soc., 70* (12), 4268–4269.

Taghizadeh, M, Ghanadi, M and Zolfonoun, E (2011) Separation of zirconium and hafnium by solvent extraction using a mixture of TBP and CYANEX 923, *J. Nucl. Mater.*, *412* (3), 334–337.

Taghizadeh, M, Ghasemzadeh, R, Ashrafizadeh, SN and Ghannadi, M (2009) Stoichiometric relation for extraction of zirconium and hafnium from acidic nitrate solutions with CYANEX 272, *Hydrometallurgy 96* (1-2), 77–80.

Taghizadeh, M, Ghasemzadeh, R, Ashrafizadeh, SN, Saberyan, K and Maragheh, MG (2008) Determination of optimum process conditions for the extraction and separation of zirconium and hafnium by solvent extraction, *Hydrometallurgy, 90* (2-4), 115–120.

Takahashi, M, Miyazaki, H and Katoh, Y (1984) New solvent extraction process for zirconium and hafnium, in *Zirconium in the Nuclear Industry*, Franklin, D and Adamson, R (Eds.), ASTM International.

Ti, VA, Esyutin, VS and Scherbinin, VP (1990a) The dependence of the zirconium tetrafluoride sublimation rate in vacuum upon the process temperature and product composition. *Kompleksn. Ispol'z. Miner. Syr'ya., 9*, 63–64.

Ti, VA, Esyutin, VS and Scherbinin, VP (1990b) The dependence of the zirconium tetrafluoride sublimation rate upon the process pressure, *Kompleksn. Ispol'z. Miner. Syr'ya, 10*, 61–63.

Ti, VA, Esyutin, VS and Scherbinin, VP (1990c) The influence of the sample height on the zirconium tetrafluoride sublimation process, *Kompleksn. Ispol'z. Miner. Syr'ya, 8,* 60–61.

Ux Consulting (2013) Nuclear Zirconium Alloy Market*,* March 2013, Roswell.

Van der Merwe, R and Snyders, E (2016) Characterisation of ZrF_4 run 2 powder*,* AC-CHRNM-REP-16015, Nuclear Materials, Necsa.

Van der Vis, MGM, Cordfunke, EHP and Konings, RJM (1997) Thermochemical properties of zirconium halides: a review, *Thermochimica Acta, 302* (1), 93–108.

Van der Westhuizen, D (2009) Separation of zirconium and hafnium via solvent extraction, PhD Thesis, North-West University, Potchefstroom.

Van der Westhuizen, D, Lachmann, G and Krieg, H (2012) Method for the selective separation and recovery of metal solutes from solution *WO Patent 2012/168915 A1*, assigned to North-West University.

Waseda, Y and Isshiki, M (2001) *Purification process and characterisation of ultra-high purity metals: application of basic science to metallurgical processing,* Springer, New York.

Welty, JR, Wicks, CE, Wilson, RE and Rorrer, G (2001) *Fundamentals of momentum, heat and mass transfer,* Wiley, New York.

Westrum, EF (1965) Zirconium tetrafluoride-heat capacity and thermodynamic properties from 5° to 307°K, *J. Chem. Eng. Data, 10* (2), 140–142.

Williams, JL and Weaver, B (1956) *Hafnium metal. I, Conversion of hafnium oxide to hafnium tetrafluoride,* US Atomic Energy Commission, Oak Ridge, Tennessee.

Withers, J, Woytek, AJ and Lileck, JT (1991) Process for the production of high purity zirconium tetrafluoride and other fluorides, *US Patent 4,983,373 (A),* assigned to Air Products and Chemicals Inc.

Xu, Z, Wang, L, Wu, Y, Chi, R, Zhang, L and Wu, M (2012) Solvent extraction of hafnium from thiocyanic acid medium in DIBK-TBP mixed system, *Trans. Nonferrous Met. Soc. China, 22* (7), 1760–1765.

Yang, XJ, Fane, AG and Pin, C (2002) Separation of zirconium and hafnium using hollow fibers: Part I. Supported liquid membranes, *Chem. Eng. J., 8* (1-3), 37–44.

Yang, XJ, Pin, C and Fane, AG (1999) Separation of hafnium from zirconium by extraction chromatography with liquid anionic exchangers, *J. Chromatogr. Sci.*, *37* (5), 171–179.

Yeatts, LB and Rainey, WT (1965) *Purification of zirconium tetrafluoride,* Technical report ORNL-TM-1292, US Atomic Energy Commission, US.

Zhan, L, Qiu, Z and Xu, Z (2009) Separating zinc from copper and zinc mixed particles using vacuum sublimation, *Sep. Purif. Technol., 68* (3), 397–402.